Time-dependent Karhunen-Loève type decomposition methods for SPDEs

by

Minseok Choi

B.S., Seoul National University; Seoul, 2002

M.S., Seoul National University; Seoul, 2007

A dissertation submitted in partial fulfillment of the
requirements for the degree of Doctor of Philosophy
in The Division of Applied Mathematics at Brown University

PROVIDENCE, RHODE ISLAND

May 2014

This dissertation by Minseok Choi is accepted in its present form
by The Division of Applied Mathematics as satisfying the
dissertation requirement for the degree of Doctor of Philosophy.

Date_____ _____

George EM Karniadakis, Ph.D., Advisor

Recommended to the Graduate Council

Date_____ _____

Boris Rozovsky, Ph.D., Reader

Date_____ _____

Themistoklis Sapsis, Ph.D., Reader

Approved by the Graduate Council

Date_____ _____

Peter M. Weber, Dean of the Graduate School

Vitae

Education

- M.S. in Mechanical engineering, Seoul National University, 2007
- B.S. in Mathematics and Mechanical engineering, Seoul National University, 2002

Publications

- M. Choi, T. Sapsis, and G.E. Karniadakis. On the equivalence of dynamically orthogonal and dynamically bi-orthogonal methods: Theory and Numerical simulations, *J. Comp. Phys., 270, 1-20, 2014*
- M. Choi, T. Sapsis, and G.E. Karniadakis. A convergence study for the SPDEs using combined polynomial chaos and dynamically orthogonal schemes, *J. Comp. Phys., 245, 281-301, 2013*
- D. Venturi, M. Choi, and G.E. Karniadakis. Supercritical quasi-conduction states in stochastic Rayleigh Benard convection, *Int. J. of Heat & Mass Transfer, 55(13-14), 3732-3743, 2012*
- X. Yang, M. Choi, G. Lin, and G.E. Karniadakis. Adaptive ANOVA decomposition of stochastic incompressible and compressible flows, *J. Comp. Phys., 231, 1587-1614, 2012*
- Z. Zhang, M. Choi, and G.E. Karniadakis. Error estimates for the ANOVA

method with polynomial chaos interpolation: Tensor product functions, *SIAM J. Sci. Comp., 34(2) A1165-A1186, 2012*

- Z. Zhang, M. Choi, G.E. Karniadakis. Anchor Points Matter in ANOVA Decomposition, *Spectral and High Order Methods for Partial Differential Equations, Lecture Notes in Computational Science and Engineering, 76, 347-355, 2011*

Acknowledgements

I would like to thank my advisor, Professor George EM Karniadakis, for his guidance, support, and patience during my PhD studies here at Brown. His motivation, curiosity and methodology has amazed me all the time and his insight and vision in physics have been vital to the completion of this thesis. I am truly grateful to the support, patience and opportunities he has provided. I would also like thank my collaborator, Professor Themistoklis Sapsis, for his support and guidance on the subject of this thesis. I wish to thank Professor Boris Rozovsky for being on my thesis committee, reading through my research, and providing useful feedback and suggestions.

I would like to acknowledge the funding support which made the research presented in this thesis possible: OSD/MURI (FA9550-09-1-0613), DOE (DE-SC0009247, DE-SC0002542), NSF/DMS (DMS-1216437, DMS-0915077), ONR (N00014-07-1-0446).

Of course, I would like to thank my family and friends, including my mom, dad, brother, sister, girlfriend, Korean friends, tennis friends, and all current and former graduate students for their support, patience and discussions, especially through the stresses of graduate school. They added balance to my graduate student life, without which my journey to a Ph.D. degree would not have been possible.

Abstract of "Time-dependent Karhunen-Loève type decomposition methods for SPDEs" by Minseok Choi, Ph.D., Brown University, May 2014

A new hybrid methodology for the stochastic partial differential equations (SPDEs) is developed based on the dynamically-orthogonal (DO) and bi-orthogonal (BO) expansions; both approaches are an extension of the Karhunen-Loève (KL) expansion. The original KL expansion provides a low-dimensional representation for square integrable random processes since it is optimal in the mean square sense. The solution to SPDEs is represented in a way that it follows the characteristics of KL expansion "on-the-fly" at any given time. To this end, both the spatial and stochastic basis in the representation are *time-dependent* unlike the traditional methods such as polynomial chaos (PC), where only one of them is time-dependent. In order to overcome the redundancy the DO imposes the dynamical constraints on the spatial basis [1] while the BO imposes the static constraints on the spatial and stochastic basis [2, 3]. We examine the relation of the BO and DO and prove theoretically and illustrate numerically their equivalence, in the sense that one method is an *exact reformulation* of the other. We show this by deriving an invertible and linear transformation matrix governed by a matrix differential equation that connects the BO and the DO. We also examine the pathology of the BO equations that occurs when there is an eigenvalue crossing leading to the numerical instability. On the other hand we observe that the DO suffers numerically when there is a high condition number of the covariance matrix for the stochastic basis. To this end, we propose a unified hybrid framework of the two methods by utilizing an invertible and linear transformation between them. We also present an adaptive algorithm to add or remove modes to better capture the transient behavior. Several numerical examples , linear and nonlinear, are presented to illustrate the DO and BO methods, their equivalence, and adaptive strategies. It is also shown numerically that two methods converge exponentially fast with respect to the number of modes giving the same

levels of accuracy, which is comparable with the PC method but with substantially smaller computational cost compared to stochastic collocation, especially when the involved parametric space is high-dimensional.

Contents

List of Tables

List of Figures

Chapter 1

Introduction

Recently, there has been a growing interest in quantifying parametric uncertainty in physical and engineering problems through the probabilistic framework. Such problems are often described by stochastic partial differential equations (SPDEs), and they arise in various fields such as fluid mechanics, solid mechanics, wave propagation through random media [4, 5, 6], random vibration [7, 8, 9], finance [10], etc. The source of stochasticity in all the above cases includes uncertainty in physical parameters, initial and/or boundary conditions, random excitations, etc. All these stochastic elements may be modeled as random processes or random variables. Several methods have been developed to study SPDEs, including Monte Carlo (MC) method and its variants and, more recently, generalized polynomial chaos (gPC), multi-element generalized polynomial chaos (ME-gPC), probabilistic collocation method (PCM) , multi-element probabilistic collocation method (ME-PCM) and many other variants (see e.g. [11, 12, 13, 14, 15, 16, 17, 18, 19, 20, 21] and references therein).

Another aspect in uncertainty quantification is order-reduction schemes or reduced-

order models (ROMs) for the simplification and analysis of high-dimensional complex systems across many physical and engineering disciplines. For many stochastic systems of practical interest, it has been known that the solution possess an inherent low-dimensional character. Many methods in ROMs have been developed in the context of deterministic framework such as proper orthogonal decomposition (POD) or principal component analysis (PCA) with applications to many disciplines such as turbulent fluid flows [22, 23], structural vibration [24, 25], image processing [26], signal processing, data compression to name a few. However, there have been a few researches on ROMs in the context of stochastic framework. To this end, we aim to address reduced-order modeling in the stochastic framework and provide the methodology and its numerical schemes in this thesis. Before introducing the methodology it is worth reviewing the stochastic spectral methods.

1.1 Stochastic spectral methods

The Polynomial Chaos (PC) method was developed in [27] in the context of the Wiener-Hermite polynomial chaos expansion. The stochastic processes are represented by a series of Hermite polynomials in terms of random variables, e.g. Brownian motion can be approximated by a series of Hermite polynomials in terms of standard Gaussian random variables [28]. A Galerkin projection of the governing equations to the subspace spanned by Hermite polynomials yields a set of deterministic equations. PC has been applied to many problems including structural mechanics [11, 29, 30], fluid mechanics [31, 32, 33, 34, 35], etc. The generalized polynomial chaos developed by [33, 16] employs non-Hermite polynomial or Askey-type orthogonal polynomial in terms of random vectors to improve efficiency for a wider class of nonlinear problems. Though gPC has been widely and successfully used

in the stochastic community, it suffers from the so-called *curse-of-dimensionality* as it requires the solution of a system of coupled deterministic problems for the gPC basis coefficients whose degree of freedom grows exponentially with respect to the dimension of parametric space and the polynomial order.

A computationally efficient version of PC is the probabilistic collocation method (PCM; also referred to as stochastic collocation (SC)) which uses collocation points based on numerical integration. The number of collocation points may grow exponentially with the dimensionality of parametric space if tensor product grids are used. In order to reduce the computational cost in multi-dimensional space the use of sparse grid quadrature, originally introduced by Smolyak [36], was proposed for stochastic collocation in [37]. It is known to weaken the curse of dimensionality for certain classes of function. The errors of sparse grid integration and interpolation have been investigated in [38, 39, 40, 41]. Sparse grid stochastic collocation has been introduced in [15] and analyzed a linear elliptic PDE with random input with low to moderate dimensions in [42], which exhibits fast convergence rates with increasing order of the expansions, provided that solutions are sufficiently smooth in the parametric space. Several variants of sparse collocation methods including anisotropic sparse grids [43] have been developed to further improve the efficiency.

Despite the significant improvements in the efficiency of the sparse grid stochastic collocation method, high-dimensional representations in the parametric space makes such simulations computationally prohibitive as the sparse grid still depends on the dimension and the regularity of the function. To this end, the ANOVA (Analysis-of-Variance) decomposition, introduced by Fisher in 1921 [44] and employed for studying U-statistics by Hoeffding in 1945 [45], have been employed to in the context of uncertainty quantification in [46, 47]. ANOVA decomposes a multi-dimensional function into a series of low-dimensional functions. It has been known

in many physical problems that high-dimensional functions often have the major contribution only from the interaction of low-dimensional functions. Therefore, by truncating the ANOVA decomposition at a low dimension we deal with a series of low-dimensional problems in lieu of one high-dimensional problem that makes high-dimensional problems computationally tractable. To this end, MEPCM-ANOVA was introduced in [48] to represent each term for greater control of accuracy and efficiency of the discrete representation. Adaptive ANOVA decomposition to further reduce the computational cost was introduced in [49] for stochastic incompressible and compressible flows with nominal dimension of parametric space up to 100.

1.2 The class of time-dependent Karhunen-Loève (KL) type methods for SPDEs

Order-reduction schemes or reduced-order models (ROMs) have been a popular approach for the simplification and analysis of high-dimensional complex systems across many scientific and engineering disciplines. For example, the stochastic framework in the analysis of fluid flows has been proven beneficial for the description of the dynamics, energy interactions, and bifurcations in unstable fluid flows [50, 51, 52, 53], for the uncertainty quantification in CFD computations [34, 54, 55, 56], as well as for the development of filtering methods for turbulent systems [57, 58, 59, 60].

The Karhunen-Loève (KL) expansion provides a low-dimensional representation for square integrable random processes as it is optimal in the mean square sense. It has been widely used in the context of the deterministic problems under the name of POD or PCA or SVD. In the stochastic framework, the KL expansion has been used mainly to represent the random processes of the input parameter with the

solution or quantity of interest being often represented as gPC basis or to find a low-dimensional structure of the solution in the post-processing as it often requires to solve a large-scale eigenvalue problem.

Schemes based on ROMs are essentially relying on the projection of the original system into a 'suitable' set of modes representing important and essential components of the dynamics. This projection can be performed either with respect to a spatially-dependent basis or with respect to a stochastically-dependent basis. For both cases, various approaches and rules have been developed for the choice, computation, or improvement of these basis elements.

For the first family of methods (spatially-dependent basis) some of the most popular methods for the basis selection include empirical criteria such as energy-based proper orthogonal decomposition (POD) (see for example [23, 22]) or more recently linear-operator-theoretic model reduction methods, such as the balanced POD [61, 62]. While these have time-independent basis, a new reduced-order modeling based on approximated Lax pairs was proposed in [63] for deterministic PDEs where the basis evolves in time with applications to progressive waves or front propagation. For the second family of methods (projection to a stochastic basis) one of the most popular approaches is the Gaussian closure (assumption that the solution has a Gaussian stochastic structure) which, however, has limited applicability for problems where the non-Gaussian character is inevitable. For this case the employment of a polynomial chaos basis and its variants may provide for many cases a reliable computational scheme [11, 16, 33, 15, 64, 42, 17].

Despite the success of these methods in many problems of practical interest there are important limitations associated with them. On the one hand, methods relying on the selection of a spatial basis present important limitations in problems with

strongly time-dependent character where the basis employed may become irrelevant as time evolves. Typical examples of problems belonging to this category are transient fluid flows even with a very small number of instabilities (See Appendix in [65]). On the other hand, methods relying on a pre-selected stochastic structure suffer from important limitations especially in problems with highly non-Gaussian structure or with strongly transient stochastic characteristics.

Motivated by these limitations an alternative approach for the solution of stochastic systems that tracks the KL representation at a given time according to the evolution equations was proposed in [1]. The new method adopts a redundant representation where both the spatial and stochastic basis evolve in time unlike the traditional methods such as gPC and POD. By imposing the *dynamical constraints* on the spatial basis, called the *dynamical orthogonality (DO) condition*, the authors were able to derive the DO evolution equations for all the components involved - mean, the spatial basis and stochastic basis. These equations (DO evolution equations) consist of a deterministic PDE describing the evolution of the mean field, a set of deterministic PDEs describing the evolution of the spatiotemporally-dependent deterministic basis, and a set of stochastic differential equations describing the evolution of the stochastic basis. The DO equations under appropriate constraints reproduce both the POD equations and the polynomial chaos equations. Adaptive strategies for the addition and removal of basis elements based on the dynamical theory on the instantaneous energy of the existing DO modes were presented in [66].

Recently, [2, 67] and independently developed by the author [3] adopted the same redundant representation used in [1]. By imposing static constraints on both the spatial and the stochastic basis, called the *bi-orthogonal (BO) condition*, an independent set of equations describing the evolution of all the quantities involved (DyBO or BO equations) was obtained. Although in both works the same projections

were employed (with respect to physical and stochastic space) the equations rely on different conditions imposed to the representation.

These two methods follow a low-dimensional structure of the solution by tracking the KL expansion of the solution at any given time on-the-fly. By imposing the *dynamical constraints* on the spatial basis in the DO and imposing the *static constraints* on both the spatial and stochastic basis in the BO, evolution equations for all components involved can be obtained. These are classes of time-dependent KL (tKL) type evolution equations for SPDEs. In this thesis, we aim to establish the relations between the two methods and integrate these methods in a unified framework. In addition, we examine the numerical aspects for these methods such as the exponential convergence with respect to the number of modes, computational complexity, adaptive strategies, etc.

1.3 Objectives and Organization of the thesis

In Chapter 2 we overview some preliminaries and background on stochastic spectral methods. We introduce generalized Polynomial Chaos expansion. The Galerkin and collocation methods are presented. The KL expansion is introduced and the use of gPC in stochastic problem is formulated.

In Chapter 3 we present the dynamically orthogonal (DO) and bi-orthogonal (BO) methods, which are two classes of time-dependent KL type methods for SPDEs. In both methods, the spatial basis as well as stochastic basis are time-dependent. In order to overcome the redundancy the DO imposes the dynamical constraints on the spatial basis while the BO imposes the static constraints on both the spatial and

stochastic basis. The evolution equations consist of a system of deterministic PDEs for the mean and spatial basis and a system of stochastic ODEs for the stochastic basis.

In Chapter 4 we establish the relation between the BO and DO via an orthogonal matrix governed by an orthogonal matrix differential equation and show that they are equivalent to each other in a sense that one can be derived from the other and vice versa. We also show that the evolution equations for one can be transformed into the evolution equations for the other via the relation between them.

In Chapter 5 we provide all necessary material for the numerical implementation for these methods. We introduce how to represent the stochastic basis using gPC or PCM. When the system has deterministic initial conditions as it is often the case in practice, a singularity arises. In order to overcome such singularity we present the hybrid method of gPC and BO or DO. We also develop adaptive strategies; i) hybrid BO-DO and ii) adaptively adding and removing modes to the system. In the hybrid BO-DO we switch from BO to DO when there is an eigenvalue crossing or switch from DO to BO when there is a zero eigenvalue. We adaptively add and remove modes when the smallest eigenvalues become larger than threshold or smaller than threshold, respectively.

In Chapter 6 and Chapter 7 we present two main examples - stochastic advection and Burgers problem to illustrate the DO and BO methods, hybrid gPC-tKL, and adaptive strategies. We document that both methods give the same accuracy as suggested by the Theorem on the equivalence of two methods. We present convergence properties of the DO and BO in comparison with the PC method, where the DO and BO methods converge exponentially fast with respect to the number of modes (for the problems considered). They also give the same levels of computational

accuracy comparable with the PC method but (in many cases) with substantially smaller computational cost compared to stochastic collocation, especially when the involved parametric space is high-dimensional. We illustrate the adaptive strategies introduced in Chapter 5 with several examples.

Chapter 2

Stochastic Spectral Expansions

In this chapter we briefly discuss the spectral methods for the stochastic processes and how they are used to solve the stochastic partial differential equations (SPDEs). Many more details can be found in [11, 68, 16, 33, 15]. In addition, we discuss the general model problem and assumptions for which methods in this paper are applicable. A brief introduction of notations is first provided. Let $(\Omega, \mathcal{A}, P)$ be a complete probability space, where Ω is the sample space, P is the probability measure, and $\mathcal{A}$ is the σ-algebra of P-measurable sets and $\mathcal{D} \subset \mathbb{R}^n, n = 1, 2, 3$ and $\partial\mathcal{D}$ be the physical domain and boundary of the domain, respectively. We denote $L_2(\Omega, P)$ the space of second-order random variables defined on $(\Omega, \mathcal{A}, P)$ equipped with the inner product $(\cdot, \cdot)$ and associated norm $\|\cdot\|_\Omega$:

$$\begin{aligned} (U, V) &\equiv \int_\Omega U(\omega)V(\omega)dP(\omega), \quad U, V \in L_2(\Omega, P) \\ \|U\|_\Omega^2 &\equiv (U, U), \quad U \in L_2(\Omega, P) \end{aligned}$$

Let us consider a real-valued stochastic process, indexed by $\mathbf{x} \in \mathcal{D} \subset \mathbb{R}^n$:

$$U : (\mathbf{x}, \omega) \in \mathcal{D} \times \Omega \mapsto U(\mathbf{x}, \omega) \in \mathbb{R}$$

where for a fixed $\mathbf{x}$, the function $U(\mathbf{x}, \cdot)$ is a random variable while for a fixed ω, the function $U(\cdot, \omega)$ is a realization of the stochastic processes. We will consider the second-order stochastic process, i.e. $U(\mathbf{x}, \omega) \in L_2(\Omega, P)$. We will also assume that the realizations $U(\cdot, \omega)$ are almost surely in the Hilbert space $L_2(\mathcal{D})$ equipped with the inner product $\langle \cdot, \cdot \rangle$ and associated norm $\| \cdot \|_{\mathcal{D}}$:

$$\begin{aligned} \langle u, v \rangle &\equiv \int_{\mathcal{D}} u(x)v(x)dx, \quad u, v \in L_2(\mathcal{D}) \\ \|u\|_{\mathcal{D}}^2 &\equiv \langle u, u \rangle, \quad u \in L_2(\mathcal{D}). \end{aligned}$$

2.1 Generalized Polynomial Chaos (gPC) Expansion

The original polynomial chaos was first proposed by Wiener where Hermite polynomials in terms of Gaussian random variables was used as a basis. The idea was then generalized to the Askey polynomial scheme associated with non-Gaussian random variables by Xiu & Karniadakis in [16]. Any second-order stochastic process

$X(\omega) \in L_2(\Omega, P)$ can be written as a series expansion of gPC basis functions:

$$\begin{aligned} X(\omega) &= a_0\Phi_0 \\ &\quad + \sum_{i_1=1}^{\infty} a_{i_1}\Phi_1(\xi_{i_1}(\omega)) \\ &\quad + \sum_{i_1=1}^{\infty}\sum_{i_2=1}^{i_1} a_{i_1 i_2}\Phi_2(\xi_{i_1}(\omega), \xi_{i_2}(\omega)) \\ &\quad + \cdots \end{aligned}$$

where $\Phi_n(\xi_{i_1}(\omega), \xi_{i_2}(\omega), ..., \xi_{i_n}(\omega))$ denotes the polynomial chaos basis function of order n in terms of the random vector $\boldsymbol{\xi} = (\xi_{i_1}(\omega), \xi_{i_2}(\omega), ..., \xi_{i_n}(\omega))$. The theorem of Cameron and Martin [69] guarantees that such expansions converge under the L_2 norm. We will adopt a condensed notation:

$$X(\omega) = \sum_{j=0}^{\infty} b_j \Psi_j(\boldsymbol{\xi}), \tag{2.4}$$

where there is a one-to-one correspondence between $\Phi_n(\xi_{i_1}(\omega), \xi_{i_2}(\omega), ..., \xi_{i_n}(\omega))$ and $\Psi_j(\boldsymbol{\xi})$. The polynomial chaos basis satisfy the orthogonality condition with respect to the probability measure P:

$$E[\Psi_i \Psi_j] \equiv (\Psi_i, \Psi_j) = \|\Psi_i\|_{\Omega}^2 \delta_{ij}, \tag{2.5}$$

where the expectation operator $E[\cdot]$ is defined as $E[X] = \int_{\Omega} X(\omega) dP(\omega)$. The probability density function (PDF) of the random variables $\boldsymbol{\xi}$ determines the polynomials $\{\Psi_i\}$ where the weight function of orthogonal polynomials is closely related to the PDF. The correspondence between PDFs and classical polynomials can be found in [16]. Wan & Karniadakis [64] extended gPC associated with well-known PDFs to gPC associated with arbitrary PDFs by numerically constructing the gPC basis whose weight function matches the arbitrary PDFs.

2.2 Karhunen-Loève Expansion

The Karhunen-Loève (KL) expansion [70] is widely used in many disciplines including signal analysis, physics, mechanics to name a few. It is also known as proper orthogonal decomposition (POD) or principal component analysis (PCA) depending on the field. This will play an important role in establishing numerical methods for the SPDEs.

Consider a second-order stochastic process $U \in L_2(\mathcal{D} \times \Omega)$ for bounded $\mathcal{D}$ and assume that U is continuous in the mean-square sense:

$$\lim_{\mathbf{y} \to \mathbf{x}} \|U(\mathbf{y}, \cdot) - U(\mathbf{x}, \cdot)\|_{\Omega}^2 = 0 \quad \forall \mathbf{x} \in \mathcal{D}.$$

The bilinear form of the covariance operator denoted by $C_U : \mathcal{D} \times \mathcal{D} \to \mathbb{R}$ has a form:

$$C_U(\mathbf{x}, \mathbf{y}) = E[(U(\mathbf{x}, \omega) - E[U](\mathbf{x}))(U(\mathbf{y}, \omega) - E[U](\mathbf{y}))], \quad \forall \mathbf{x}, \mathbf{y} \in \mathcal{D} \tag{2.6}$$

and it can be shown that the C_U is continuous on $\mathcal{D} \times \mathcal{D}$ and

$$\int_{\mathcal{D}} \int_{\mathcal{D}} C_U(\mathbf{x}, \mathbf{y}) d\mathbf{x} d\mathbf{y} < \infty. \tag{2.7}$$

Hence, the inner operator defined by

$$\langle Kf, g \rangle = \int_{\mathcal{D}} \int_{\mathcal{D}} C_U(\mathbf{x}, \mathbf{y}) f(\mathbf{x}) g(\mathbf{y}) d\mathbf{x} d\mathbf{y}, \tag{2.8}$$

is a symmetric semi-positive Hilbert-Schmidt operator on $\mathcal{H} = L_2(\mathcal{D}, \mathbb{R})$ equipped with the inner product $(\cdot, \cdot)$ where K is called the correlation kernel. We then have

the following results [70]:

- there exists a set of eigenvalues and eigenfunctions $\{\lambda_i, \phi_i\}$ of the following eigenvalue problem

$$\int_{\mathcal{D}} C_U(\mathbf{x}, \mathbf{y})\phi_i(\mathbf{x})d\mathbf{x} = \lambda_i\phi_i(\mathbf{y}), \mathbf{y} \in \mathcal{D}; \tag{2.9}$$

- eigenvalues λ_i are real and non-negative and arranged in decreasing order

$$\lambda_1 \geq \lambda_2 \geq \lambda_3 \geq \cdots ;$$

- the set of eigenfunctions $\{\phi_i\}$ consists of an orthonormal basis of $\mathcal{H}$, i.e. $\langle \phi_i, \phi_j \rangle = \delta_{ij}$.

The KL expansion of the stochastic process U admits

$$U(\mathbf{x}, \omega) = E[U](\mathbf{x}) + \sum_{i \geq 1} \sqrt{\lambda_i}\phi_i(\omega)\eta_i(\omega), \tag{2.10}$$

where the random variable $\eta_i(\omega)$ are given by

$$\eta_i(\omega) = \frac{1}{\sqrt{\lambda_i}} \langle U(\mathbf{x}, \omega) - E[U](\mathbf{x}), \phi_i(\mathbf{x}) \rangle . \tag{2.11}$$

It can be easily shown that the random variables $\{\eta_i\}$ have zero mean and mutually uncorrelated, i.e. $E[\eta_i] = 0, E[\eta_i\eta_j] = \delta_{ij}$.

The KL is widely used in many disciplines as mentioned above because the KL expansion is optimal in the mean square sense. Indeed, when we have a truncation of the KL expansion up to the first N terms denoted by $U_N = \sum_{i=1}^{N} \sqrt{\lambda_i}\phi_i(\omega)\eta_i(\omega)$

where we assume, without loss of generality, $E[U] = 0$ and the eigenvalues are arranged in decreasing order, i.e. $\lambda_1 \geq \lambda_2 \geq \lambda_3 \cdots$, the truncated KL expansion U_N minimizes the mean square error:

$$\begin{aligned} \epsilon_N^2 &\equiv E\left[\|U(\mathbf{x},\cdot) - U_N(\mathbf{x},\cdot)\|_{\mathcal{D}}^2\right] \\ &= \sum_{i,j>N} \sqrt{\lambda_i \lambda_j}\, \langle \phi_i, \phi_j \rangle\, E[\eta_i \eta_j] \\ &= \sum_{i,j>N} \sqrt{\lambda_i \lambda_j}\, \delta_{ij} \delta_{ij} \\ &= \sum_{i>N} \lambda_i. \end{aligned}$$

This implies that no other approximation of U in a series of N terms can give a better approximation with a mean square error.

2.3 gPC and KL in stochastic problem

In this section we briefly overview how gPC and KL are applied to the stochastic problems such as stochastic ordinary differential equations (SODEs) or stochastic partial differential equations. We consider the following stochastic problem: find $u : \bar{\mathcal{D}} \times \Omega \to \mathbb{R}$ such that P-almost everywhere (a.e.) in Ω the following equation holds:

$$\mathcal{L}(\mathbf{x}, \omega; u) = f(\mathbf{x}, \omega), \quad \mathbf{x} \in \mathcal{D}, \tag{2.13a}$$

$$\mathcal{B}(\mathbf{x}; u) = g(\mathbf{x}), \quad \mathbf{x} \in \partial\mathcal{D}. \tag{2.13b}$$

We assume that f and g have sufficient regularity so that the problem is well-posed P-a.e. We also assume that the random dependence of operators $\mathcal{L}$ and f satisfy

a few properties. The first requirement referred to as a *finite dimensional noise assumption* [15, 18] is that the random input can be represented by a finite set of random variables $\{Y_1(\omega), Y_2(\omega), ..., Y_N(\omega)\}$ with a known joint density function $\rho(\mathbf{Y})$. The problem (2.13) then can be restated as follows: find $u : \bar{\mathcal{D}} \times \Omega \to \mathbb{R}$ such that

$$\mathcal{L}(\mathbf{x}, Y_1(\omega), ..., Y_N(\omega); u) = f(\mathbf{x}, Y_1(\omega), ..., Y_N(\omega))$$

holds for every $\mathbf{x} \in \mathcal{D}$ and for P-a.e. $\omega \in \Omega$. The Doob-Dynkin Lemma [71] guarantees that the solution $u(\mathbf{x}, \omega)$ can be written as $u(\mathbf{x}, \mathbf{Y}(\omega))$ with $\mathbf{Y} = (Y_1, Y_2, ..., Y_N)$. Then, the problem may be recast from the space Ω into the range space of the N random variables $(Y_1, ..., Y_N)$ with the joint probability density function of Y as follows:

$$\mathcal{L}(\mathbf{x}, \mathbf{y}; u) = f(\mathbf{x}, \mathbf{y}), \quad \mathbf{x} \in \mathcal{D}, \tag{2.14a}$$

$$\mathcal{B}(\mathbf{x}; u) = g(\mathbf{x}), \quad \mathbf{x} \in \partial\mathcal{D}, \tag{2.14b}$$

where $\mathbf{y} = (y_1, y_2, ..., y_N) \in \Gamma \equiv \prod_{i=1}^{N} \Gamma_i$, and Γ_i is the image of $Y_i(\Omega), i = 1, ..., N$.

2.3.1 gPC: Galerkin projection

With the assumptions made in the above subsection, we have corresponding orthogonal polynomials $\Psi(\mathbf{Y})$ associated with the joint probability density function $\rho(\mathbf{Y})$. Then we seek in a series of polynomial basis the solution that is a spatial random process:

$$u(\mathbf{x}, \omega) = \sum_{j=0}^{M} \hat{u}_j(\mathbf{x}) \Psi_j(\mathbf{Y}), \tag{2.15}$$

where $M+1$ is the number of terms in the truncated expansion and is a function of the number of random dimensions N and the maximum polynomial order p by

$$M(p,N) = \frac{(N+p)!}{N!p!} - 1. \tag{2.16}$$

We then substitute gPC expansions (2.15) into equation (2.14a) and perform a Galerkin projection onto each basis function Ψ_i:

$$E\left[\mathcal{L}\left(\mathbf{x},\mathbf{y};\sum_{j=0}^{M}\hat{u}_j(\mathbf{x})\Psi_j(\mathbf{Y})\right)\Psi_i\right] = E[f\Psi_i], \quad i=0,...,M. \tag{2.17}$$

We obtain a system of $M+1$ deterministic equations for the gPC coefficients $\hat{u}_j$ to be solved. This system is usually coupled unless the system is linear. In order to solve these deterministic coupled equations any standard numerical method can be employed.

The moments can be easily computed using the orthogonality condition of the gPC basis once the coefficients $\hat{u}_i, i=0,...,M$ are obtained. For example, the first and second moment of the solution u is

$$E[u](\mathbf{x}) = \hat{u}_0 \tag{2.18a}$$

$$E[u^2](\mathbf{x}) = \sum_{i=0}^{M}\hat{u}_i^2(\mathbf{x})E[\Psi_i^2]. \tag{2.18b}$$

It has been shown that the stochastic Galerkin projection method based on gPC basis shows the spectral convergence provided that the gPC basis is chosen accordingly [16, 33]. On the other hand, it suffers the long time integration and multi-element Galerkin method like *h-type finite element* was proposed to overcome [64]. There are also many variations of the stochastic Galerkin method in the literature,

including a multi-resolution formulation based on multi-wavelet basis [72].

2.3.2 gPC: collocation projection

While the stochastic Galerkin projection method is spectrally convergent with the right choice of gPC basis, it can be computationally prohibitive in particular when the number of terms M is high due to either high dimensional parametric space or large polynomial order because of the coupled nature of the system of deterministic equations. The collocation projection method may be useful in this case. In this method, a set of M collocation points and corresponding weights $\{y_i, w_i\}_{i=1}^{M}$ is defined on the space Γ. Then, collocation projections are defined with the measure being Dirac delta centered at each collocation points and performed on both sides of the model problem (2.14a) obtaining:

$$\mathcal{L}(\mathbf{x}, y_i; u) = f(\mathbf{x}, y_i), \quad i = 1, ..., M. \tag{2.19}$$

Then we have M uncoupled deterministic equations, and equation (2.19) can be solved using any existing deterministic numerical solver and can be easily parallelized since they are uncoupled. The solution u then can be approximated via interpolation on the $\{y_i\}$. The moments can be easily computed through numerical integration based on the collocation points and corresponding weights, e.g. the first and second moments are:

$$\begin{aligned} E[u](\mathbf{x}) &= \sum_{i=1}^{M} u(\mathbf{x}, y_i) w_i \\ E[u^2](\mathbf{x}) &= \sum_{i=1}^{M} u^2(\mathbf{x}, y_i) w_i. \end{aligned}$$

The collocation projection allows to use the existing deterministic solver but it may still suffer the curse-of-dimensionality when the parametric space is high-dimensional. The sparse grids has been proposed in [36] to reduce the number of points in multi-dimensional parametric space while keeping accuracy and been widely used in the stochastic problem [38, 39, 40]. The counterpart of multi-element gPC in the collocation projection method called ME-PCM has been proposed in [48] and successfully applied to mid-dimensional parametric space.

Chapter 3

Dynamically-orthogonal and Bi-orthogonal Method

3.1 Introduction

In this chapter we introduce time-dependent KL type decomposition methods to solve SPDEs - dynamically orthogonal (DO) and bi-orthogonal (BO) method [1, 2]. While the traditional methods such as gPC and proper orthogonal decomposition (POD) to solve SPDEs have time-independent basis in either parametric or physical space and evolution equations for the corresponding coefficients, the DO and BO have time-dependent basis for both physical and parametric space. It achieves the characteristics of the KL expansion for every time t and hence follows the intrinsic low-dimensional structure of the system *on-the-fly*. Since the spatial and stochastic basis are time-dependent, there exists redundancy in the equations. In order to overcome this redundancy the DO imposes the *dynamical constraints* on the spatial

basis while the BO imposes the *static constraints* on both the spatial and stochastic basis, which will be described in more detail in the following sections.

3.2 Model Problem

We consider the following stochastic partial differential equations

$$\frac{\partial u}{\partial t} = \mathcal{L}(u(t,x;\omega)), \quad x \in D, \omega \in \Omega \tag{3.1a}$$

$$u(t_0,x;\omega) = u_0(x;\omega), \quad x \in D, \omega \in \Omega \tag{3.1b}$$

$$\mathcal{B}[u(t,x;\omega)] = h(t,x;\omega), \quad x \in \partial D, \omega \in \Omega, \tag{3.1c}$$

where $\mathcal{L}$ is a differential operator and $\mathcal{B}$ is a linear differential operator. D is a bounded domain in $\mathcal{R}^d$ where $d = 1, 2$, or 3. We assume that the problem is well-posed such that the set of solution $u(x,t;\omega)$ forms a Hilbert space $\mathcal{H} \equiv L_2(\mathcal{D} \times \Omega)$ for every t. The randomness may come from different sources including parameter, initial condition and boundary condition.

A new approach, called dynamically orthogonal (DO) method, was developed in [1]; the idea is to represent the solution in a more general expansion, i.e.,

$$u(x,t;\omega) = \bar{u}(x,t) + \sum_{i=1}^{N} u_i(x,t) Y_i(t;\omega) \tag{3.2}$$

where u_i and Y_i for $i = 1, ..., N$ are the spatial and stochastic basis, respectively. Note that both the spatial and stochastic basis are time-dependent while the traditional methods have only one of them time-dependent. The time-dependence on *both* the spatial and stochastic basis makes the above representation very flexible for the

representation of strongly transient, non-stationary responses. However, this same property makes the representation redundant and the derivation of well-posed equations for all the quantities involved is not a straightforward problem. In addition, we require that, at a given time t, the spatial and stochastic basis has the similar properties to what the KL expansion do. The questions arise that there exists such representation and if there exists, then how the all components $\bar{u}, \{u_i, Y_i\}_{i=1}^N$ evolve in time. In the following sections we seek the answers to these questions.

3.3 Dynamically orthogonal (DO) method

Using a time-dependent generalization of the KL expansion [1], we have that every random field $u(x,t;\omega) \in \mathcal{H}$ at a given time t can be approximated by a finite series of the form

$$u(x,t;\omega) = \bar{u}(x,t) + \sum_{i=1}^{N} u_i(x,t) Y_i(t;\omega) = \bar{u}(x,t) + \mathbf{U}(x,t)\mathbf{Y}^T(t;\omega), \tag{3.3}$$

where $\mathbf{U} = (u_1, ..., u_N), \mathbf{Y} = (Y_1, ..., Y_N)$, $u_i(x,t)$ are the spatial basis, and $Y_i(t;\omega)$ are zero-mean stochastic basis whose variance $E[\mathbf{Y}^T\mathbf{Y}]$ is equal to the corresponding eigenvalue $\lambda_i(t)$ of the eigenvalue problem of the KL expansion:

$$\int_D C_u(x,y) u_i(x,t) dx = \lambda_i(t) u_i(y,t), \quad y \in D, \tag{3.4}$$

where $C_u(x,y)$ is the covariance kernel defined in Equation (2.6). We define the linear subspace $V_S = span\{u_i(x,t)\}_{i=1}^N$ spanned by the N eigenfunctions associated with the N largest eigenvalues. Note that both the stochastic basis $Y_i(t;\omega)$ and the spatial basis $u_i(x,t)$ are time-dependent (and they are evolving according to the system dynamics) unlike other methods such as the standard PC where the

stochastic basis or gPC basis are time-independent. In [73], a similar expansion with time evolving PC basis is presented but the time-dependent basis is obtained according to the PDF of the solution; in DO it is obtained through an evolution equation.

All quantities $\bar{u}(x,t), u_i(x,t), Y_i(t;\omega), i = 1,...,N$ in the representation (3.3) are time-dependent and hence there exists some redundancy in the representation. Therefore, additional constraints need to be imposed in order to formulate a well posed problem for the unknown quantities. As first proposed in [1], we impose *dynamical constraints* on the spatial basis; the evolution of the spatial basis $\{u_i(x,t)\}_{i=1}^N$ be *normal* to the space V_S. This can be expressed through the following condition:

$$\frac{dV_S}{dt} \perp V_S \Leftrightarrow \left\langle \frac{\partial u_i(x,t)}{\partial t}, u_j(x,t) \right\rangle = 0 \quad i,j = 1,...,N. \tag{3.5}$$

This condition is referred to as the *dynamically orthogonal (DO) condition*. Note that the DO condition preserves orthonormality of the spatial basis since

$$\frac{\partial}{\partial t} < u_i(\cdot,t), u_j(\cdot,t) >=< \frac{\partial u_i(\cdot,t)}{\partial t}, u_j(\cdot,t) > + < u_i(\cdot,t), \frac{\partial u_j(\cdot,t)}{\partial t} >= 0, \quad i,j = 1,...,N.$$

We can derive the evolution equations for all components by projecting the operator for the SPDE on the spatial and stochastic basis. First we insert the DO representation into the SPDE (3.1a) to obtain

$$\frac{\partial \bar{u}}{\partial t} + \sum_{i=1}^{N} \frac{dY_i}{dt} u_i + \sum_{i=1}^{N} Y_i \frac{\partial u_i}{\partial t} = \mathcal{L}[u]. \tag{3.6}$$

By applying the expectation operator on both sides we obtain the evolution equation

for the mean:

$$\frac{\partial \bar{u}}{\partial t} = E[\mathcal{L}[u]] \tag{3.7}$$

where we used $E[Y_i] = 0, i = 1, ..., N$. By projecting Equation (3.6) on the spatial basis we have

$$\left\langle \frac{\partial \bar{u}}{\partial t}, u_j \right\rangle + \sum_{i=1}^{N} \langle u_i, u_j \rangle \frac{dY_i}{dt} + \sum_{i=1}^{N} Y_i \left\langle \frac{\partial u_i}{\partial t}, u_j \right\rangle = \langle \mathcal{L}[u], u_j \rangle , \quad j = 1, ..., N$$

By utilizing the DO condition and the evolution equation for the mean we obtain the evolution equations for the stochastic basis:

$$\frac{dY_j}{dt} = \left\langle \tilde{\mathcal{L}}[u], u_j \right\rangle , \quad j = 1, ..., N \tag{3.8}$$

where $\tilde{\mathcal{L}}[u] \equiv \mathcal{L}[u] - E[\mathcal{L}[u]]$. Note that $E[\tilde{\mathcal{L}}[u]] = E[\mathcal{L}[u]] - E[E[\mathcal{L}[u]]] = 0$ and $E[\tilde{\mathcal{L}}[u]Y_i] = E[\mathcal{L}[u]Y_i]$ using the linearity of the expectation and mean-zero property of the stochastic basis. We multiply Equation (3.6) with Y_j and apply the expectation operator to get

$$\sum_{i=1}^{N} E\left[\frac{dY_i}{dt} Y_j\right] u_i + \sum_{i=1}^{N} C_{ij} \frac{\partial u_i}{\partial t} = E[\mathcal{L}[u]Y_j] \tag{3.9}$$

where $C_{ij} \equiv E[Y_i Y_j]$ is the covariance matrix of the stochastic basis and we used the fact that the stochastic basis have mean zero. By putting Equation (3.8) into the above equation and using the interchangeability of the inner product on the physical and stochastic domain, we have

$$\sum_{i=1}^{N} \langle E[\mathcal{L}[u]Y_j], u_i \rangle u_i + \sum_{i=1}^{N} C_{ij} \frac{\partial u_i}{\partial t} = E[\mathcal{L}[u]Y_j] \tag{3.10}$$

from which we obtain the evolution equations for the spatial basis:

$$\begin{aligned}\sum_{i=1}^{N} C_{ij}\frac{\partial u_i}{\partial t} &= E[\mathcal{L}[u]Y_j] - \sum_{i=1}^{N}\langle E[\mathcal{L}[u]Y_j], u_i\rangle\, u_i \\ &= \prod_{V_s^{\perp}} E[\mathcal{L}[u]Y_j] \end{aligned} \tag{3.11}$$

where the projection in the orthogonal complement of the linear subspace is defined as $\prod_{V_S^{\perp}} F(x) = F(x) - \prod_{V_S} F(x) = F(x) - \sum_{k=1}^{N}\langle F, u_k\rangle\, u_k$.

For simplicity we introduce the vector and matrix notation. Denote the vector of spatial and stochastic basis by $\mathbf{U} = (u_1, ..., u_N)$ and $\mathbf{Y} = (Y_1, ..., Y_N)$, respectively. The evolution equations for each component involve the projection of the differential operator on the spatial and stochastic basis. We define the following quantities:

$$\Lambda = diag(\lambda_1, ..., \lambda_N) \tag{3.12a}$$

$$C_{ij} = E[Y_i Y_j] \tag{3.12b}$$

$$G_{ij} = < E[\mathcal{L}[u]Y_j], u_i > \tag{3.12c}$$

$$h_j = < \tilde{\mathcal{L}}[u], u_j > \tag{3.12d}$$

$$p_j = E[\mathcal{L}[u]Y_j]. \tag{3.12e}$$

Now we have the following theorem for the evolution equations for all DO components [1]:

Theorem 1. *Under the assumptions of the DO representation, the original SPDE*

(3.1a)-(3.1c) is reduced to the following system of equations

$$\begin{aligned} \frac{\partial \bar{u}(x,t)}{\partial t} &= E[\mathcal{L}[u(x,t;\omega)]], && \text{(3.13a)} \\ \frac{d\mathbf{Y}(t;\omega)}{dt} &= \left\langle \tilde{\mathcal{L}}(\cdot,t;\omega), \mathbf{U}(\cdot,t) \right\rangle && \text{(3.13b)} \\ \frac{\partial \mathbf{U}(t,x)}{\partial t} C &= \mathbf{p} - \mathbf{U}G && \text{(3.13c)} \end{aligned}$$

The associated boundary conditions have the form

$$\begin{aligned} \mathcal{B}[\bar{u}(\xi,t;\omega)]|_{\xi\in\partial D} &= E[h(\xi,t;\omega)], \\ \mathcal{B}[u_i(\xi,t)]|_{\xi\in\partial D} &= E[Y_j(t;\omega)h(\xi,t;\omega)]C^{-1}_{Y_i(t)Y_j(t)}, \end{aligned}$$

and the initial conditions for the DO components are given by

$$\begin{aligned} \bar{u}(x,t_0) &= E[u_0(x;\omega)], \\ Y_i(t_0;\omega) &= < u_0(\cdot,\omega) - \bar{u}(x,t_0), v_i(\cdot) >, \\ u_i(x,t_0) &= v_i(x), \end{aligned}$$

for all $i = 1, ..., n$, where $v_i(x)$ are the eigenfields of the covariance operator $C_{u(\cdot,t_0)}$ defined by the following eigenvalue problem for $t = t_0$:

$$\int_D C_{u(\cdot,t_0)}(x,y)v_i(x)dx = \lambda_i(t)v_i(y), \quad y \in D. \tag{3.14}$$

Remark 1. *It is shown in [1] that by imposing suitable restrictions on the DO representation the equations for methods such as Polynomial Chaos or Proper Orthogonal Decomposition (POD) can be recovered from the DO evolution equations. For example, PC can be recovered by setting $Y_i(t;\omega) = \Psi_i(\xi(\omega))$, where $\Psi_i(\xi)$ is an orthogonal polynomial in terms of ξ.*

Remark 2. *From the DO representation, the moments can be readily computed. For example, the first moment, i.e., the mean, appears in the DO representation as* $\bar{u}(x,t)$ *while the variance is directly computed as follows:*

$$\begin{aligned} Var[u] &= E[(u-\bar{u})^2] \\ &= E\left[\left(\sum_{i=1}^{N} u_i Y_i\right)^2\right] \\ &= \sum_{i,j=1}^{N} u_i E[Y_i Y_j] u_j \\ &= \mathbf{U} C \mathbf{U}^T. \end{aligned}$$

As the DO representation at any fixed time t can be seen as the KL decomposition, there is a relationship between the eigenpairs for the covariance matrix of $Y_i(t;\omega), i = 1, ..., N$ and the eigenpairs for the covariance operator of $u(x,t;\omega)$. For the covariance matrix C whose (i,j)-th element is $C_{ij} = C_{Y_i(t)Y_j(t)}$, we have a set of eigenvalues and eigenvectors that satisfies the following eigenvalue problem

$$C(t)\phi_k(t) = \rho_k \phi_k(t), k = 1, ..., N, \tag{3.15}$$

where $\phi_k(t) = (\phi_{k1}(t), \cdots, \phi_{kN}(t))^T$. Similarly, for the covariance operator for $u(x,t;\omega)$, there exists a set of eigenvalues and eigenfields for $C_u(x,y)$ through the Karhunen-Loeve decomposition such that

$$\int_D C_u(x,y) v_k(x,t) dx = \lambda_k v_k(y,t), \tag{3.16}$$

where $C_u(x,y) = E[(u(x,t;\omega) - \bar{u}(x,t))(u(y,t;\omega) - \bar{u}(y,t))]$. In order to relate the eigenvalues and eigenvectors for Y_i with those for $u(x,t;\omega)$, we substitute the DO representation of u into $C_u(x,y)$ and compare Equations (3.15) and (3.16) to obtain

the following relations:

$$\lambda_k = \rho_k \ ; \quad v_k(x,t) = \phi_{kl}(t) u_l(x,t).$$

This shows that the stochastic coefficients Y_i together with the modes u_i provide the necessary information to describe both the shape and magnitude of the uncertainty that characterizes a stochastic field but also the principal directions in $\mathcal{H}$ over which this stochasticity is distributed.

3.4 Bi-orthogonal (BO) method

The DO imposes the *dynamical constraints* on the evolution of the spatial basis in order to derive the evolution equations. On the other hand, the BO imposes the *static constraints* on both the spatial and stochastic basis:

$$\langle u_i, u_j \rangle = \lambda_i \delta_{ij}, \quad E[Y_i Y_j] = \delta_{ij}, \quad i,j = 1, ..., N, \tag{3.17}$$

where the λ_i are eigenvalues of the solution. This condition is referred to as the *bi-orthogonal (BO) condition*. Note that this is exactly the characteristics that the spatial and stochastic components in the KL expansion at a given time t have. Note also the difference between the DO and BO condition; the basis in the DO condition evolves normal to the space V_s, which maintains the basis to be orthogonal in time, while both the basis and the stochastic coefficients in the BO condition are orthogonal in time in the associated space, respectively. There is also a slight difference between the DO and BO representation; the stochastic basis carry the eigenvalues of the covariance operator in the DO representation while the spatial

basis carry the eigenvalues of the covariance operator in the BO representation.

Remark 3. *Both the spatial and stochastic basis change in time while maintaining the orthogonality. Define the matrix S and M whose entries are*

$$S_{ij} = \left\langle u_i, \frac{\partial u_j}{\partial t} \right\rangle, \tag{3.18}$$

$$M_{ij} = E\left[Y_i \frac{dY_j}{dt} \right]. \tag{3.19}$$

Then, by taking the derivative of the first term in Equation (3.17) with respect to time, we have $\left\langle \frac{\partial u_i}{\partial t}, u_j \right\rangle + \left\langle u_i, \frac{\partial u_j}{\partial t} \right\rangle = 0$ for $i \neq j$ and $\left\langle \frac{\partial u_i}{\partial t}, u_i \right\rangle = \frac{1}{2}\frac{d\lambda_i(t)}{dt}$ for $i = j$ or $S_{ij} = -S_{ji}$ for $i \neq j$ and $S_{ii} = \frac{1}{2}\frac{d\lambda_i(t)}{dt}$. Similarly, we have $M_{ij} = -M_{ji}$ for $i \neq j$ and $M_{ii} = 0$. Note that M is skew-symmetric. It will be shown later that the matrices S and M, i.e. the rate of how the basis and the stochastic coefficients change in time, have explicit form.

The procedure of deriving the BO evolution equations are very similar to the one for DO. By doing the exact steps as we did in the DO we are able to derive the BO evolution equations

$$\frac{\partial \bar{u}(x,t)}{\partial t} = E[\mathcal{L}[u]], \tag{3.20a}$$

$$\lambda_j \frac{dY_j(t;\omega)}{dt} = -\sum_{i=1}^{N} S_{ji} Y_i + h_j, \quad j = 1, ..., N, \tag{3.20b}$$

$$\frac{\partial u_j(x,t)}{\partial t} = -\sum_{i=1}^{N} M_{ji} u_i + p_j, \quad j = 1, ..., N, \tag{3.20c}$$

The evolution equations $(3.20a) - (3.20c)$ can be recasted into matrix form with

$\mathbf{u} = (u_1, ..., u_N), \mathbf{Y} = (Y_1, ..., Y_N)$ and $\Lambda = diag(\lambda_1, ..., \lambda_N)$ as follows:

$$\frac{\partial \bar{u}(x,t)}{\partial t} = E[\mathcal{L}[u]], \tag{3.21a}$$

$$\frac{d\mathbf{Y}(t;\omega)}{dt}\Lambda = -\mathbf{Y}S^T + \mathbf{h}, \tag{3.21b}$$

$$\frac{\partial \mathbf{u}(x,t)}{\partial t} = \mathbf{u}M + \mathbf{p}, \tag{3.21c}$$

where S^T is the transpose of the matrix S and we used the skew-symmetricity of M. The question arises that there exists a closed form for the matrix M and S that contains information on how the spatial and stochastic basis evolve. The answer is affirmative as shown in the following lemma.

Lemma 1. *Assume that there is no eigenvalue crossing in a given time domain, i.e.* $\lambda_i \neq \lambda_j$. *There exists a unique and closed form for the matrix* M *and* S *as follows:*

$$M_{ij} = \begin{cases} \frac{G_{ij}+G_{ji}}{-\lambda_i+\lambda_j}, & \text{if } i \neq j \\ 0, & \text{if } i = j \end{cases} \tag{3.22a}$$

$$S_{ij} = \begin{cases} G_{ij} + \lambda_i M_{ij}, & \text{if } i \neq j \\ G_{ii}, & \text{if } i = j \end{cases}. \tag{3.22b}$$

(3.22c)

Proof. By multiplying Y_k on the both sides in equation (3.20b) and then taking the expectation we get

$$\lambda_j M_{kj} = -\sum_{i=1}^{N} S_{ji} E[Y_i Y_k] + \langle E[\mathcal{L}[u] Y_k], u_j \rangle \tag{3.23}$$

where we use $E[(\mathcal{L}[u] - E[\mathcal{L}[u]])Y_k] = E[\mathcal{L}[u]Y_k]$ because of the linearity of the

expectation and $E[Y_k] = 0$. By applying the BO condition we have

$$\lambda_j M_{kj} = -S_{jk} + G_{jk}. \tag{3.24}$$

Interchanging the indices k and j yields

$$\lambda_k M_{jk} = -S_{kj} + G_{kj}. \tag{3.25}$$

This holds for $j \neq k$. For $j = k$, we have $S_{jj} = G_{jj}$ since the diagonal entries of M are zero. Summing up the last two equations and using skew-symmetric properties for S for non-diagonal elements and M yield

$$M_{jk} = \begin{cases} \frac{G_{jk}+G_{kj}}{-\lambda_j+\lambda_k}, & \text{if } j \neq k \\ 0, & \text{if } j = k \end{cases} \tag{3.26}$$

and substituting it back into equation (3.24) we get the explicit form for S

$$S_{jk} = \begin{cases} \frac{\lambda_k}{-\lambda_j+\lambda_k} G_{jk} + \frac{\lambda_j}{-\lambda_j+\lambda_k} G_{kj}, & \text{if } j \neq k \\ G_{jj}, & \text{if } j = k. \end{cases} \tag{3.27}$$

□

We now have the following theorem for the BO evolution equations.

Theorem 2. *We assume that the spatial and stochastic basis satisfy the BO condition and there is no eigenvalue crossing throughout the time domain. Then the original*

SPDE (3.1a)-(3.1c) is reduced to the following system of equations:

$$\begin{aligned} \frac{\partial \bar{u}(x,t)}{\partial t} &= E[\mathcal{L}[u]], \\ \frac{d\mathbf{Y}(t;\omega)}{dt}\Lambda &= -\mathbf{Y}S^T + \mathbf{h}, \\ \frac{\partial \mathbf{u}(x,t)}{\partial t} &= \mathbf{u}M + \mathbf{p}. \end{aligned}$$

We note that the rate of change of the basis and stochastic coefficients is associated with the matrix G whose entries are $G_{ij} = \langle E[\mathcal{L}[u]Y_j], u_i \rangle$, i.e. $S = G + \Lambda M$, and the matrix S and M have closed form. If two eigenvalues are identical, the denominator in the non-diagonal entries of the matrix M in Equation (3.22a) is singular and thus can lead to the numerical instability for the BO when two eigenvalues are getting close to each other.

The diagonal entries for S account for how the eigenvalues change in time $S_{ii} = \frac{1}{2}\frac{d\lambda_i(t)}{dt}$ as discussed in Remark 3, which can be computed exactly by Equation (3.22b). This can be used as a useful adaptive criterion in the computation to decide when to add or remove modes; if the lowest eigenvalue grows quickly and is larger than a certain value, a new mode needs to be added. This will be described in more detail in Section 5.4.2. Another possible adaptive strategy proposed in [66] is to use as a criterion the instantaneous energy of the existing DO modes.

Remark 4. *Both DO and BO representations can be viewed as an extension of KL representation so that they track the low-dimensional structure for every time. It is shown in Section 4.2 that they are equivalent through the invertible matrix differential equation; in other words, there is an one-to-one mapping between the BO components and DO components. However, we have observed that the BO is numerically more stable than the DO, in particular for high modes in non-linear problems. While the*

stochastic basis in the DO carry the eigenvalues the spatial basis in the BO carry the eigenvalues. On the other hand the BO suffers from the numerical instability due to the aforementioned singularity when the eigenvalues cross while the DO does not. In Section 5.4.1, the method to overcome the aforementioned disadvantage of each method will be described.

Chapter 4

The equivalence of the DO and BO

4.1 Introduction

In the previous chapter, we derived the DO and BO evolution equations by imposing the *dynamical constraints* and the *static constraints* on the basis, respectively as shown in Table 4.1. Both representation have time-dependence on both the spatial and stochastic basis. In this chapter we seek the relation between two methods and show that they are equivalent to each other in the sense that the one can be derived from the other and vice versa through the orthogonal matrix governed by the orthogonal matrix differential equation.

BO	DO
$\left\langle \mathbf{U}^T\mathbf{U} \right\rangle = \Lambda, \quad E[\mathbf{Y}^T\mathbf{Y}] = I_N$	$\left\langle \frac{\partial \mathbf{U}^T}{\partial t}\mathbf{U} \right\rangle = O_N$

Table 4.1: The BO and DO conditions.

We present the DO and BO evolution equations in Table 4.2.

	DO	BO
mean	$\frac{\partial \bar{\mathbf{u}}^{DO}}{\partial t} = E[\mathcal{L}(u)]$	$\frac{\partial \bar{\mathbf{u}}^{BO}}{\partial t} = E[\mathcal{L}(u)]$
spatial basis	$\frac{\partial \mathbf{U}^{DO}}{\partial t} = (\mathbf{p} - \mathbf{U}^{DO}G)C^{-1}$	$\frac{\partial \mathbf{U}^{BO}}{\partial t} = \mathbf{U}^{BO}M + \mathbf{p}$
stochastic basis	$\frac{d\mathbf{Y}^{DO}}{dt} = \mathbf{h}$	$\frac{d\mathbf{Y}^{BO}}{dt} = (-\mathbf{Y}^{BO}S^T + \mathbf{h})\Lambda^{-1}$

Table 4.2: The BO and DO evolution equations. $\mathbf{U}^{DO}$ and $\mathbf{Y}^{DO}$ are the DO components of the basis and stochastic coefficients and $\mathbf{U}^{BO}$ and $\mathbf{Y}^{BO}$ are the BO components.

The vector and matrix in the evolution equations are defined as:

$$\Lambda = diag(\lambda_1, ..., \lambda_N) \tag{4.1a}$$

$$C_{ij} = E[Y_i Y_j] \tag{4.1b}$$

$$G_{ij} = < E[\mathcal{L}[u]Y_j], u_i > \tag{4.1c}$$

$$M_{ij} = \begin{cases} \frac{G_{ij}+G_{ji}}{-\lambda_i+\lambda_j}, & \text{if } i \neq j \\ 0, & \text{if } i = j \end{cases} \tag{4.1d}$$

$$S_{ij} = \begin{cases} G_{ij} + \lambda_i M_{ij}, & \text{if } i \neq j \\ G_{ii}, & \text{if } i = j \end{cases} \tag{4.1e}$$

$$h_j = < \tilde{\mathcal{L}}[u], u_j > \tag{4.1f}$$

$$p_j = E[\mathcal{L}[u]Y_j]. \tag{4.1g}$$

Note that the vectors such as $\mathbf{h}, \mathbf{p}, G$ in Table 4.2 are computed in the corresponding components, e.g. $\mathbf{h} = \langle \tilde{\mathcal{L}}[u]\mathbf{U}^{DO} \rangle$ in the DO evolution equations and $\mathbf{h} = \langle \tilde{\mathcal{L}}[u]\mathbf{U}^{BO} \rangle$ in the BO evolution equations. Note that $\lambda_i, i = 1, ..., N$ are eigenvalues of the system. For the BO it is equivalent to the inner product of the spatial basis, i.e. $\Lambda =< \mathbf{U}^T\mathbf{U} >$ while for the DO it is equivalent to the eigenvalues of the

covariance matrix $C = E[\mathbf{Y}^T\mathbf{Y}]$. Note also that the matrix M is skew-symmetric and S is quasi-skew-symmetric meaning that the diagonal entries can be non-zero.

4.2 The equivalence of BO and DO

We now prove the equivalence between the BO and DO solutions. In particular, we will prove that there is a linear transformation for the spatial and stochastic basis that (i) leaves the total solution invariant, and (ii) transforms the pair of spatial and stochastic basis of the BO solution to a set of spatial and stochastic basis that satisfy the DO equations. We will also show that this transformation is *invertible*, and thus it can be applied to transform the DO components to the corresponding BO components. Based on this fact we will conclude that the two sets of equations are just a reformulation of each other since they describe the same approximate (in the sense of finite-dimensionality) solution.

For notation simplicity denote the spatial and stochastic basis for the BO and DO by $\check{U} = (\check{u}_1, \check{u}_2, ..., \check{u}_N), \hat{U} = (\hat{u}_1, \hat{u}_2, ..., \hat{u}_N), \check{Y} = (\check{Y}_1, \check{Y}_2, ..., \check{Y}_N)$ and $\hat{Y} = (\hat{Y}_1, \hat{Y}_2, ..., \hat{Y}_N)$, respectively, i.e. $\check{U} = \mathbf{U}^{BO}, \hat{U} = \mathbf{U}^{DO}, \check{Y} = \mathbf{Y}^{BO}, \hat{Y} = \mathbf{Y}^{DO}$ in Table 4.2. We consider the linear transformation from the DO to the BO components:

$$\check{Y} = \hat{Y}P\Lambda^{-\frac{1}{2}}, \tag{4.2a}$$

$$\check{U} = \hat{U}P\Lambda^{\frac{1}{2}}, \tag{4.2b}$$

where P satisfies the matrix differential equation

$$\begin{aligned} \frac{dP}{dt} &= P\Lambda^{-\frac{1}{2}}\Sigma\Lambda^{-\frac{1}{2}}, \\ P(0) &= I_N, \end{aligned} \tag{4.3}$$

where I_N is the $N \times N$ identity matrix, and Σ is the skew-symmetric part of the matrix S in Equation (4.1e), i.e. $\Sigma_{ij} = S_{ij}$ for $i \neq j$ and $\Sigma_{ii} = 0$ for $i = 1, ..., N$. This leads to the following theorem:

We first prove the invertibility of the linear transformation through the following:

Lemma 2. *The solution $P(t)$ to the matrix differential equation (4.3) remains orthogonal for every time $t \geq 0$ given that the initial condition $P(0)$ is an orthogonal matrix. Indeed, the coefficient $F(t) \equiv \Lambda^{-\frac{1}{2}}\Sigma\Lambda^{-\frac{1}{2}}$ of P in Equation (4.3) is skew-symmetric because Σ is skew-symmetric, and thus we have*

$$\begin{aligned} \frac{d}{dt}\big(P(t)P^T(t)\big) &= \dot{P}(t)P^T(t) + P(t)\dot{P}^T(t) \\ &= (PF)P^T + P(PF)^T \\ &= P(F + F^T)P^T \\ &= O_N, \quad t \geq 0, \end{aligned}$$

where O_N is $N \times N$ zero matrix and the overdots denote differentiation with respect to t. Thus $\dot{P} \equiv \frac{dP}{dt}$. Therefore $P(t)P^T(t) = P(0)P^T(0) = I_N, t \geq 0$.

We are now ready to establish the connection between the BO and the DO components.

Theorem 3. *Suppose that $\check{U}$ and $\check{Y}$ satisfy the BO equations. Assume that the eigenvalues $\lambda_i, i = 1, ..., N$ of the covariance operator in Equation (3.17) are dis-*

crete at any time. Then the linear transformation (4.2a)-(4.2b) defines a new set of stochastic coefficients and basis elements for which (i) $\check{Y}\check{U}^T = \hat{Y}\hat{U}^T$ the total solution remains invariant, and (ii) $\hat{U}$ satisfies the DO condition. Hence, $(\hat{U}, \hat{Y})$ is a solution of the DO equations. The invertibility of the transformation allows for the application of the Theorem in the inverse direction.

Proof. Assume that $\check{Y}$ and $\check{U}$ are the solutions to the BO evolution equations (3.20a)-(3.20c). Then we will prove that $\hat{Y}$ and $\hat{U}$ are the solutions to the DO evolution equations (3.13a)-(3.13c) by showing the following three properties: (i) $\hat{U}$ is an orthonormal basis, (ii) $\check{Y}\check{U}^T = \hat{Y}\hat{U}^T$, and (iii) $\hat{U}$ satisfy the DO condition and $(\hat{U}, \hat{Y})$ are DO components.

According to the BO assumption on the basis $\check{U}$, we have

$$\begin{aligned} \Lambda &= < \check{U}^T \check{U} > \\ &= \langle \Lambda^{\frac{1}{2}} P^T \hat{U}^T \hat{U} P \Lambda^{\frac{1}{2}} \rangle \\ &= \Lambda^{\frac{1}{2}} P^T \langle \hat{U}^T \hat{U} \rangle P \Lambda^{\frac{1}{2}} \end{aligned}$$

because Λ and P is a function of time so that we can take them out of the integral with respect to the physical domain. Multiplying $P\Lambda^{-\frac{1}{2}}$ and $\Lambda^{-\frac{1}{2}}P^T$ to the left and right, respectively, on the both sides yields

$$\begin{aligned} < \hat{U}^T \hat{U} > &= P \underbrace{\Lambda^{-\frac{1}{2}} \Lambda \Lambda^{-\frac{1}{2}}}_{I} P^T \\ &= P P^T \\ &= I \end{aligned}$$

where we used the fact that P is orthogonal. Hence $\hat{U}$ is an orthonormal basis.

Second, the BO and DO representations to the solution $u(x,t;\omega)$ have the same form:

$$\begin{aligned} u(x,t;\omega) &= \bar{u}(x,t) + \sum_{i=1}^{N} \check{u}_i(x,t)\check{Y}_i(t;\omega) \\ &= \bar{u}(x,t) + \sum_{i=1}^{N} \hat{u}_i(x,t)\hat{Y}_i(t;\omega), \end{aligned}$$

where $(\check{u}_i, \check{Y}_i)_{i=1}^N$ and $(\hat{u}_i, \hat{Y}_i)_{i=1}^N$ are the BO and DO components, respectively. Indeed, we obtain this directly using Equations (4.2a)-(4.2b)

$$\check{U}\check{Y}^T = \hat{U}P\Lambda^{\frac{1}{2}}(\hat{Y}P\Lambda^{-\frac{1}{2}})^T = \hat{U}P\Lambda^{\frac{1}{2}}\Lambda^{-\frac{1}{2}}P^T\hat{Y}^T = \hat{U}PP^T\hat{Y}^T = \hat{U}\hat{Y}^T.$$

Finally, we have by the definition of the transformation

$$\check{U} = \hat{U}P\Lambda^{\frac{1}{2}}$$

from which we have

$$\begin{aligned} \dot{\check{U}} &= \dot{\hat{U}}P\Lambda^{\frac{1}{2}} + \hat{U}\dot{P}\Lambda^{\frac{1}{2}} + \frac{1}{2}\hat{U}P\Lambda^{-\frac{1}{2}}\dot{\Lambda} \\ &= \dot{\hat{U}}P\Lambda^{\frac{1}{2}} + \hat{U}(P\Lambda^{-\frac{1}{2}}\Sigma\Lambda^{-\frac{1}{2}})\Lambda^{\frac{1}{2}} + \frac{1}{2}\hat{U}P\Lambda^{-\frac{1}{2}}\dot{\Lambda} \\ &= \dot{\hat{U}}P\Lambda^{\frac{1}{2}} + \hat{U}P\Lambda^{-\frac{1}{2}}\left(\Sigma + \frac{\dot{\Lambda}}{2}\right) \end{aligned}$$

where $\frac{d\Lambda^{\frac{1}{2}}}{dt} = \Lambda^{-\frac{1}{2}}\dot{\Lambda}$. Note $S = \Sigma + \frac{1}{2}\dot{\Lambda}$. We have by the definition of the matrix S as in Equation (3.18)

$$S = \langle \check{U}^T\dot{\check{U}} \rangle$$

and putting the above two equations for $\check{U}$ and $\dot{\check{U}}$ all together yields

$$\begin{aligned} S &= \langle \check{U}^T (\dot{\hat{U}} P \Lambda^{\frac{1}{2}} + \hat{U} P \Lambda^{-\frac{1}{2}}) \rangle \\ &= \Lambda^{\frac{1}{2}} P^T \langle \hat{U}^T \dot{\hat{U}} \rangle P \Lambda^{\frac{1}{2}} + \Lambda^{\frac{1}{2}} P^T \langle \hat{U}^T \hat{U} \rangle P \Lambda^{-\frac{1}{2}} S \end{aligned}$$

where we employed $< \hat{U}^T \hat{U} >= I$. Hence, we have

$$\Lambda^{\frac{1}{2}} P^T \langle \hat{U}^T \dot{\hat{U}} \rangle P \Lambda^{\frac{1}{2}} = O_N.$$

Since P and Λ are invertible, we obtain $\langle \hat{U}^T \dot{\hat{U}} \rangle = O_N$ that is precisely the DO condition in vector notation. This completes the proof that $\hat{Y}$ and $\hat{U}$ are the solutions to the DO evolution equations.

The same procedure can be used to prove that if $\hat{Y}$ and $\hat{U}$ are the solutions to the DO evolution equations, then $\check{Y}$ and $\check{U}$ are the solutions to the BO evolution equations. This completes the proof.

□

If we plug Equations (4.2a)-(4.2b) into the BO evolution equations, we obtain the DO evolution equations and vice versa. First we seek the relation between the vectors or matrices corresponding to the BO and DO. For notation simplicity denote the components for the BO and DO by $\check{\cdot}$ and $\hat{\cdot}$, respectively. For example, $\check{\mathbf{h}} = \langle \tilde{\mathcal{L}}[u], \check{U} \rangle$ and $\hat{\mathbf{h}} = \langle \tilde{\mathcal{L}}[u], \hat{U} \rangle$. Then we have the following relations between the

BO and DO components via Equations (4.2a)-(4.2b):

$$\begin{aligned}
\check{\mathbf{p}} &= E[\mathcal{L}[u]\check{Y}] = E[\mathcal{L}[u]\hat{Y}P\Lambda^{-\frac{1}{2}}] = E[\mathcal{L}[u]\hat{Y}]P\Lambda^{-\frac{1}{2}} = \hat{\mathbf{p}}P\Lambda^{-\frac{1}{2}} && (4.4a)\\
\check{\mathbf{h}} &= \langle\tilde{\mathcal{L}}[u]\check{U}\rangle = \langle\mathcal{L}[u]\hat{U}\rangle P\Lambda^{-\frac{1}{2}} = \hat{\mathbf{h}}P\Lambda^{-\frac{1}{2}} && (4.4b)\\
\check{G} &= \langle\check{U}^T\check{\mathbf{p}}\rangle \\
&= \langle\Lambda^{\frac{1}{2}}P^T\hat{U}^T\hat{\mathbf{p}}P\Lambda^{-\frac{1}{2}}\rangle \\
&= \Lambda^{\frac{1}{2}}P^T\hat{G}P\Lambda^{-\frac{1}{2}}. && (4.4c)
\end{aligned}$$

First we obtain the DO evolution equations from the BO evolution equations for the stochastic basis. The BO evolution equations for the stochastic basis is

$$\frac{d\check{Y}}{dt} = (-\check{Y}S^T + \check{\mathbf{h}})\Lambda^{-1}. \tag{4.5}$$

Substituting Equation (4.2a) into the left hand side of the above equation yields

$$\begin{aligned}
\frac{d\check{Y}}{dt} &= \frac{d(\hat{Y}P\Lambda^{-\frac{1}{2}})}{dt} \\
&= \frac{d\hat{Y}}{dt}P\Lambda^{-\frac{1}{2}} + \hat{Y}\dot{P}\Lambda^{-\frac{1}{2}} - \frac{1}{2}\hat{Y}P\Lambda^{-\frac{3}{2}}\dot{\Lambda} \\
&= \frac{d\hat{Y}}{dt}P\Lambda^{-\frac{1}{2}} + \hat{Y}P\Lambda^{-\frac{1}{2}}\Sigma\Lambda^{-1} - \frac{1}{2}\hat{Y}P\Lambda^{-\frac{3}{2}}\dot{\Lambda}
\end{aligned}$$

where we used $\frac{d\Lambda^{-\frac{1}{2}}}{dt} = -\frac{1}{2}\Lambda^{-\frac{3}{2}}\dot{\Lambda}$ and $\dot{P} = P\Lambda^{-\frac{1}{2}}\Sigma\Lambda^{-\frac{1}{2}}$. The right hand side is

$$\begin{aligned}
\text{RHS} &= (-\check{Y}S^T + \check{\mathbf{h}})\Lambda^{-1} \\
&= (-\hat{Y}P\Lambda^{-\frac{1}{2}}S^T + \hat{\mathbf{h}}P\Lambda^{\frac{1}{2}})\Lambda^{-1}.
\end{aligned}$$

Multiplying Λ from the right on both sides and moving the last two terms in the

LHS to the RHS we have:

$$\begin{aligned}\frac{d\hat{Y}}{dt}P\Lambda^{\frac{1}{2}} &= \hat{\mathbf{h}}P\Lambda^{\frac{1}{2}} - \hat{Y}P\Lambda^{-\frac{1}{2}}S^T - \hat{Y}P\Lambda^{-\frac{1}{2}}\Sigma + \frac{1}{2}\hat{Y}P\Lambda^{-\frac{1}{2}}\dot{\Lambda} \\ &= \hat{\mathbf{h}}P\Lambda^{\frac{1}{2}} - \hat{Y}P\Lambda^{-\frac{1}{2}}\left(S^T + \Sigma - \frac{1}{2}\dot{\Lambda}\right).\end{aligned}$$

Note that we can decompose the matrix S into the non-diagonal part Σ and diagonal part $\frac{1}{2}\dot{\Lambda}$ using the definition for S, hence $S = \Sigma + \frac{1}{2}\dot{\Lambda}$. Utilizing the skew-symmetricity for Σ yields $S^T = -\Sigma + \frac{1}{2}\dot{\Lambda}$. Therefore, the last term on the right hand side vanishes and we have the DO evolution equations for the stochastic basis because P and $\Lambda^{\frac{1}{2}}$ are orthogonal:

$$\frac{d\hat{Y}}{dt} = \hat{\mathbf{h}}.$$

Second we obtain the DO evolution equations from the BO evolution equations for the spatial basis. The BO evolution equations for the spatial basis is

$$\frac{\partial\check{U}}{\partial t} = \check{U}M + \check{\mathbf{p}}. \tag{4.8}$$

Substituting Equation (4.2b) into the left hand side of the above equation yields

$$\begin{aligned}\frac{\partial\check{U}}{\partial t} &= \frac{\partial(\hat{U}P\Lambda^{\frac{1}{2}})}{\partial t} \\ &= \frac{\partial\hat{U}}{\partial t}P\Lambda^{\frac{1}{2}} + \hat{U}\dot{P}\Lambda^{\frac{1}{2}} + \frac{1}{2}\hat{U}P\Lambda^{-\frac{1}{2}}\dot{\Lambda} \\ &= \frac{\partial\hat{U}}{\partial t}P\Lambda^{\frac{1}{2}} + \hat{U}P\Lambda^{-\frac{1}{2}}\Sigma + \frac{1}{2}\hat{U}P\Lambda^{-\frac{1}{2}}\dot{\Lambda}.\end{aligned}$$

where we used $\frac{d\Lambda^{\frac{1}{2}}}{dt} = \Lambda^{-\frac{1}{2}}\dot{\Lambda}$. Substituting (4.2a) and (4.4a) into the right hand side

of Equation (4.8) yields: The right hand side is

$$\begin{aligned} \text{RHS} &= \check{U}M + \check{\mathbf{p}} \\ &= (\hat{U}P\Lambda^{\frac{1}{2}})M + \hat{\mathbf{p}}P\Lambda^{-\frac{1}{2}}. \end{aligned}$$

Multiplying $\Lambda^{\frac{1}{2}}P^T$ from the right on both sides and moving the last two terms in the LHS to the RHS we have:

$$\begin{aligned} \frac{\partial \hat{U}}{\partial t}P\Lambda P^T &= \hat{\mathbf{p}} + \hat{U}P\Lambda^{\frac{1}{2}}M\Lambda^{\frac{1}{2}}P^T - \hat{U}P\Lambda^{-\frac{1}{2}}\left(\Sigma + \frac{\dot{\Lambda}}{2}\right) \\ &= \hat{\mathbf{p}} - \hat{U}P\left(\Lambda^{-\frac{1}{2}}\left(\underbrace{\Sigma + \frac{\dot{\Lambda}}{2}}_{S}\right) - \Lambda^{\frac{1}{2}}M\right)\Lambda^{\frac{1}{2}}P^T \\ &= \hat{\mathbf{p}} - \hat{U}P\Lambda^{-\frac{1}{2}}\left(\underbrace{S - \Lambda M}_{\check{G}}\right)\Lambda^{\frac{1}{2}}P^T \\ &= \hat{\mathbf{p}} - \hat{U}\underbrace{P\Lambda^{-\frac{1}{2}}\check{G}\Lambda^{\frac{1}{2}}P^T}_{\hat{G}} \\ &= \hat{\mathbf{p}} - \hat{U}\hat{G}. \end{aligned}$$

It remains to show that $C = E[\hat{Y}^T\hat{Y}] = P\Lambda P^T$. Indeed,

$$\begin{aligned} C &= E[\hat{Y}^T\hat{Y}] \\ &= E[(\check{Y}\Lambda^{\frac{1}{2}}P^T)^T\check{Y}\Lambda^{\frac{1}{2}}P^T] \\ &= P\Lambda^{\frac{1}{2}}E[\check{Y}^T\check{Y}]\Lambda^{\frac{1}{2}}P^T \\ &= P\Lambda P^T \end{aligned}$$

where we used the orthonormality of the stochastic basis for the BO. Therefore, we obtain the DO evolution equations for the spatial basis from the BO evolution equations. We have the following Lemma.

Lemma 3. *Suppose that* $\check{U}$ *and* $\check{Y}$ *satisfy the BO evolution equations. Assume that the eigenvalues* $\lambda_i, i = 1, ..., N$ *of the covariance operator in Equation (3.17) are discrete at any time. We obtain the DO evolution equations for the spatial and stochastic basis via the following relations:*

$$\begin{aligned} \check{Y} &= \hat{Y}\Lambda^{\frac{1}{2}}P^T \\ \check{U} &= \hat{U}\Lambda^{-\frac{1}{2}}P^T \\ \dot{P} &= P\Lambda^{-\frac{1}{2}}\Sigma\Lambda^{-\frac{1}{2}}. \end{aligned}$$

In summary, the BO and DO representation come from the KL decomposition and require that both the spatial and stochastic basis are time-dependent. Hence, there exists some redundancy in the representation. In order to remove this redundancy different constraints are imposed; the DO imposes the *dynamic constraints* on the basis (called *DO condition*) from which the static connection for the basis as well as the evolution equations for the components are derived. In contrast, the BO imposes the *static constraints* on the basis and coefficients (called *BO condition*) from which the dynamic connection for the basis and coefficients as well as the evolution equations for the components are derived. However, Theorem 3 implies that both methods are equivalent in the sense that one can be derived from the other, and vice versa through the orthogonal matrix as in Equations (4.2a)-(4.2b).

Chapter 5

Numerical implementation

5.1 Introduction

In this chapter we deal with numerical implementation of the BO and DO methods. Denote these two methods by time-dependent KL (tKL) methods when there is no ambiguity. tKL evolution equations is a combination of deterministic PDEs (3.13a) and (3.13c) for the DO or (3.20a) and (3.20c) for the BO and SODEs (3.13b) for the DO and (3.20b) for the BO. For the deterministic PDEs for the mean and spatial basis, we can apply any spatial discretization schemes and time-integrators to solve them numerically. For this paper, we use the spectral methods in order to maintain high-order convergence in the spatial space so that the numerical error due to the spatial discretization scheme can be negligible that allows us to focus on the methods in the stochastic framework. Many more details can be found in [74, 75, 76]. We use high-order time-integrators throughout the paper, including the third-order Adams-Bashforth, third-order Runge-Kutta (RK) or fourth-order RK methods. We present

the stochastic discretization schemes to represent the stochastic basis $\mathbf{Y}(t;\omega)$ that are introduced in Section 2.3. This will be introduced in Section 5.2.

The tKL evolution equations require that the initial conditions are random so that the stochastic basis evolves in time according to the evolution equations. However, there are systems where the randomness are not from initial conditions but other parameters or boundary conditions. In this case, there exists singularity initially that would affect the time-integration throughout the time interval. A small perturbation is given to the initial condition in order to avoid this singularity in [1, 54]. However, this intrinsically introduces the errors associated with the magnitude of the perturbation and may not be suitable if higher accuracy is needed. To this end we propose the *hybrid gPC-tKL* i.e., hybrid gPC-DO or hybrid gPC-BO; when there is a deterministic initial condition, we solve the problem initially using gPC or PCM for some time and when the stochasticity evolves, then we switch to tKL methods, i.e. BO or DO. This will be introduced in Section 5.3.

The BO evolution equations (3.20a)-(3.20c) require that there is no eigenvalue crossing in the time interval because the matrix can be singular in the presence of eigenvalue crossing, e.g. $M_{ij} \equiv E\left[Y_i \frac{dY_j}{dt}\right] = \frac{G_{ij}+G_{ji}}{-\lambda_i+\lambda_j}$ for $i \neq j$. However, the DO does not suffer from eigenvalue crossing. On the other hand it is observed numerically as will be shown later that the DO suffers when the ratio of the smallest eigenvalue to the largest eigenvalue or the condition number of the covariance matrix C is very large because the evolution equations for the spatial basis involve the inverse of the covariance matrix C. However, the BO does not suffer from this condition. Since we showed that the two methods are related through the orthogonal matrix P as shown in Equations (4.2a)-(4.2b), we can switch from the BO to the DO when there is eigenvalue crossing or from the DO to the BO when the ratio of the smallest eigenvalue to the largest eigenvalue is very large. We refer this method to as *hybrid*

BO-DO. This will be introduced in Subsection 5.4.1.

If the system is strongly transient and nonlinear e.g. in turbulent systems, the KL truncation with a fixed number of modes to represent the solution may not be enough to maintain within a prescribed accuracy and in such cases we need to adaptively add modes when the smallest eigenvalue is larger than a certain threshold or remove modes when the smallest eigenvalue is smaller than a certain threshold. This may enhance the accuracy of the methods and efficiency of the algorithm. This will be introduced in Subsection 5.4.2.

5.2 Representation for stochastic basis

The stochastic basis $\mathbf{Y}(t;\omega)$ is a vector of random processes. There are, in essence, two ways to represent the stochastic basis: spectral representations such as gPC [16] or wavelet based Polynomial chaos or ensemble representations such as tensor product or sparse grid stochastic collocation [48, 42, 15] depending on the dimensionality of the parametric space or Monte Carlo. We will present two methods: generalized Polynomial chaos and stochastic collocation method introduced in Chapter 2.

5.2.1 Generalized Polynomial Chaos

In Section 2.3, we assume that the random input can be represented by a finite set of independent random variables $\boldsymbol{\eta} = \{\eta_1(\omega), ..., \eta_N(\omega)\}$ with a known joint density function $\rho(\boldsymbol{\eta})$. Then the solution to the SPDE (3.1) is a function of these random variables, i.e. $u(x,t;\omega) = u(x,t;\boldsymbol{\eta})$. The stochastic basis can be represented by these

random variables as well:

$$Y_i(t;\omega) = \sum_{j=1}^{M} \alpha_{ij}(t)\Psi_j(\boldsymbol{\eta}(\omega)), \quad i = 1, ..., N \tag{5.1}$$

where N is the number of tKL modes and M is the number of gPC modes and Ψ_j are orthogonal polynomials associated with random variables $\boldsymbol{\eta}$. The set of orthogonal polynomials associated with well-known standard random variables can be found in [16]. We assume that the number of gPC modes M is the same for every stochastic basis. It can be chosen adaptively as the stochastic basis exhibits multi-scale type representation; the higher tKL mode may imply the more gPC modes as it represents small scale. The vector of stochastic basis $\mathbf{Y}$ can be represented with the coefficients and orthonormal polynomials:

$$\mathbf{Y}(t;\omega) = \boldsymbol{\Psi}(\boldsymbol{\eta}(\omega))\boldsymbol{\alpha}(t), \tag{5.2}$$

where $\boldsymbol{\alpha} \in \mathbb{R}^{M\times N}$. We rescale the orthogonal polynomials to be orthonormal polynomials for convenience and hence $E[\boldsymbol{\Psi}^T(\boldsymbol{\eta})\boldsymbol{\Psi}^T(\boldsymbol{\eta})] = \mathbf{I}$. Then the representation of the solution $u(x,t;\omega)$ reads

$$u(x,t;\omega) = \bar{u}(x,t) + \mathbf{U}\boldsymbol{\alpha}^T(t)\boldsymbol{\Psi}^T(\boldsymbol{\eta}(\omega)). \tag{5.3}$$

The evolution equations for $\mathbf{Y}$ become the evolution equations for the coefficients $\boldsymbol{\alpha}$. Then we have the following evolution equations for the DO and BO.

- (DO) The evolution equations read

$$\frac{d\boldsymbol{\alpha}(t)}{dt} = \langle E[\boldsymbol{\Psi}^T(\boldsymbol{\eta})\tilde{\mathcal{L}}[u]]\mathbf{U}\rangle \tag{5.4a}$$

$$\frac{\partial \mathbf{U}(t,x)}{\partial t}C = E[\mathcal{L}[u]\boldsymbol{\Psi}(\boldsymbol{\eta})]\boldsymbol{\alpha} - \mathbf{U}\langle \mathbf{U}^T E[\mathcal{L}[u]\boldsymbol{\Psi}(\boldsymbol{\eta})]\boldsymbol{\alpha}\rangle \tag{5.4b}$$

where we used the fact that the gPC basis is orthonormal, i.e. $E[\boldsymbol{\Psi}^T(\boldsymbol{\eta})\boldsymbol{\Psi}(\boldsymbol{\eta})] = I$.

- (BO) The evolution equations read

$$\frac{d\boldsymbol{\alpha}(\boldsymbol{t})}{dt}\Lambda = -\boldsymbol{\alpha}(\boldsymbol{t})S^T + E[\boldsymbol{\Psi}^T(\boldsymbol{\eta})\mathbf{h}] \tag{5.5a}$$

$$\frac{\partial \mathbf{U}(x,t)}{\partial t} = \mathbf{U}M + E[\mathcal{L}[u]\boldsymbol{\Psi}(\boldsymbol{\eta})]\boldsymbol{\alpha}. \tag{5.5b}$$

5.2.2 Probabilistic collocation methods

While gPC have a well-established theory on the convergence, in particular for the elliptic problems, it suffers from the curse of dimensionality as the number of modes given by $M = \frac{(R+p)!}{R!p!} - 1$ grows exponentially where R is the dimensionality of parametric space and p the maximum polynomial order. Furthermore, from the implementation viewpoint, the deterministic solver can not be reused but the whole solver needs to be implemented from the scratch and it may cost lots of work to do, in particular in problems with random nonlinearities. The PCM can be a good alternative to avoid these drawbacks from gPC; (i) the deterministic solver can be reused as for each sampling point, the problem turns into a deterministic one and hence it can be easily parallelized and (ii) the curse-of-dimensionality can be lifted up to some extent choosing a clever sampling method such as sparse grid.

We suppose that we have a set of collocation points and corresponding weights $\{\boldsymbol{\xi}_i, w_i\}_{i=1}^{N_r}$ where N_r is the number of points. We use the sparse grid or tensor product quadrature rule to generate the collocation points depending on the dimensionality of parametric space throughout the paper. For each collocation point

$\boldsymbol{\xi}_i = (\xi_1^i, \xi_2^i, ..., \xi_R^i)$, we solve the evolution equations for the stochastic basis.

$$\text{BO:} \quad \frac{d\mathbf{Y}(t;\boldsymbol{\xi}_i)}{dt}\Lambda = -\mathbf{Y}(t;\boldsymbol{\xi}_i)S^T + \mathbf{h}, \tag{5.6a}$$

$$\text{DO:} \quad \frac{d\mathbf{Y}(t;\boldsymbol{\xi}_i)}{dt} = \left\langle \tilde{\mathcal{L}}(x,t;\boldsymbol{\xi}_i), \mathbf{U}(x,t) \right\rangle. \tag{5.6b}$$

The quantity of interest such as moment can be easily computed with the solution at each collocation point and corresponding weight, e.g. the covariance matrix of $\mathbf{Y}$ can be computed as follows:

$$C = E[\mathbf{Y}^T\mathbf{Y}](t) = \sum_{i=1}^{N_r} \mathbf{Y}^T(t;\boldsymbol{\xi}_i)\mathbf{Y}(t;\boldsymbol{\xi}_i)w_i.$$

If the dimensionality of parametric space is high enough that the sparse grids does not work, the ANOVA method can be employed where it decompose the R-dimensional function into the series of low-dimensional functions. More details can be found in [48, 49]. In this paper, we mainly use PCM rather than gPC for the representation of $\mathbf{Y}$.

5.3 Hybrid gPC-tKL

In Theorem 1 or 2, it is assumed that the initial condition for the SPDE is random from which the corresponding initial conditions for DO or BO components are derived. However, in practice in many cases the initial condition for the SPDE is deterministic while the randomness comes from other sources such as random coefficients or random forcing. Then $Y_i, i = 1, ..., N$ at the initial time become zero, which makes the covariance matrix for Y_i singular. Although the singular limit for the DO

or BO equations exist, the transition to finite covariance creates numerical issues. More importantly, in such a case it is not clear what is the optimal choice to initiate the stochastic subspace. To this end, we propose a hybrid approach of Polynomial Chaos (PC) and DO or BO methods in order to avoid the aforementioned problems called *hybrid gPC-tKL*. Specifically, for PC we employ the probabilistic collocation method (PCM) or multi-element PCM (ME-PCM), which was found to effectively deal with problems exhibiting low regularity in parametric space as well as for long-term integration [17]. We first use PCM or ME-PCM from the initial time t_0 up to some time, say t_s, provided that the stochasticity is sufficiently developed, and then switch over to the DO or BO methods at t_s and employ the KL decomposition to initialize $\bar{u}, \mathbf{Y}$ and $\mathbf{U}$.

First, we construct the covariance matrix $C_{u(\cdot,t_s)}(x,y)$

$$C_{u(\cdot,t_s)}(x,y) = E\left[\left(u(x,t_s;\omega) - \bar{u}(x,t_s)\right)^T \left(u(y,t_s;\omega) - \bar{u}(y,t_s)\right)\right],$$

where u and $\bar{u}$ at $t = t_s$ are known from PC computations. Then, we compute the eigenpairs for $C_{u(\cdot,t_s)}(x,y)$ by solving

$$\int_D C_{u(\cdot,t_s)}(x,y)\phi(x)dx = \lambda\phi(y).$$

We assume that the eigenfunctions $\phi(y)$ are orthonormalized. The Table 5.1 shows how to initialize the BO and DO components at $t = t_s$ and we are ready to solve the DO evolution equations. This procedure is summarized in Algorithm 1.

	spatial basis	stochastic basis
BO	$u_i(x,t_s) = \sqrt{\lambda_i}\phi_i(x,t_s)$	$Y_i(t_s,\omega) = \frac{1}{\sqrt{\lambda_i}}\langle u(x,t_s;\omega) - \bar{u}(x,t), \phi_i\rangle$
DO	$u_i(x,t_s) = \phi_i(x,t_s)$	$Y_i(t_s,\omega) = \langle u(x,t_s;\omega) - \bar{u}(x,t), \phi_i\rangle$

Table 5.1: The initialization for the BO and DO components at $t = t_s$.

Algorithm 1: Hybrid gPC-tKL: combining gPC and tKL (either BO or DO)

- Run PCM or ME-PCM up to $t = t_s$ from $t = 0$.
- At $t = t_s$, use the KL decomposition for the solution:

$$u(x, t_s; \omega) = \bar{u}(x, t_s) + \sum_{i=1}^{N} Y_i(t_s; \omega)\phi_i(x, t_s).$$

- From the KL decomposition, we can initialize $\bar{u}(x, t_s)$, $\mathbf{Y}(t_s; \omega)$ and $\mathbf{U}(x, t_s)$ for tKL methods as shown in Table 5.1.
- Switch over to the DO method up to time $t = t_f$.

5.4 Adaptive algorithm

Theorem 3 states that the BO and DO are equivalent in the sense that one can be derived from the other, and vice versa through the orthogonal matrix as in Equations (4.2a)-(4.2b). However, the BO evolution equations assume that there is no eigenvalue crossing. In practice, when two eigenvalues are getting close to each other, the numerical instability can occur due to the singularity, e.g. the non-diagonal entries for the matrix M. On the contrary, the DO evolution equations involve the inverse of the covariance matrix C for the stochastic basis, and it is observed that the evolution equations for the spatial basis become stiff when the condition number of C is very large, e.g. the eigenvalue is getting close to zero. In order to avoid the numerical instabilities that the BO and DO may cause under the aforementioned conditions we take advantage of Theorem 3 when either facing eigenvalue crossing to switch from BO to DO or facing zero eigenvalue to switch from DO to BO. We present this method called the *hybrid BO-DO* in subsection 5.4.1

The KL representation may not have a fixed number of modes to represent the solution within a prescribed accuracy e.g. due to the nonlinearity of the system and

in such cases we need to adaptively add modes when the smallest eigenvalue is larger than a certain threshold ϵ_a or remove modes when the smallest eigenvalue is smaller than a certain threshold ϵ_r. This may enhance the accuracy of the methods and efficiency of the algorithm.

5.4.1 Hybrid BO-DO: switching between the BO and DO

In order to avoid the disadvantages of each method, we switch from the one to the other via the matrix differential equations whenever there is either eigenvalue crossing or high condition number of the covariance matrix. The algorithm is shown in Algorithm 2. We start with the BO and solve the BO evolution equations as well as the matrix differential equation for P. When two eigenvalues are getting close to each other in the BO at time t_e, i.e. $|\lambda_i(t_e) - \lambda_j(t_e)| < \epsilon_e$, then we switch over to DO. We can initialize the DO components at t_e through Equations (4.2a)-(4.2b). When the eigenvalue is getting close to zero in the DO at t_c, i.e. $\lambda_i(t_c) < \epsilon_c$, then we switch over to BO. We continue the switching between the BO and DO until the final time is reached.

5.4.2 Adding and removing modes

The eigenvalues determine the energy of the system and can be easily computed; for the BO they are the diagonal entries of the covariance matrix of the spatial basis $< \check{U}^T \check{U} >$ while for the DO they are the eigenvalues of the covariance matrix of the stochastic basis $E[\hat{Y}^T \hat{Y}]$. Let us assume that there are N modes and eigenvalues are arranged in a decreasing order, i.e. $(\lambda_1, \lambda_2, ..., \lambda_N)$ where $\lambda_1 \geq \lambda_2 \geq \cdots \geq \lambda_N$. As adaptive criteria we consider the slope of the smallest eigenvalue as well as the

Algorithm 2: Switching between the BO and DO

Input: Start with the BO evolution equations with a given time-integration method.
t=0; $isBO$=true;
repeat
  if $|\lambda_i - \lambda_j| < \epsilon_e$ *and* $isBO == true$ **then**
    $isBO$ = false; (switch to DO)
  end
  if $cond(C) < \epsilon_c$ *and* $isBO == false$ **then**
    $isBO$ = true; (switch to BO)
  end
  if $isBO$ **then**
    Integrate BO evolution equations.
  else
    Integrate DO evolution equations.
  end
until $t < t_f$;

smallest eigenvalue because the slope gives the information on how fast the eigenvalue increases. The criteria are as follows:

$$\lambda_N > \epsilon_a^1, \quad \frac{d\lambda_N}{dt} > \epsilon_a^2. \tag{5.7}$$

When the smallest eigenvalue λ_N at time t_a is larger than a certain threshold ϵ_a, we add a new set of components (u_{N+1}, Y_{N+1}) via the probabilistic collocation method as follows:

1. Reconstruct the path-wise solution $u(x, t_a; \xi_i) = \bar{u}(x, t_a) + \sum_{n=1}^{N} u_i(x, t_a) Y_i(t_a; \xi_i)$ from the BO or DO components to initialize the probabilistic collocation method.

2. Run the PCM for some time steps.

3. Construct the covariance matrix from PCM solution $u(x, t; \xi_i), i = 1, ..., N_r$ and perform the KL decomposition to add new pair of the spatial and stochastic basis (u_{N+1}, Y_{N+1}).

When the smallest eigenvalue λ_N at time t_r is smaller than a certain threshold ϵ_r, then we remove the last mode of the spatial and stochastic basis (u_N, Y_N) and hence the number of modes is reduced to be $N-1$.

Chapter 6

Applications to linear problems: Advection equations

The objective of this chapter is to give a general algorithmic framework to solve stochastic advection (linear) partial differential equations using the DO and BO methods. The problems we are interested in has the form

$$\frac{\partial u}{\partial t} + V(t;\omega)\frac{\partial u}{\partial x} = 0, \quad \forall (t,x) \in [0,T] \times D = [0,2\pi] \tag{6.1a}$$

$$u(0,x) = g(x) = \sin(x), \quad \forall x \in D. \tag{6.1b}$$

The randomness comes from the advection velocity $V(t;\omega)$, which is considered to be either time-independent or time-dependent. For the time-independent case it is assumed to be a Gaussian random variance with mean zero and variance σ^2, i.e., $V(t;\omega) = V(\omega) = \xi \sim N(0,\sigma^2)$, while for the time-dependent case a stochastic process whose covariance kernel is exponential, i.e, $C_V(t_1,t_2) = \sigma \exp\left(-\frac{|t_1-t_2|}{L}\right)$, with L being the correlation length. It is known in [77] that the stochastic advection

equation (6.1) has exact solutions for the mean and variance.

In case when the advection velocity is random process, we approximate the random process via the truncated KL decomposition with the first M terms as shown in Chapter 2:

$$V(t,\omega) = E[V](t) + \sum_{i=1}^{M} \sqrt{\lambda_i}\phi_i(t)Z_i, \tag{6.2}$$

where $\{Z_i\}_{i=1}^{M}$ are uncorrelated random variables with zero mean and unit variance, and $\{\phi_i(t), \lambda_i\}_{i=1}^{M}$ are the eigenpairs corresponding to the covariance kernel $C_V(t_1, t_2)$, *i.e.* satisfying

$$\int_D C_V(t_1,t_2)\phi_i(t_2)dt_2 = \lambda_i\phi_i(t_1), \tag{6.3}$$

where the exponential covariance kernel has a closed form for the eigenfunctions [77]:

$$\phi_i(t) = \frac{w\cos(wt)/c + \sin(wt)}{\sqrt{(1+w^2/c^2)T/2 + (w^2/c^2-1)\sin(2wT)/(4w) + (1-\cos(2wT))/(2c)}}, \tag{6.4}$$

where $c = 1/L$ and $w = \sqrt{2c/\lambda_i - c^2}$. The eigenvalues are arranged in decreasing order. The theorem of Cameron and Martin [69] guarantees that the truncated decomposition converges to V as M goes to infinity; further, we assume that $E[V](t) = 0$.

Using the tKL representation i.e., the BO or DO representation $u(x,t;\omega) = \bar{u}(x,t) + \sum_{i=1}^{N} u_i(x,t)Y_i(t;\omega)$, we obtain the evolution operator $\mathcal{L}$ in terms of their components:

$$\mathcal{L}(u) = -V(t;\omega)\left(\frac{\partial\bar{u}}{\partial x}(x,t) + \sum_{i=1}^{N}\frac{\partial u_i}{\partial x}(x,t)Y_i(t;\omega)\right).$$

6.1 Numerical solution of the evolution equations

The DO evolution equations (3.13a)-(3.13c) and BO evolution equations (3.20a)-(3.20c) involve the numerical integration in physical space as well as in random space. We define the collocation points and weights for physical space by $(x_k, w_k)_{k=1}^{N_s}$ and random space by $(\xi_j, \gamma_j)_{j=1}^{N_r}$. We choose Fourier collocation points for $x_k, k = 1, ..., N_s$, and sparse grids based on Gauss-Hermite in one dimension for $\xi_j, j = 1, ..., N_r$. N_s and N_r are the number of collocation points in physical and random space, respectively. For the time discretization, we use explicit methods for all DO evolution equations (3.13a)-(3.13c) or BO evolution equations (3.20a)-(3.20c). Essentially the procedure to solve the BO and DO evolution equations are the same; all coefficients in the evolution equations need to be computed in the corresponding components. For the convenience we show only the DO problems in detail but can be easily applied to the BO. Two inner products are involved in tKL equations, given in discrete form below:

- **inner product in the physical space**

$$< h(x), g(x) >= \int_D h(x)g(x)dx \approx \sum_{k=1}^{N_s} h(x_k)g(x_k)w_k.$$

- **inner product in the random space, *i.e.*, expectation operator**

$$E[h(\omega), g(\omega)] = \int_\Omega h(\omega)g(\omega)\rho(\omega)d\omega \approx \sum_{j=1}^{N_r} h(\xi_j)g(\xi_j)\gamma_j.$$

Substituting these equations into the DO equations (3.13b) yields

$$\begin{aligned}
\frac{dY_i(t;\omega)}{dt} &= < \mathcal{L}[u(\cdot,t;\omega)] - E[\mathcal{L}[u(\cdot,t;\omega)]], u_i(\cdot,t) > \\
&= \sum_{k=1}^{N_s} \left(\mathcal{L}(t,x_k) - E[\mathcal{L}(u)](t,x_k)\right) u_i(t,x_k) w_k \\
&= \sum_{k=1}^{N_s} \left(-V(t,\omega)\frac{\partial \bar{u}}{\partial x}(t,x_k) - \sum_{j=1}^{N} \left(V(t,\omega)Y_j(t,\omega) - E[VY_j](t)\right) \frac{\partial u_j}{\partial x}(t,x_k) \right) u_i(t,x_k) w_k \\
&= -B_i V(t,\omega) - V(t,\omega) \sum_{j=1}^{N} Y_j(t,\omega) A_{ji} + \sum_{j=1}^{N} E[VY_j] A_{ji}, \quad i = 1, ..., N
\end{aligned}$$

where we used $E[V](t) = 0$ and

$$B_i = \sum_{k=1}^{N_s} \frac{\partial \bar{u}}{\partial x}(t,x_k) u_i(t,x_k) w_k \text{ and } A_{ji} = \sum_{k=1}^{N_s} \frac{\partial u_j}{\partial x}(t,x_k) u_i(t,x_k) w_k.$$

Note that for each i the above stochastic differential equation is a vector equation of size N_r because we solve the equation at the collocation points $\xi_j, j = 1, ..., N_r$. Therefore, there are $N \times N_r$ equations for Y_i.

The equation for the mean $\bar{u}$ becomes

$$\frac{\partial \bar{u}(t,x)}{\partial t} = E^{\omega}[\mathcal{L}[u(\cdot,t;\omega)]] = -\sum_{i=1}^{N} E[VY_i](t) \frac{\partial u_i}{\partial x}(t,x)$$

since $E[V](t) = 0$. Note that we solve this equation at the collocation points $x_k, k = 1, ..., N_s$ and $E[VY_i]$ is independent of the physical space.

The evolution equations for the spatial basis $u_i(t,x), i = 1, ..., N$ become

$$\begin{aligned}\sum_{i=1}^{N} C_{ij}\frac{\partial u_i}{\partial t}(t,x) &= \prod_{V_s^{\perp}}[E^{\omega}[\mathcal{L}[u(\cdot,t;\omega)Y_j]] \\ &= E^{\omega}[\mathcal{L}[u(\cdot,t;\omega)Y_j] - \sum_{k=1}^{N} < E^{\omega}[\mathcal{L}[u(\cdot,t;\omega)Y_j](t,x), u_k(t,x) > u_k(t,x)\end{aligned}$$

where

$$C_{ij} = C_{Y_i(t)Y_j(t)} = E[Y_i(t,\omega)Y_j(t,\omega)] = \sum_{k=1}^{N_r} Y_i(t,\xi_k)Y_j(t,\xi_k)\gamma_k.$$

The term $E[\mathcal{L}[u(\cdot,t;\omega)Y_j](t,x)$ can be computed as follows:

$$D_{kj} = E[\mathcal{L}[u(\cdot,t;\omega)Y_j](t,x_k) = -E[VY_j](t)\frac{\partial \bar{u}}{\partial x}(t,x_k) - \sum_{i=1}^{N} E[VY_iY_j](t)\frac{\partial u_i}{\partial x}(t,x_k).$$

6.2 Exact formulas of BO and DO components

In this section, we derive the exact formulas of BO and DO components u_i and $Y_i, i = 1, ..., N$ for the stochastic advection equation. First for the stochastic advection equation we have the exact path-wise solution and then after some manipulation can derive the closed form for the mean and variance: [77]:

- **Time-independent** $V(\omega)$

$$u(x,t;\omega) = g(x-\xi t) = \sin(x-\xi t), \tag{6.5a}$$

$$E[u](t,x) = \sin(x)\exp\left(-\frac{\sigma^2 t^2}{2}\right), \tag{6.5b}$$

$$Var[u](t,x) = \frac{1}{2}\left[1-\cos(2x)\exp(-2\sigma^2 t^2)\right] - E[u]^2, \tag{6.5c}$$

- **Time-dependent** $V(t;\omega)$

$$
\begin{aligned}
u(x,t;\omega) &= \sin\left(x - \int_0^t V(s;\omega)ds\right), && \text{(6.6a)}\\
E[u](x,t) &= \sin(x-\bar{V}t)\exp(-a^2\sigma^2/2), && \text{(6.6b)}\\
V[u](x,t) &= \frac{1-\cos(2(x-\bar{V}t))\exp(-2\sigma^2a^2)}{2} - E[u]^2, && \text{(6.6c)}
\end{aligned}
$$

where $a = a(t)$ depends on the type of the process $V(t;\omega)$ we model, *i.e.*,

$$
a^2 = \begin{cases} t^2, & \text{if fully correlated,} \\ 2L(t - L(1-\exp(-t/L))), & \text{partially correlated,} \\ t\Delta t, & \text{mutually independent} \end{cases}
$$

Now we are ready to find the exact closed form for all DO or BO components for two cases of advection velocity: time-independent and time-dependent advection velocities.

Time-independent $V(\omega)$

First we consider a *time-independent* case, *i.e.,* $V(t;\omega) = V(\omega) = \xi(\omega)$ where $\xi(\omega)$ is a Gaussian random variable with mean zero and variance σ^2. The path-wise solution for Equation (6.1) is $u(x,t;\omega) = \sin(x-\xi t)$, and hence by the property of trigonometric function we have

$$
u(x,t;\omega) = \sin(x)\cos(\xi t) - \cos(x)\sin(\xi t). \tag{6.7}
$$

In the BO or DO representation, the solution is expressed as $u(x,t;\omega) = E[u](x,t) + \sum_{i=1}^{N} u_i(x,t)Y_i(t;\omega)$ and comparing this with Equation (6.7) yields

$$\begin{aligned}\sum_{i=1}^{N} u_i(x,t)Y_i(t;\omega) &= u(x,t;\omega) - E[u](x,t) \\ &= -\cos(x)\sin(\xi t) + \sin(x)\left(\cos(\xi t) - \exp\left(-\frac{\sigma^2 t^2}{2}\right)\right),\end{aligned}$$

where the last term is the mean of the solution. Hence we have a *finite* number of modes, *i.e.,* $N = 2$, and we can derive the exact formulas for $(\mathbf{U}^{DO}, \mathbf{Y}^{DO})$ and $(\mathbf{U}^{BO}, \mathbf{Y}^{BO})$ that satisfy the DO and BO condition, respectively:

- **DO**

$$\begin{aligned}u_1(x,t) &= \frac{\cos(x)}{\sqrt{\pi}}, && (6.8a)\\ u_2(x,t) &= \frac{\sin(x)}{\sqrt{\pi}}, && (6.8b)\\ Y_1(t;\omega) &= -\sqrt{\pi}\sin(\xi t), && (6.8c)\\ Y_2(t;\omega) &= -\sqrt{\pi}\left(\cos(\xi t) - \exp\left(-\frac{\sigma^2 t^2}{2}\right)\right). && (6.8d)\end{aligned}$$

- **BO**

$$\begin{aligned}u_1(x,t) &= \alpha_1(t)\cos(x), && (6.9a)\\ u_2(x,t) &= \alpha_2(t)\sin(x), && (6.9b)\\ Y_1(t;\omega) &= \frac{1}{\alpha_1(t)}\sin(\xi t), && (6.9c)\\ Y_2(t;\omega) &= \frac{1}{\alpha_2(t)}\left(\cos(\xi t) - \exp\left(-\frac{\sigma^2 t^2}{2}\right)\right), && (6.9d)\end{aligned}$$

where $\alpha_1(t) = E[\sin^2(\xi t)]$ and $\alpha_2(t) = E\left[\left(\cos(\xi t) - \exp\left(-\frac{\sigma^2 t^2}{2}\right)\right)^2\right]$.

Note that the DO or BO components are the same up to the sign, *i.e.*, $\sum_i u_i Y_i = \sum_i (-u_i)(-Y_i)$.

Time-dependent $V(t;\omega)$

In a similar way we can derive the exact formulas of DO or BO components when $V(t;\omega)$ is *time-dependent* with covariance kernel being $C_V(t_1,t_2) = \sigma^2 \exp\left(-\frac{|t_1-t_2|}{L}\right)$. We have again $N = 2$ and the exact formulas for u_i and Y_i are:

- **DO**

$$
\begin{aligned}
u_1(x,t) &= \frac{\cos(x)}{\sqrt{\pi}}, && \text{(6.10a)}\\
u_2(x,t) &= \frac{\sin(x)}{\sqrt{\pi}}, && \text{(6.10b)}\\
Y_1(t;\omega) &= -\sqrt{\pi}\sin\left(\int_0^t V(s;\omega)ds\right), && \text{(6.10c)}\\
Y_2(t;\omega) &= -\sqrt{\pi}\left(\cos\left(\int_0^t V(s;\omega)ds\right) - \exp\left(-\frac{a^2(t)\sigma^2}{2}\right)\right), && \text{(6.10d)}
\end{aligned}
$$

- **BO**

$$
\begin{aligned}
u_1(x,t) &= \beta_1(t)\cos(x), && \text{(6.11a)}\\
u_2(x,t) &= \beta_2(t)\sin(x), && \text{(6.11b)}\\
Y_1(t;\omega) &= \frac{1}{\beta_1(t)}\sin\left(\int_0^t V(s;\omega ds\right), && \text{(6.11c)}\\
Y_2(t;\omega) &= \frac{1}{\beta_2(t)}\left(\cos\left(\int_0^t V(s;\omega)ds\right) - \exp\left(-\frac{a^2(t)\sigma^2}{2}\right)\right), && \text{(6.11d)}
\end{aligned}
$$

where $\beta_1(t) = E\left[\left(\sin\left(\int_0^t V(s;\omega ds\right)\right)^2\right]$ and
$\beta_2(t) = E\left[\left(\cos\left(\int_0^t V(s;\omega)ds\right) - \exp\left(-\frac{a^2(t)\sigma^2}{2}\right)\right)^2\right]$.

Note that the time-dependent modes are given by semi-analytical forms.

6.3 Numerical results for time-independent $V(\omega)$

In this section, we consider the case where $V(t;\omega)$ is a Gaussian random variable with mean zero and variance σ^2. We present two different methods to solve the DO evolution equations (3.13a)-(3.13c). For the first method we assume that $Y_i(0;\omega) = 0$ and $u_i(x,0)$ are orthogonal polynomials while for the second one we use the hybrid gPC-tKL proposed in Section 5.3. The parameters are as follows:

$$\triangle t = 0.001, t_f = 5, N = 2, N_s = 128, N_r = 32, \sigma = 0.1,$$

where t_f is the final time. Fourier collocation in the physical space and Hermite collocation in the parametric (or random) space are used to discretize the space. (The number of collocation points in the physical space is denoted by N_s while the number in the random space N_r.) We use the third-order Adams-Bashforth (AB3) as a time-integrator to minimize the error due to the time discretization. Indeed, Figure 6.1 shows that AB3 is much better than the Euler method with errors approaching machine accuracy. Although this is expected, we want to obtain the absolute errors of time integration so that we will only consider the errors in parametric space later. Also, this temporal accuracy will be very important when we switch from gPC to the DO or BO method. The relative L_2 error for the mean is defined as $|E(u_{num}) - E(u_{exact})|_{L_2}/|E(u_{exact})|_{L_2}$ where u_{num} is the numerical solution and u_{exact} is the exact solution.

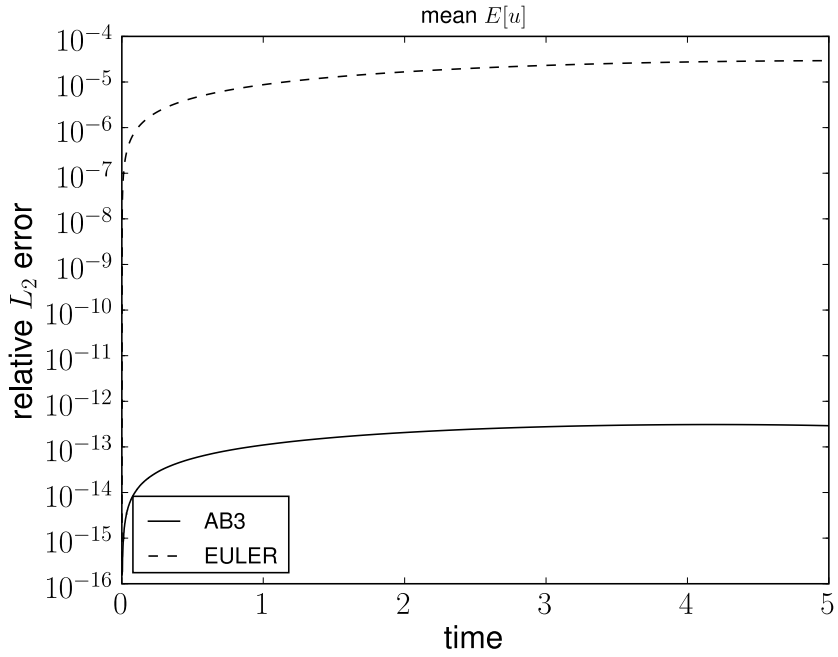

Figure 6.1: $V(t;w) = V(w) = \xi \sim N(0, \sigma^2)$ with $\sigma = 0.1$. The mean of the solution using AB3 has eight orders of magnitude better accuracy than the Euler method.

6.3.1 DO method with initial basis being orthogonal polynomials

Since the initial condition is deterministic, the stochastic coefficients $Y_i(0;\omega), i = 1, ..., N$ are zero. To illustrate how the solution evolves in time through the DO evolution equations, we choose initially the linear subspace V_S spanned by orthogonal polynomials with the stochastic coefficients Y_i being zero. The orthogonal polynomials on $[0, 2\pi]$ can be constructed using Gram-Schmidt orthogonalization.

Figure 6.2 shows how the basis for V_S evolves in time through the DO evolution equation (3.13c). As mentioned, orthogonal polynomials on $[0, 2\pi]$ are chosen as a basis for the initial condition for $u_i, i = 1, ..., N$ and they are evolving and converge to the Fourier basis of period one. Once they become the Fourier basis, the linear subspace V_S does not change but remains invariant in time. Indeed, the

exact formulas for the spatial basis in Equations (6.8a)-(6.8b) suggest that they are time-independent Fourier basis of period one. The mean and variance are shown in Figure 6.3 and they agree well with the exact solution at $t_f = 5$. This shows that the DO method can recover ("on-the-fly") the optimal basis as it evolves according to the evolution equations.

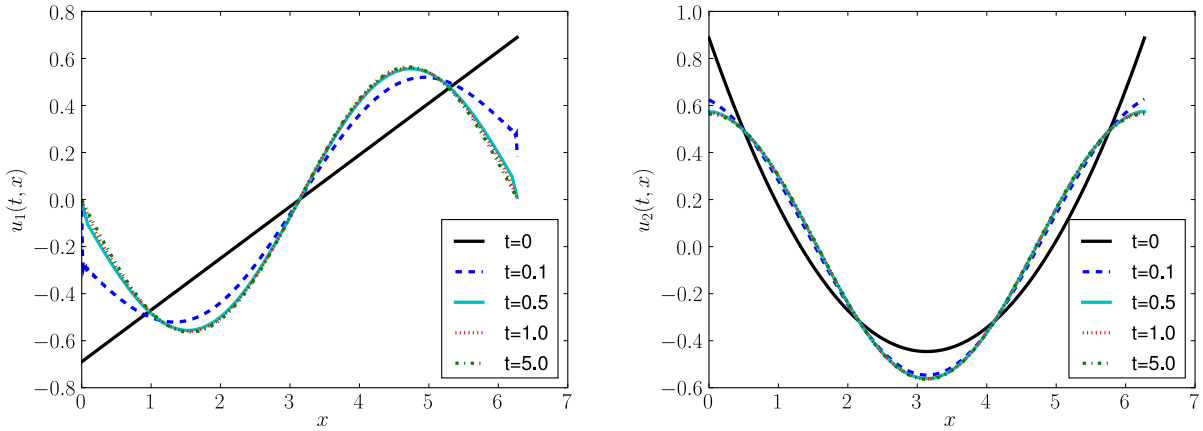

Figure 6.2: $V(t;w) = V(w) = \xi \sim N(0, \sigma^2)$ with $\sigma = 0.1$. Left: u_1, Right: u_2. Initially u_1 and u_2 are polynomials of first and second-degree, respectively. They evolve via the DO evolution equation and change into the Fourier basis. Once they become the Fourier basis, they are invariant.

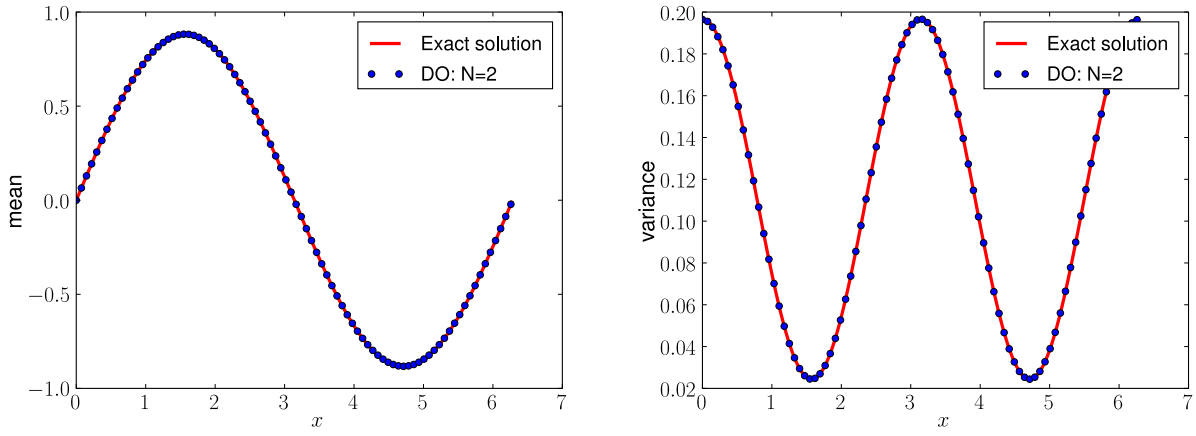

Figure 6.3: $V(t;w) = V(w) = \xi \sim N(0, \sigma^2)$ with $\sigma = 0.1$. Mean (left) and variance (right) of the advection equation at $t_f = 5$ with the initial condition for u_i being orthogonal polynomials. The parameters are $\sigma = 0.1, N_s = 128$ and $N_r = 32$.

6.3.2 Hybrid gPC-tKL method

We only present hybrid gPC-DO method but hybrid gPC-BO shows as good an accuracy as the gPC-DO. The number of DO modes N should be chosen in such a way that the KL decomposition of the solution with N terms approximates well the solution $u(x,t;\omega)$. The switching time from gPC to DO is chosen as $t_s = 0.001$. In other words, for this simple linear problem only one time step for the probabilistic collocation method may be used to switch over to DO method. The spatial basis derived from KL decomposition at $t_s = 0.001$ is, in fact, the Fourier basis so it does not change in time as suggested by the exact DO formulas for the spatial basis, *i.e.* the linear subspace does not evolve but remains invariant in time. Figure 6.4 shows the mean and variance at $t = 5$ with the hybrid method with $t_s = 0.001$.

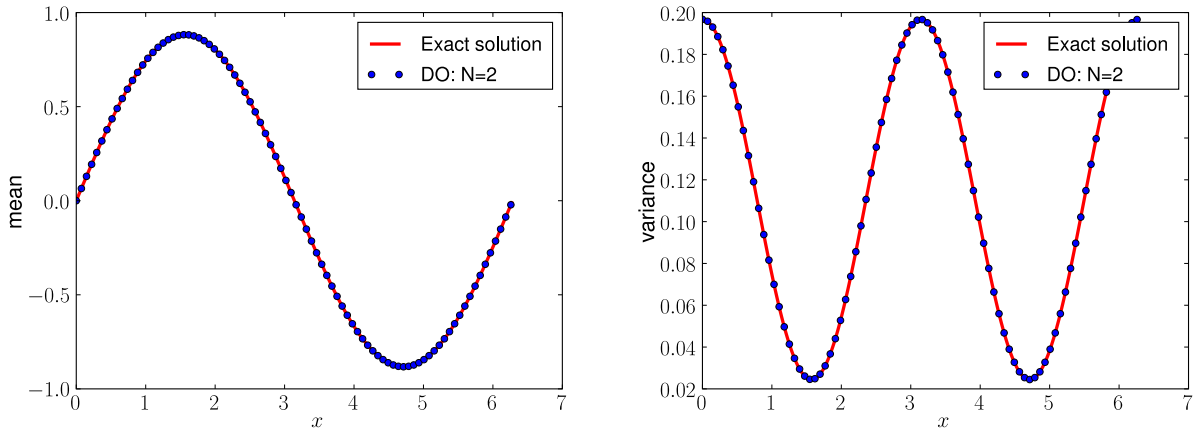

Figure 6.4: $V(t;w) = V(w) = \xi \sim N(0,\sigma^2)$ with $\sigma = 0.1$. Mean (left) and variance (right) of the advection equation at $t_f = 5$ from hybrid gPC-DO. They agree well with the exact solution. The parameters are $\sigma = 0.1, N_s = 128$ and $N_r = 32$.

We now examine the error of the mean and variance and compare them with those from PCM. Both have the same parameters such as Δt, N_s and N_r for numerical discretization. As shown in Figure 6.5, DO have as good an accuracy as PCM does for the mean and variance. However, DO are faster than PCM as will be demonstrated

in the next section.

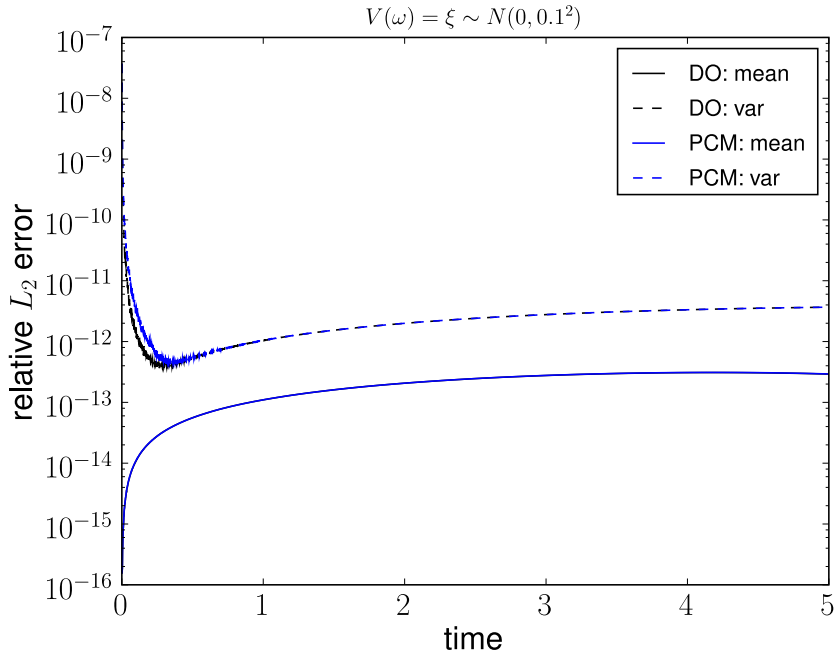

Figure 6.5: $V(t;w) = V(w) = \xi \sim N(0, \sigma^2)$ with $\sigma = 0.1$. Errors in the mean and variance using DO and PCM are identical.

Since the exact formulas for the spatial and stochastic basis are known as in Equations (6.8a)-(6.8d) we can compute the errors of each component, and they are shown in Figure 6.6. While the error of u_i stays constant in time, the error of Y_i increases in time, hence it accounts for the increase of the error of the variance since the covariance matrix of the stochastic coefficients is involved in the variance.

6.4 Numerical results for time-dependent $V(t;\omega)$

We consider the case where $V(t;\omega)$ is described by the exponential covariance in time, *i.e.* $C_V(t_1, t_2) = \sigma \exp(-\frac{|t_1 - t_2|}{L})$ and L is the correlation length that characterizes the stochastic process.

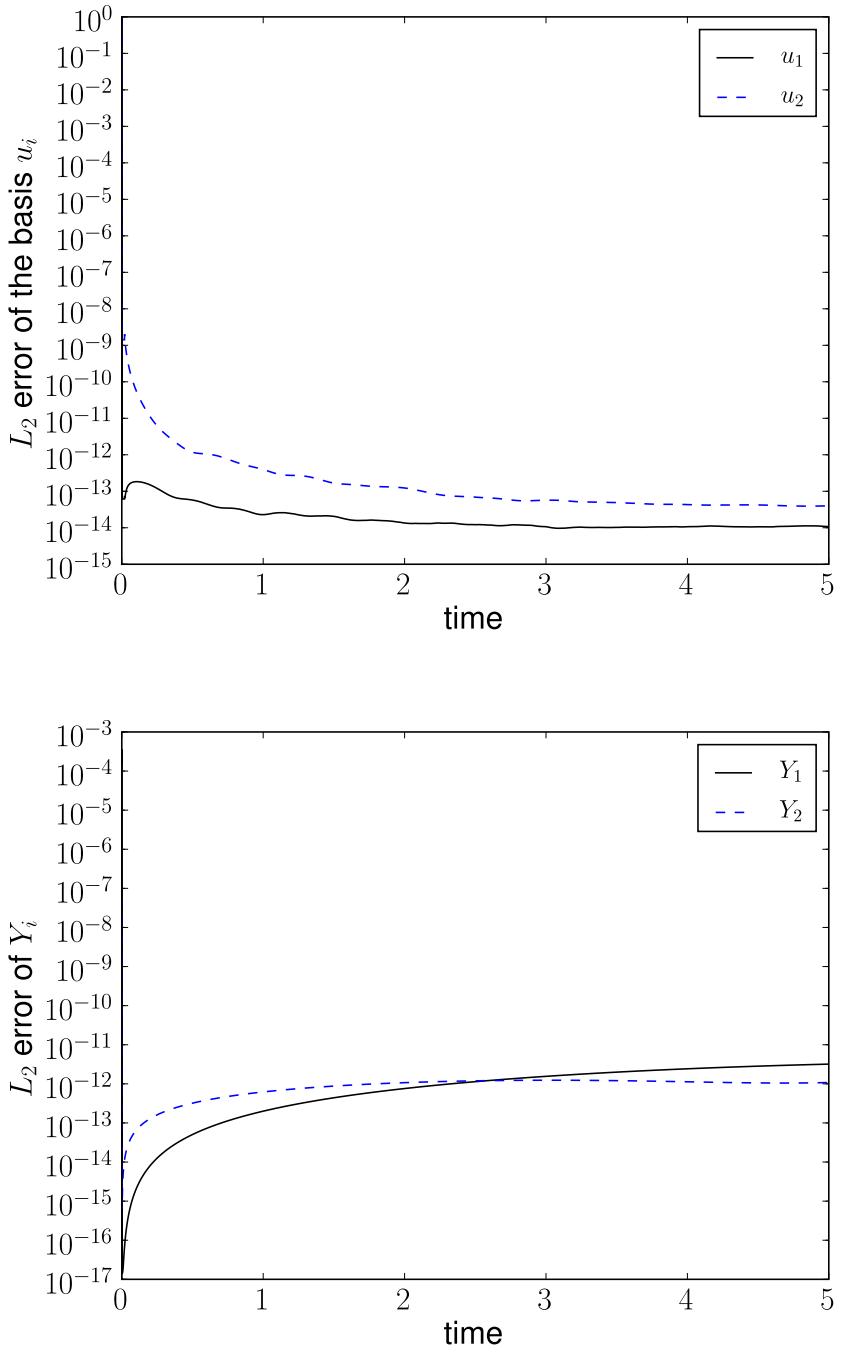

Figure 6.6: $V(t;w) = V(w) = \xi \sim N(0, \sigma^2)$ with $\sigma = 0.1$. The error of DO components u_i (top) and Y_i (bottom) , $i = 1, 2$. The error for Y_i increases in time, and it accounts for the increase of the error of the variance.

The parameters are

$$\Delta t = 10^{-3}, L = 5, \sigma = 0.1, t_f = 5, N_s = 128.$$

Energy	Dimension (M)
95%	5
99%	18
99.9%	68

Table 6.1: Dimension (or number of terms in the KL decomposition) of the parametric space with respect to energy.

We use the third-order Adams-Bashforth (AB3) as a time-integrator to minimize the error due to the time discretization. We use KL decomposition to discretize $V(t;\omega)$ and the dimension of random space is determined by how many terms in the KL decomposition we keep. Table 6.1 shows the dimension of the parametric space with respect to the percentage of energy above which we keep the terms. The more terms M we keep the more energy we have. Therefore if we keep more terms, we expect better accuracy as they approximate better to true $V(t;\omega)$. However this makes parametric space high-dimensional and hence computation more challenging. We solve the stochastic advection equation using three methods; the first two are the hybrid gPC-BO and gPC-DO methods and the other one is the probabilistic collocation method (PCM) which is one of the stochastic spectral methods along with the generalized Polynomial Chaos (gPC) [15, 42, 48]. As we increase the dimensionality of the parametric space by adding more terms in the KL decomposition of $V(t;\omega)$, the error of the mean and variance decreases as shown in Figure 6.7. Note that, like the time-independent case, DO or BO and PCM has the same order of magnitude of the error when they use the same parameters for numerical discretization. However, DO or BO is much faster than PCM, especially for high-dimensional parametric space as shown in Figure 6.8. This reveals one of the advantages of the tKL methods over gPC.

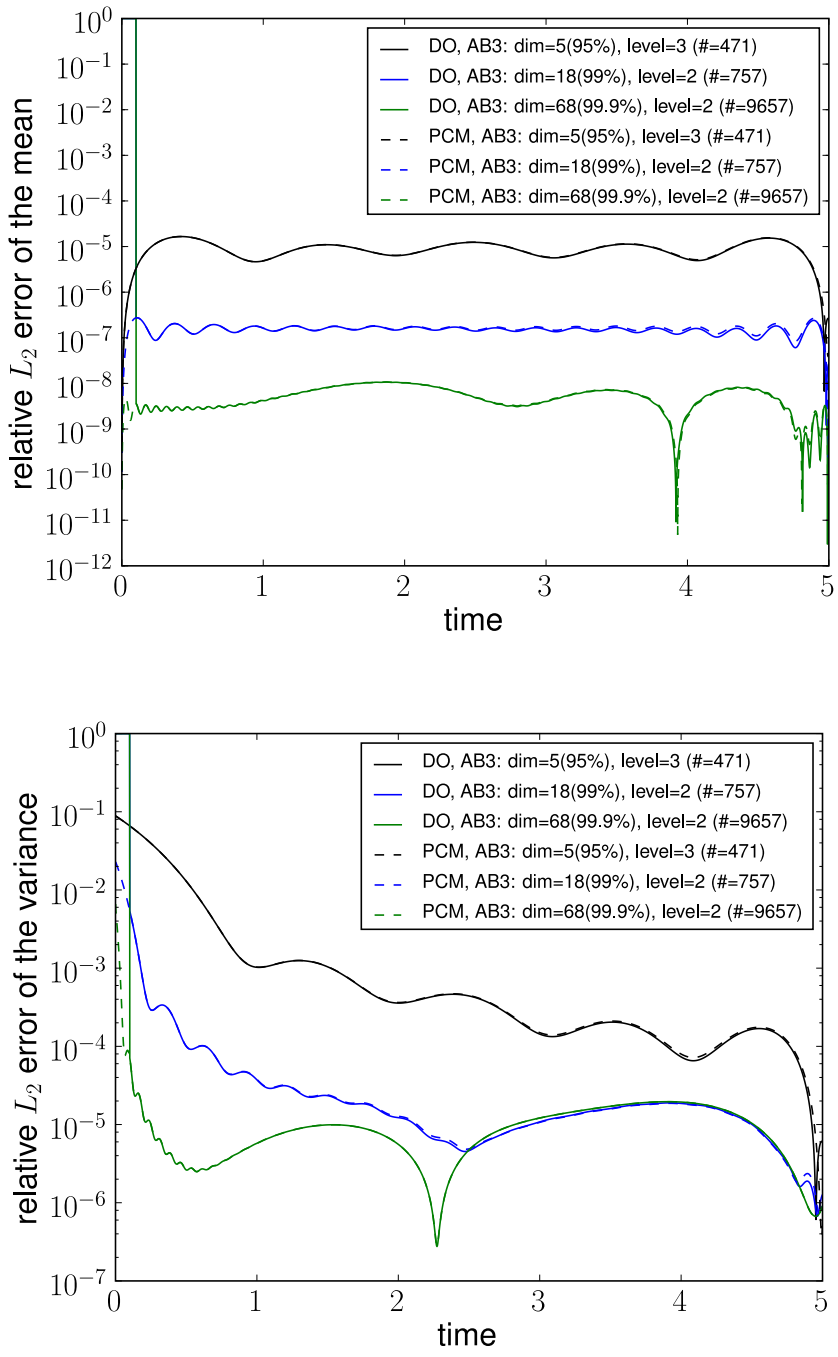

Figure 6.7: Relative L_2 error for the mean (top) and variance (bottom). The reference solution for the mean and variance is from the exact formula. As we increase the dimension of the random space i.e. we approximate $V(t;\omega)$ better with more terms, the relative L_2 error decreases. Note that BO results do not appear in these plots but they have exactly the same accuracy as DO. (AB3 refers to the third-order Adams-Bashforth integration, and "level" refers to the level of the sparse grid.)

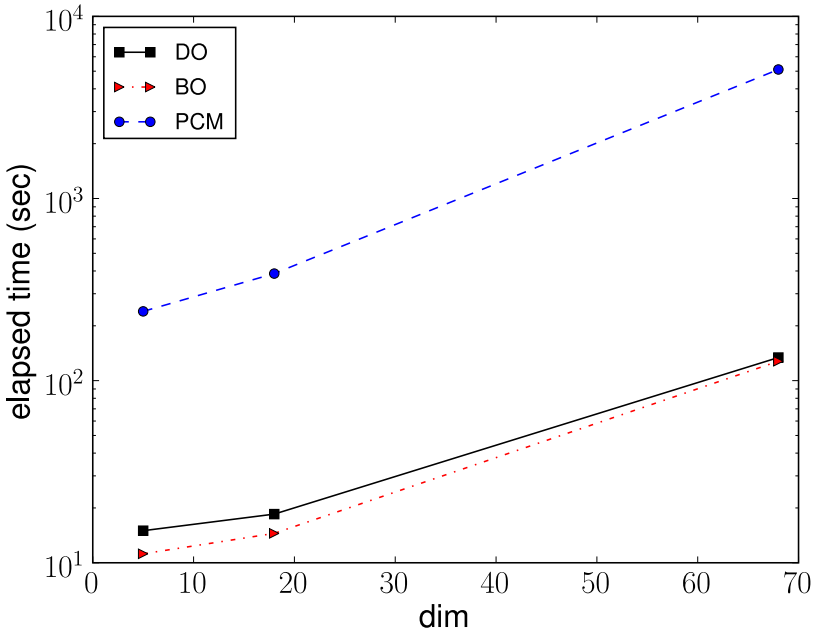

Figure 6.8: Computational time on Intel Xeon X5550 2.67GHz to solve the advection problem up to time $t = 5$ using DO, BO and PCM. DO is much faster than PCM, especially in high dimensions, and BO is slightly faster than DO for low dimensions.

Chapter 7

Applications to non-linear problems: Burgers equations

The objective of this chapter is to give a general algorithmic framework to solve stochastic Burgers (nonlinear) equations using the DO and BO methods. The problems we are interested in has the form

$$\begin{aligned} \frac{\partial u}{\partial t} + u\frac{\partial u}{\partial x} &= \nu\frac{\partial^2 u}{\partial x^2} + F(x,t;\omega), \quad \forall (t,x) \in [0,T] \times D = [0,2\pi] \qquad (7.1a) \\ u(0,x) &= g(x), \quad \forall x \in D, \end{aligned}$$

where $F(x,t;\omega)$ is a forcing term. The Burgers equation is nonlinear and has many interesting behaviors that make it a good problem to test the developed methodology i.e., the DO and BO in this thesis.

We consider various cases; in Section 7.1, assuming that the basis and stochastic coefficients are known exactly, we obtain the proper forcing in the Burgers equation and show that the DO method tracks the non-Gaussian behavior of the stochastic

basis well. In Section 7.2, we consider the Burgers equation with random forcing and demonstrate convergence with respect to the number of DO or BO modes. In Section 7.3, we illustrate how the BO suffers from eigenvalue crossing and then in Section 7.4, we present the examples to show how the adaptive strategies such as switching between the BO and DO and adaptively adding and removing modes can be applied to increase the accuracy.

7.1 Case A: exact DO components

In this section we consider the basis to be periodic in space and time as follows:

$$u_n(x,t) = \frac{1}{\sqrt{\pi}} \cos(nx - c_n t), \quad x \in [0, 2\pi], \quad n = 1, 2, ..., \quad c_n \in \mathbb{R}.$$

Then, we can easily show that the spatial basis defined above satisfy the DO condition, i.e.

$$\left\langle \frac{\partial u_n}{\partial t}, u_m \right\rangle = 0 \quad \text{and} \quad \langle u_n, u_m \rangle = \delta_{nm}.$$

We consider the stochastic basis as follows:

$$Y_i(t;\omega) = R_i \left(1 - e^{-t/T_i}\right) \cos(\lambda_i t + \varphi_i(\omega)) + \xi_i(\omega), \tag{7.2}$$

where $\xi_i(\omega)$ is a Gaussian random variable with mean zero and variance $\rho_i^2 R_i^2$, and $\varphi_i(\omega)$ is a uniform distribution in $[0, 2\pi]$, T_i and λ_i are timescales, and R_i are given positive quantities defining the magnitude of the stochastic basis.

By construction we can check that $E^\omega[Y_i(t;\omega)] = 0$, and moreover, for $i \neq j$, $E^\omega[Y_i(t;\omega) Y_j(t;\omega)] = 0$ while, for $i = j$,

$$E^{\omega}\left[Y_i\left(t;\omega\right)Y_j\left(s;\omega\right)\right] = R_i^2\left[\rho_i^2 + \tfrac{1}{2}\left(1-e^{-t/T_i}\right)\left(1-e^{-s/T_i}\right)\cos\left[\lambda_i\left(t-s\right)\right]\right].$$

For $t=0$, we have $Y_i\left(t;\omega\right)|_{t=0} = \xi_i(\omega)$, *i.e.*, the stochastic coefficients are normally distributed while, for large t, we have that

$$Y_i\left(t;\omega\right) = R_i\cos\left(\lambda_i t + \varphi_i\left(\omega\right)\right) + \xi_i\left(\omega\right)$$

since $1-e^{-t/T_i} \approx 1$. Depending on the coefficients R_i and λ_i, Y_i evolves from Gaussian into non-Gaussian as time goes on. We assume that the mean of the solution is zero for every time. Then, we have:

$$u\left(x,t;\omega\right) = \sum_{n=1}^{N}\frac{1}{\sqrt{\pi}}\left(R_n\left(1-e^{-t/T_n}\right)\cos\left(\lambda_n t + \varphi_n\left(\omega\right)\right) + \xi_n\left(\omega\right)\right)\cos\left(nx - c_n t\right) \tag{7.3}$$

and the Burgers equation

$$\frac{\partial u}{\partial t} + \frac{\partial u}{\partial x}u - \nu\frac{\partial^2 u}{\partial x^2} = F\left(x,t;\omega\right), \tag{7.4}$$

where the corresponding forcing is given by

$$\begin{aligned}
F\left(x,t;\omega\right) \;=\; & \sum_{n=1}^{N}\frac{R_n}{\sqrt{\pi}}\frac{e^{-t/T_n}}{T_n}\cos\left(\lambda_n t + \varphi_n\left(\omega\right)\right)\cos\left(nx - c_n t\right) \\
& - \sum_{n=1}^{N}\frac{R_n}{\sqrt{\pi}}\lambda_n\left(1-e^{-t/T_n}\right)\sin\left(\lambda_n t + \varphi_n\left(\omega\right)\right)\cos\left(nx - c_n t\right) \\
& + \sum_{n=1}^{N}\frac{c_n}{\sqrt{\pi}}Y_n\left(t;\omega\right)\sin\left(nx - c_n t\right) \\
& + \nu\sum_{n=1}^{N}\frac{n^2}{\sqrt{\pi}}Y_n\left(t;\omega\right)\cos\left(nx - c_n t\right) \\
& - \sum_{n=1}^{N}\sum_{m=1}^{N}\frac{m}{\pi}Y_n\left(t;\omega\right)Y_m\left(t;\omega\right)\cos\left(nx - c_n t\right)\sin\left(mx - c_m t\right).
\end{aligned}$$

7.1.1 PDF of Y_i and the solution

We can derive the exact formula of the probability density function (PDF) of the stochastic basis in Equation (7.2) and hence the solution $u(x,t;\omega)$. For simplicity, we consider $N=1$ but it can be extended easily to the case with many dimensions. We need the following two lemmas [78].

Lemma 4. *Let X, Z be two $\mathcal{R}$-valued independent random variables and let $Y = X+Z$. If X and Y has a density f_X and f_Z, respectively, then the PDF of Y is the convolution of f_X and f_Z:*

$$f_Y(y) = \int f_X(z-y) f_Z(z) dz = \int f_X(x) f_Z(y-x) dx. \tag{7.5}$$

Lemma 5. *Let $S \in \mathcal{B}^n$ be partitioned into disjoint subsets $S_0, S_1, ..., S_m$ such that $\cup_{i=0}^m S_i = S$, and such that $m_n(S_0) = 0$ where m_n is a Lebesgue measure on $(\mathcal{R}^n, \mathcal{B}^n)$, and that for each $i = 1, ..., , g : S_i \to \mathcal{R}^n$ is injective and continuously differentiable with non-vanishing Jacobian. Let $Y = g(X)$, where X is an $\mathcal{R}^n$-valued random variable with values in S and with density f_X. Then, Y has a density given by*

$$f_Y(y) = \sum_{i=1}^{m} f_X(g_i^{-1}(y)) |det J_{g_i^{-1}}(y)| \tag{7.6}$$

where g_i^{-1} denotes the inverse map $g_i^{-1} : g(S_i) \to S_i$ and $J_{g_i^{-1}}$ is its corresponding Jacobian matrix.

Let $\Theta = \varphi, X = \xi \sim N(0, \sigma^2), Z = a(t)\cos(\lambda t + \Theta) = g(\Theta)$ and $Y = X + Z$ with $\sigma = R\rho$ and $a(t) = R(1 - \exp(-t/T))$. First, we compute the PDF of Z using Lemma 5. We can decompose $S = [0, 2\pi] = S_1 \cup S_2$, where $S_1 = [0, \pi]$ and $S_2 = [\pi, 2\pi]$. Since Θ is a uniform distribution on $S_1 \cup S_2$ and $g(\theta)$ is identical on S_1 and S_2 (up to sign), we only need to consider the domain S_1 to compute the PDF of Z. The phase

does not affect the PDF of Z and hence, in this case λt can be omitted to compute PDF of Z, *i.e.*, $f_Z = f_{a(t)cos(\Theta)}$. Note that

$$\begin{aligned} f_\Theta(\theta) &= \frac{1}{\pi}, \quad \text{for } \theta \in S_1 \\ g^{-1}(z) &= \arccos(z), \quad J_{g^{-1}}(z) = -\frac{1}{\sqrt{1-z^2}} \text{ for } z \in [0,\pi], \end{aligned}$$

which gives us

$$f_Z(z) = \frac{1}{a\pi\sqrt{1-(z/R)^2}}.$$

Now we use Lemma 4 to derive the exact PDF of Y:

$$\begin{aligned} f_Y(y) &= \int_{-a}^{a} f_X(y-w) f_Z(w) dw \\ &= \int_{-a}^{a} \frac{1}{\sqrt{2\pi\sigma^2}} \exp\left(-\frac{(y-w)^2}{2\sigma^2}\right) \frac{1}{a\pi\sqrt{1-(w/a)^2}} dw \\ &= \int_{-1}^{1} \frac{1}{\sqrt{2\pi\sigma^2}} \exp\left(-\frac{(y-aw)^2}{2\sigma^2}\right) \frac{1}{\pi\sqrt{1-w^2}} dw \\ &= \frac{1}{\pi\sigma\sqrt{2\pi}} \int_0^{\pi} \exp\left(-\frac{(y-a\cos(x))^2}{2\sigma^2}\right) dx \end{aligned} \tag{7.7}$$

where the third and fourth equality follows from the change of variables. The integration in Equation (7.7) can be computed with high accuracy using Gaussian quadrature points since the integrand is smooth.

We can now derive the exact PDF of the solution $u(x,t;\omega)$ at x and time t by using Lemma 5 applied to $f_Y(y)$ because u is the multiplication of Y_1 by $u_1(x,t)$ that is a constant at fixed x and t. Hence, for a fixed x and t, the exact PDF of the solution is as follows:

$$f_u(\omega) = \frac{1}{A} f_Y\left(\frac{1}{A}\omega\right), \tag{7.8}$$

where $A = \frac{1}{\sqrt{\pi}}\cos(x - c_1 t)$. This result will be verified numerically in the next

subsection.

7.1.2 Computational results

The stochastic basis Y_1 depends on a number of parameters which determine the PDF. Here we study two different cases as shown in Table 7.1.

	Case I	Case II
T	0.1	0.1
λ	1	1
R	0.1	0.1
ρ	1	0.1

Table 7.1: Two different cases of parameters for Y_1.

Initially Y_1 is a Gaussian random variable with mean zero and variance $\rho^2 R^2$ but as time goes on, a uniform distribution is introduced through the trigonometric function in Equation (7.2) and hence, the PDF of Y_1 changes depending on the parameters. For case I and II, the PDF at time $t = 0$ and $t = 1$ is shown in Figure 7.1. For case I, the PDF follows the form of Gaussian PDF in time while, for case II, the PDF becomes bimodal so that it has two peaks whose value is far away from zero.

We solve the corresponding Burgers equation using the DO method and estimate the PDF of the stochastic coefficients and the solution at different times and compare them with exact PDF from Equations (7.7) and (7.8). The parameters for numerical discretization are as follows:

$$\Delta t = 0.001, t_f = 1, N = 1, N_s = 128, N_r = 16,$$

where N_r is the number of collocation points based on one-dimensional parametric

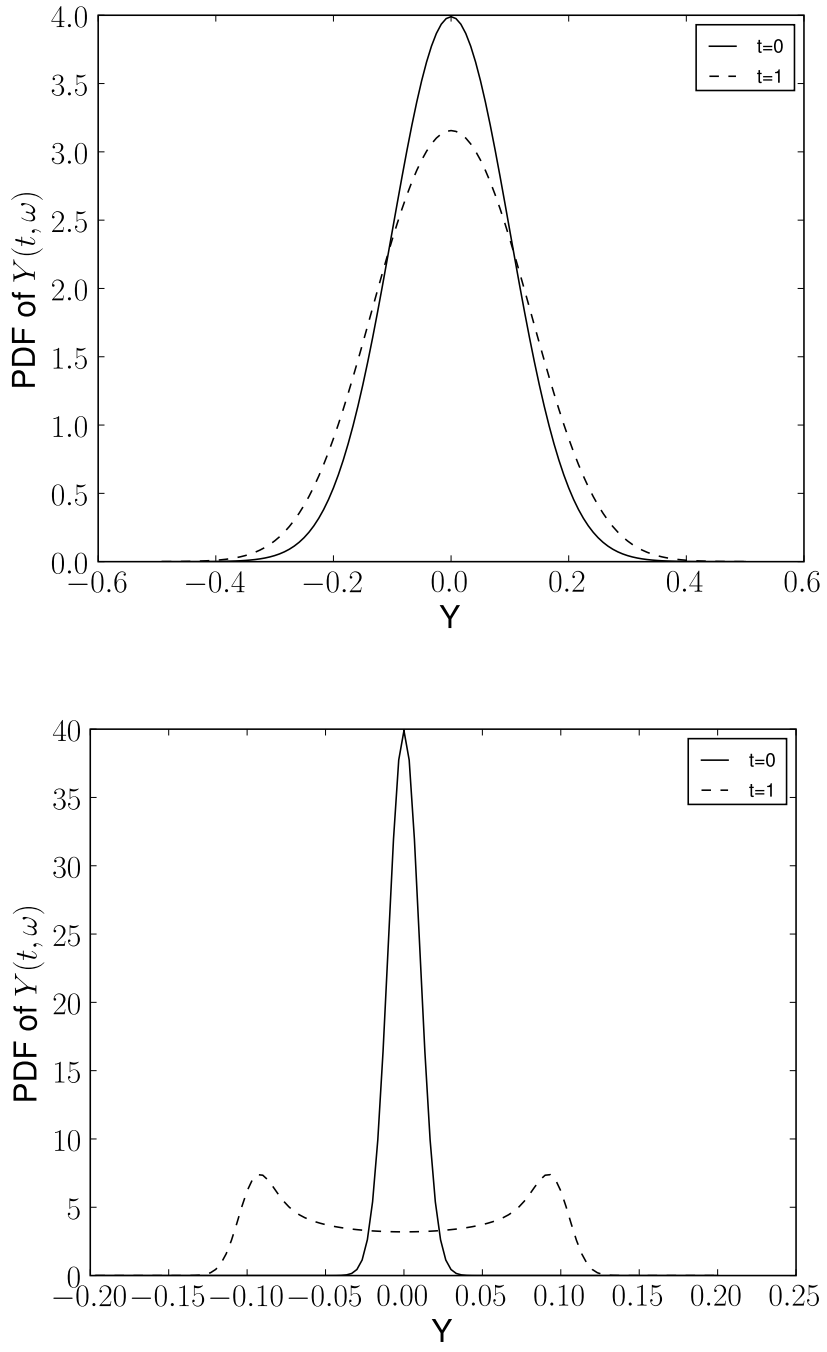

Figure 7.1: Case I (top) and case II (bottom). The PDF at $t = 0$ for both cases is Gaussian but as time goes on, the PDF for case II is bimodal while the PDF for case I remains Gaussian with larger variance.

space, and a tensor product representation is employed for the numerical discretization in the parametric space as the dimension of the parametric space, in this case two since we have two random variables for Y_1, is low.

Figure 7.2 shows the PDF of the stochastic basis and the solution at three different times $t = 0.1, 0.3$, and 1.0. The PDF of the stochastic coefficient maintains the Gaussian form in time with the variance being widened. Figure 7.3 shows the PDF of the stochastic coefficient and the solution at three different times $t = 0.1, 0.2$, and 1.0. The PDF of Y becomes non-Gaussian and has two peaks whose distance is increasing in time. The plots demonstrate that the DO method is able to capture both Gaussian and non-Gaussian behavior well.

DO and PCM are employed to compute the Burgers equation for comparison, and the L_2 errors of the mean and variance are shown in Figure 7.4. The same parameters are used for both DO and PCM and the errors are almost identical. Next, we compare the computational efficiency. In the advection equation where the dimension of the parametric space is high, we showed in Figure 6.8 that DO is much faster than PCM. The computational times with respect to the number of points in the parametric space are shown in Figure 7.5; DO is faster than PCM for this problem that has a low dimensional parametric space while the accuracy for both DO and PCM remains the same.

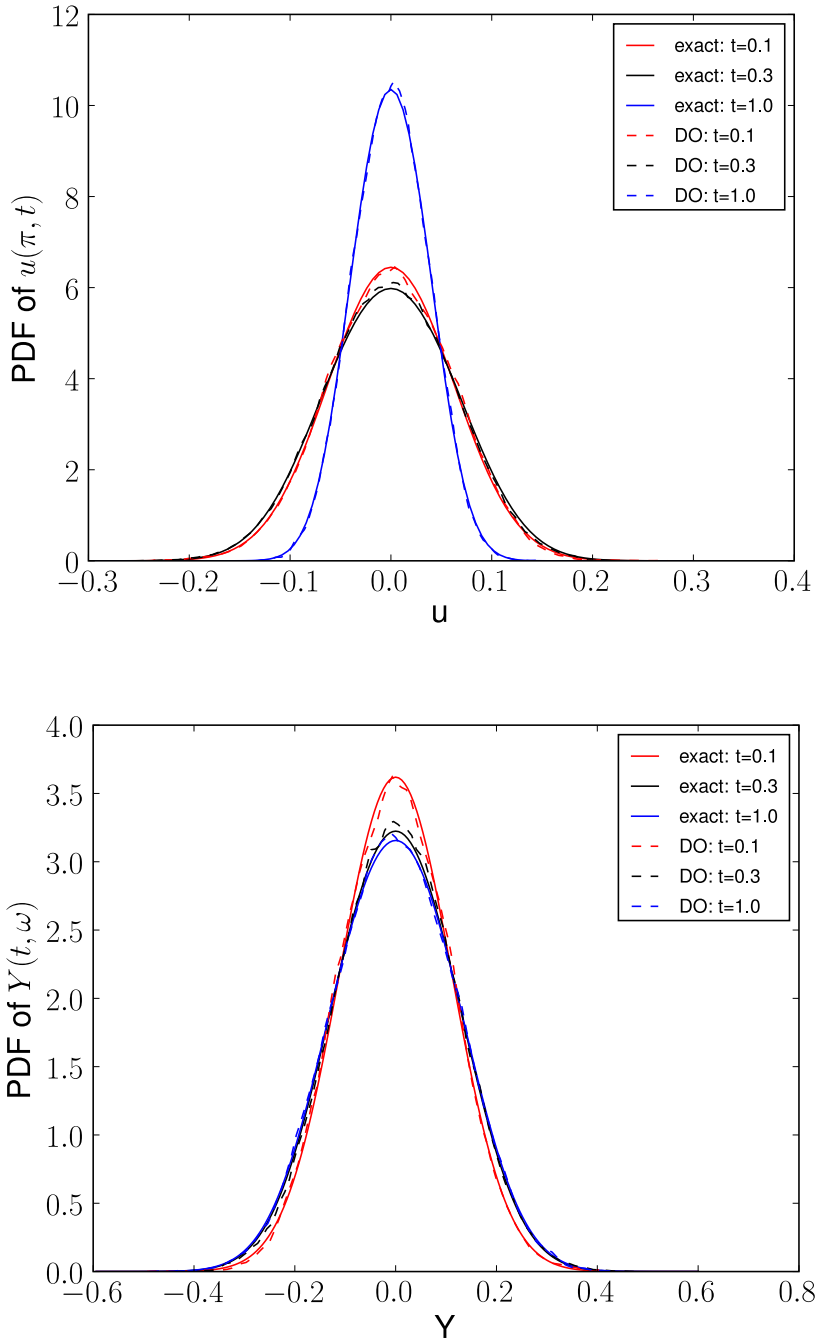

Figure 7.2: Case I. The PDF of the solution at $x = \pi$ (top) and the stochastic coefficient (bottom). The PDF maintains the Gaussian form at time $t = 1$, and DO is able to capture the PDF of the solution as well as the stochastic coefficients well.

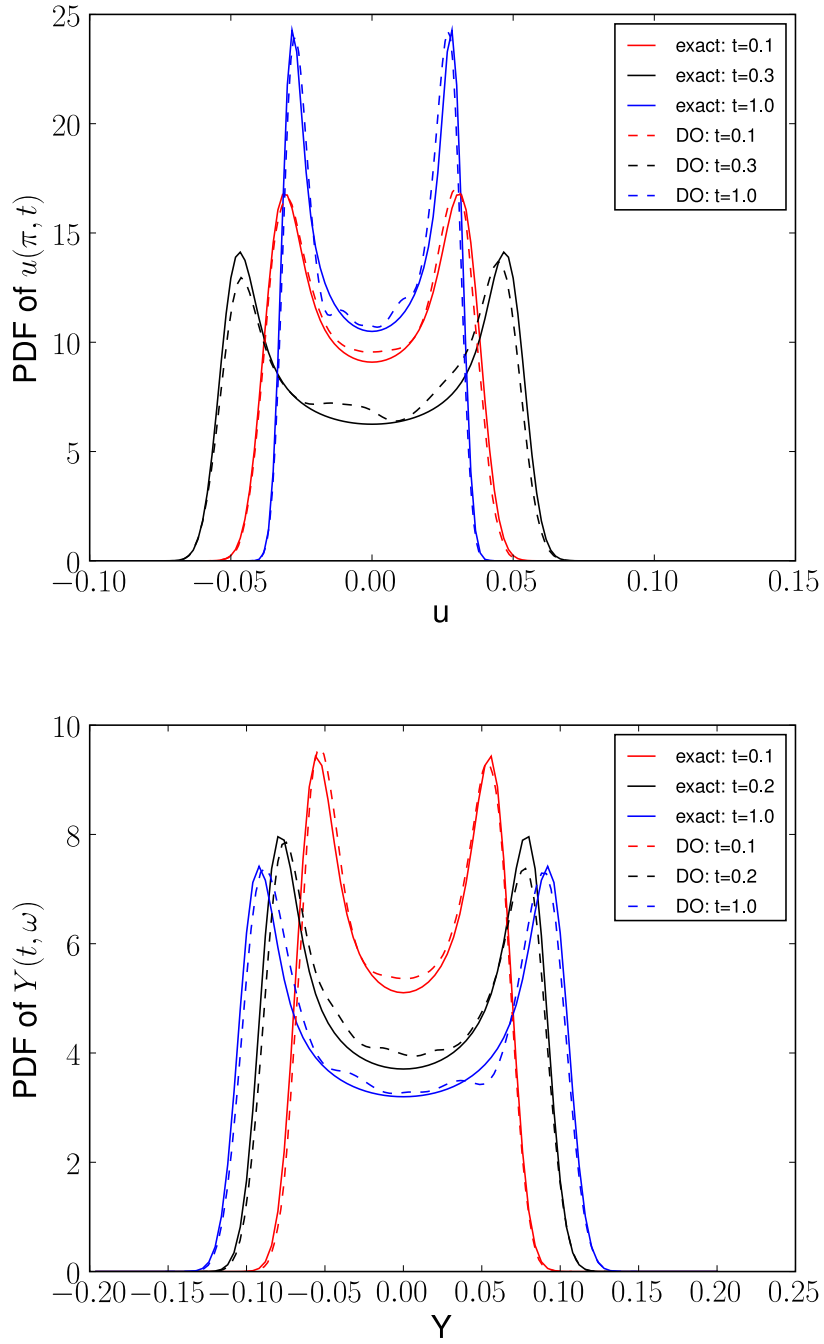

Figure 7.3: Case II. The PDF of the solution at $x = \pi$ (top) and the stochastic coefficient (bottom). The PDF evolves from Gaussian to non-Gaussian form, and DO is able to capture this behavior well.

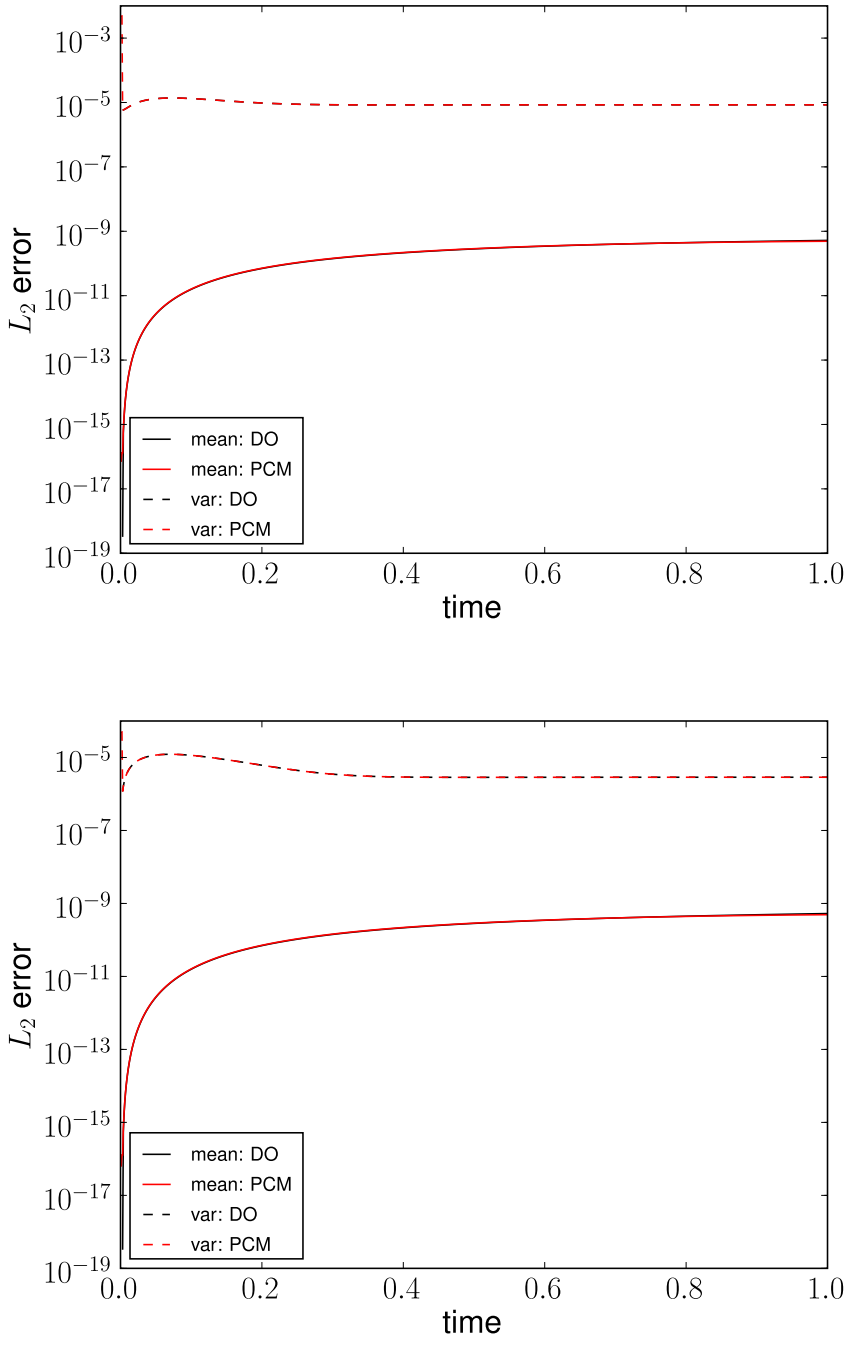

Figure 7.4: L_2 error of the mean and variance for case I (top) and case II (bottom). For both, DO and PCM exhibit the same accuracy.

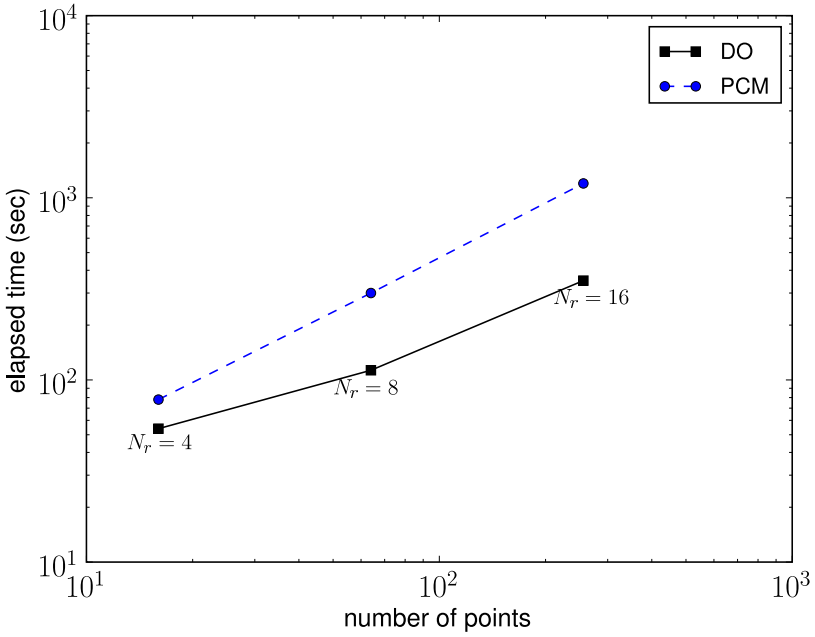

Figure 7.5: Computational time for PCM and DO. All parameters are the same for both PCM and DO. The number of the collocation points in one direction is denoted by N_r. Hence the total number of collocation points are N_r^2 since the dimension is 2 and tensor product is used. DO is faster than PCM while the accuracy for both methods is the same.

7.2 Case B: random forcing

In this section, we consider the following stochastic Burgers equation with random forcing

$$\begin{aligned} \frac{\partial u}{\partial t} + u\frac{\partial u}{\partial x} &= \nu\frac{\partial^2 u}{\partial x^2} + \frac{1+\xi}{2}\sin(2\pi t), \quad \forall (t,x) \in [0,T]\times D = [0,2\pi] \\ u(0,x) &= g(x), \quad \forall x \in D, \end{aligned} \tag{7.9}$$

where $\xi(\omega) \in [-1,1]$ is a uniformly distributed random variable and the initial condition $g(x)$ is given as

$$g(x) = 0.5\left(\exp(\cos(x)) - 1.5\right)\sin(x + 2\pi\cdot 0.37). \tag{7.10}$$

We take $\nu = 0.05$. Note that the period of the forcing is one. Using the DO representation, we obtain the form of the evolution operator $\mathcal{L}$ and some necessary forms:

$$\begin{aligned}
\mathcal{L}[u(x,t;\omega)] &= -uu_x + \nu u_{xx} + \frac{1+\xi}{2}\sin(2\pi t) \\
&= -\bar{u}\bar{u}_x - Y_i\frac{\partial}{\partial x}(u_i\bar{u}) - Y_iY_ju_i\frac{\partial u_j}{\partial x} + \nu\left(\bar{u}_{xx} + Y_i\frac{\partial^2 u_i}{\partial x^2}\right) + \frac{1+\xi}{2}\sin(2\pi t) \\
E[\mathcal{L}(u)] &= -\bar{u}\bar{u}_x - C_{ij}u_i\frac{\partial u_j}{\partial x} + \nu\bar{u}_{xx} + 0.5\sin(2\pi t) \\
E[\mathcal{L}(u)Y_j] &= -\left(C_{ij}u_i\bar{u}_x + C_{kj}\frac{\partial u_k}{\partial x}\bar{u} + C_{ikj}u_i\frac{\partial u_k}{\partial x}\right) \\
&\quad +\nu C_{ij}\frac{\partial^2 u_i}{\partial x^2} + E[\frac{\xi}{2}Y_j]\sin(2\pi t),
\end{aligned}$$

where $C_{ijk} = E[Y_iY_jY_k]$ and we employed the Einstein notation for simplifying equations. Note that $E[\mathcal{L}Y_j]$ involves the third moment of the stochastic coefficients and hence the PDE for u_i is more complicated than the linear problem, e.g. the stochastic advection equation in Chapter 6. Since the initial condition is deterministic, the $Y_i, i = 1, ..., N$ at the initial time become zero, which makes the covariance matrix for Y_i singular. We use the *hybrid gPC-tKL* introduced in Section 5.3 to avoid the singularity due to the deterministic initial condition, where it starts with PCM at the beginning and switches over to DO or BO after the stochasticity of the solution develops.

7.2.1 Numerical results: hybrid gPC-tKL methods

We need to march for many time steps to allow the stochasticity of the system to develop fully. We have performed sensitivity studies to investigate how to choose the switching time from PC to DO but a more systematic future study is required. We can choose the number of modes at the switching time based on the eigenvalues of

$C_{u(\cdot,t_s)}(x,y)$. The ten largest eigenvalues at ten different times $t = 0.5j, j = 1, ..., 10$ are shown in Figure 7.6. The eigenvalues increase as time goes on, which suggests that we need to adaptively add modes to maintain the accuracy in time.

The parameters are as follows:

$$\Delta t = 0.001, t_s = 1, t_f = 5, N_s = 128, N_r = 64, N = 6.$$

We choose $N = 6$ because, at the switching time $t_s = 1$, the sixth mode is the largest eigenmode whose eigenvalue is larger than a pre-specified threshold value. Fourier collocation in the physical space and Legendre-Gauss collocation in the parametric space are used for discretization, and third-order Adams-Bashforth (AB3) is used for a time integration. The mean and variance from the probabilistic collocation method with $N_r = 512$ using the fourth-order Runge-Kutta method are considered to be the reference solution.

The L_2 error for the mean and variance are shown in Figure 7.7; BO has better accuracy in variance than DO by one order of magnitude. DO and BO are tested with different number of modes up to 6. They have the same accuracy for the first four modes but BO is better than DO for higher modes. While they are equivalent as shown in section 4.2 this suggests that BO gives numerically more stable scheme than DO as shown in Figure 7.8; the DO evolution equation for the basis needs an inverse of matrix whose condition number for higher number is large that may affect numerical accuracy; further research is required in order to document this point. Figure 7.8 shows the exponential convergence obtained with respect to the number of modes at time $t = 5$. As mentioned above both DO and BO have the same accuracy with lower modes but BO is more accurate than DO with higher modes 5 and 6. This example is the first demonstration of the fast convergence of the DO or

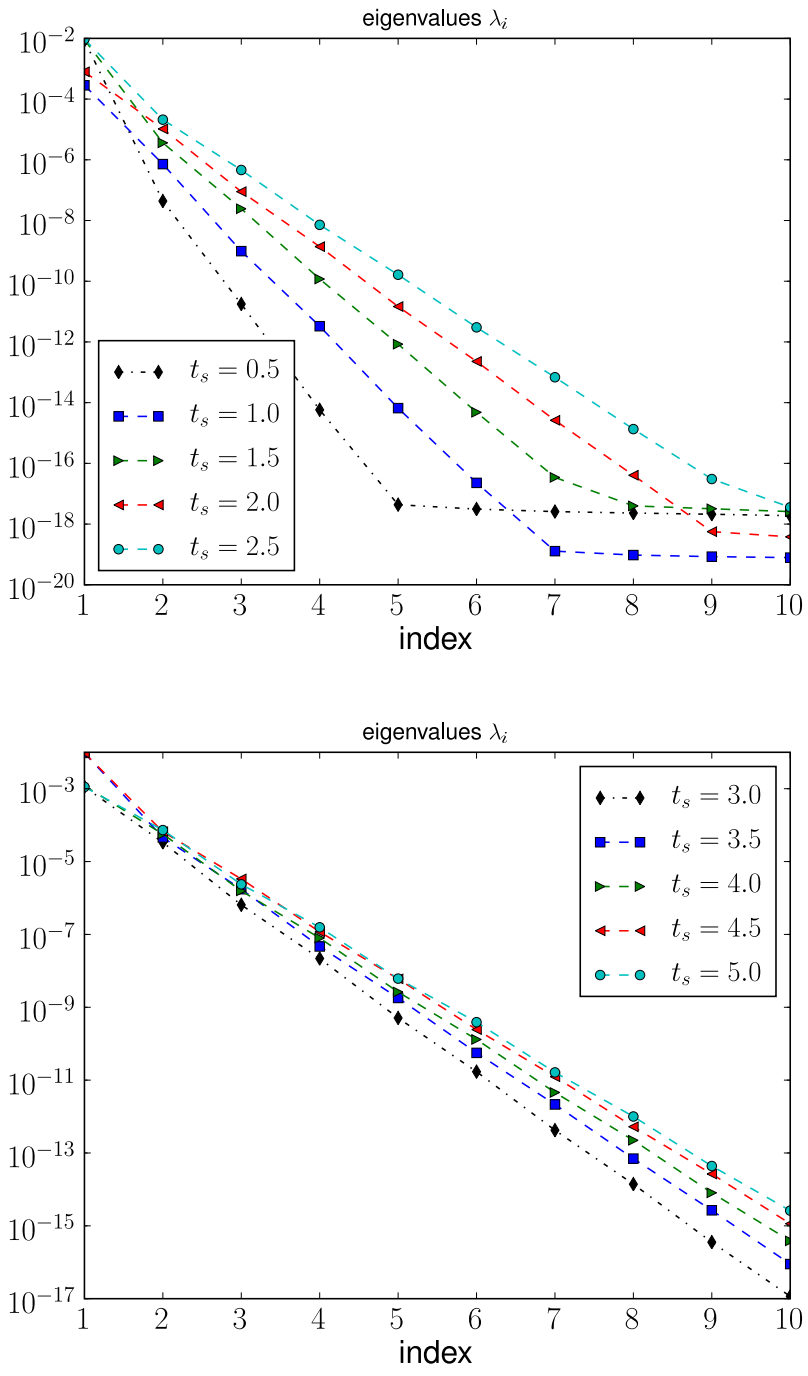

Figure 7.6: Ten largest eigenvalues of the KL expansion at ten different time $t = 0.5j, j = 1, ..., 10$. As time increases, the magnitude of eigenvalues increases. This provides a guideline on how many modes we need when switching from gPC to tKL. This also suggests that we need to adaptively add modes as time goes on that will be demonstrated in later section.

BO method for a nonlinear SPDE.

We now test the equivalence of DO and BO proved in the section 4.2. From the BO evolution equations we have the BO components at every time step. Then we derive the DO components not from the DO evolution equations but from equations (4.2a)-(4.2b) with P obtained from the matrix differential equation (4.3). The numerical integration method that preserves the orthogonality of the matrix P is employed. We compute the variance for the DO components derived from the BO components and compare this with the variances from the BO and DO. Figure 7.9 shows the error in the variances of these three methods. The variance from the DO via the matrix differential equation from the BO is in between that of the BO and DO. It is worse than the BO because a first-order time integration method for the matrix differential equation is employed while a third-order time integration method is employed for the BO and DO. This verifies numerically the equivalence of the BO and DO in the sense that one can be obtained from the other through the matrix differential equations and vice versa.

7.3 Case C: Eigenvalue crossing

When the eigenvalues of the system cross each other in time, the BO evolution equations become singular because the matrix M and S in the Equations (3.19) and (3.18) are singular. In this section we consider the Burgers equation where eigenvalues cross in time. For this we assume that the solution has an explicit form

$$u_\infty(x,t;\omega) = \xi_1(\omega)a_1(t)\cos(x-t) + \xi_2(\omega)a_2(t)\cos(2x-3t). \tag{7.11}$$

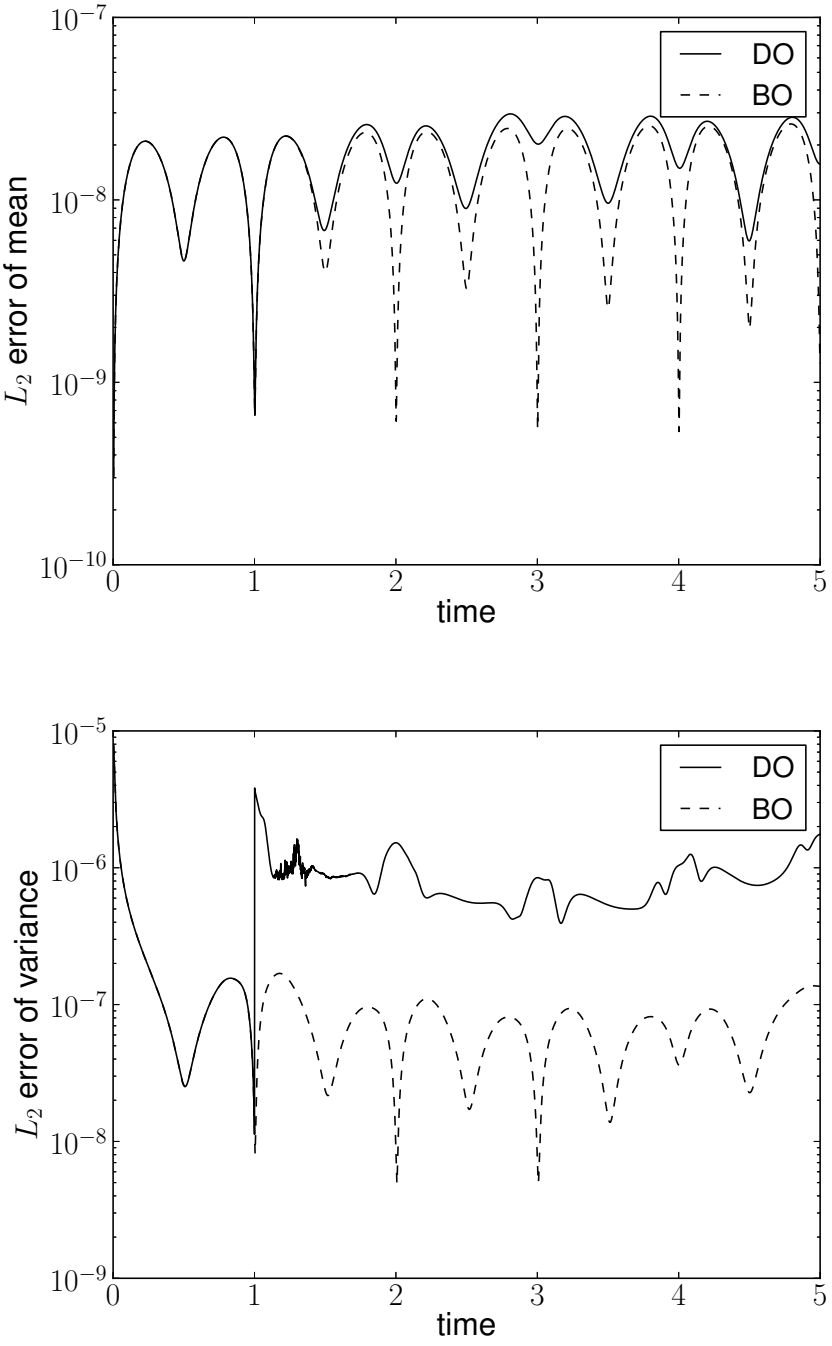

Figure 7.7: Relative L_2 error for the mean (top) and variance (bottom) of the solution for the Burgers equation with random forcing using DO and BO with $N = 6$. Both methods have the same accuracy for the mean while BO is an order of magnitude more accurate compared to DO for the variance. BO is numerically more stable than DO for high modes while they have the same accuracy for low modes. Note that the switching time is 1 and the error before the switching time is the same as collocation method is used in the hybrid method.

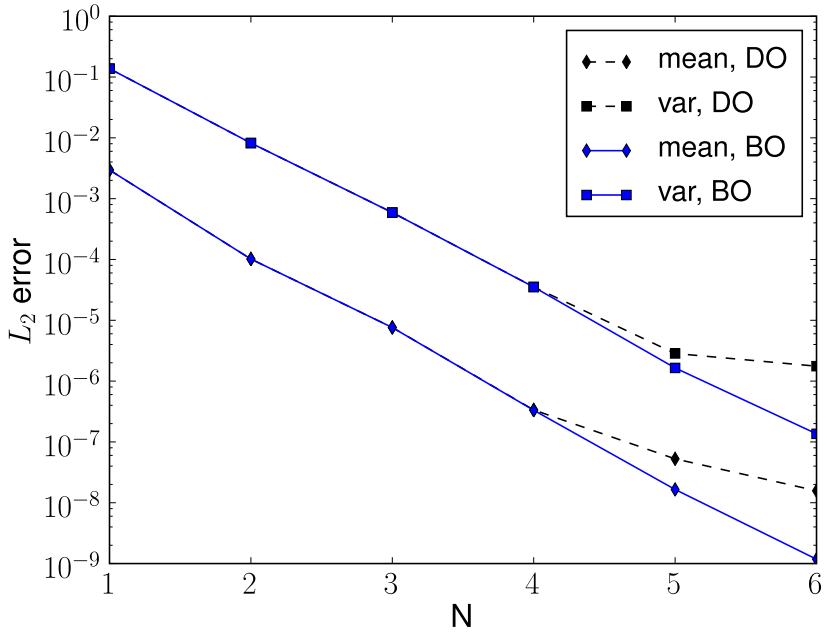

Figure 7.8: Relative L_2 error for the mean and variance at $t = 5$. Exponential convergence is observed as the number of modes increases. They have the same accuracy through $N = 4$ but BO is better than DO for high modes.

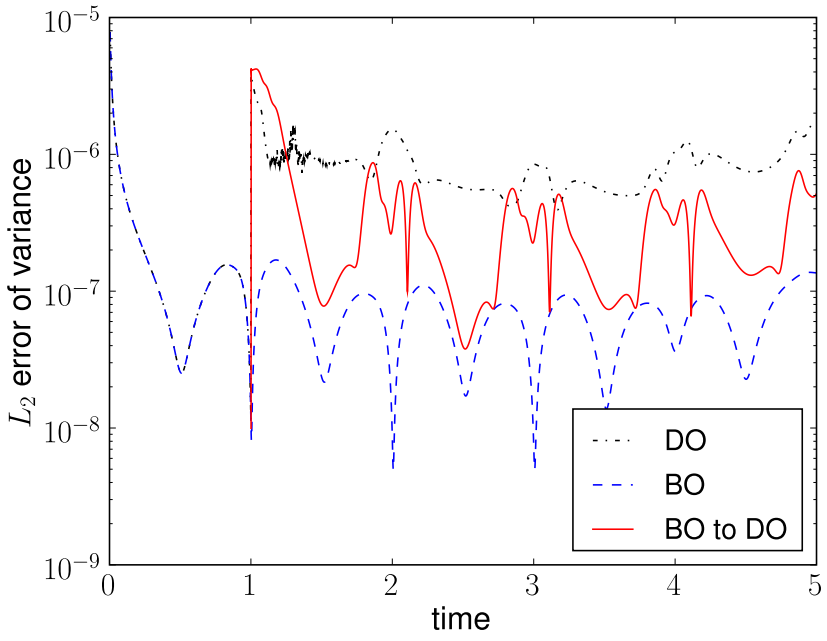

Figure 7.9: Relative L_2 error for the variance at $t = 5$ with $N = 6$. The top one is the variance from the DO evolution equations; the bottom from the BO evolution equations; the middle one from the DO components via the dynamical transformation from the BO.

The forcing term is chosen accordingly. We assume

$$a_1(t) = \sin(t), \quad a_2(t) = \cos(3t), \tag{7.12}$$

and ξ_1 and ξ_2 follow the uniform distribution on $[0, 1]$. Then the exact solution for the mean and variance has an explicit form by taking the expectation on u_∞. The eigenvalues of the system are

$$\lambda_1(t) = \frac{\pi}{12} a_1^2(t), \quad \lambda_2(t) = \frac{\pi}{12} a_2^2(t). \tag{7.13}$$

The BO and DO methods are tested with the following parameters:

$$\delta t = 10^{-4}, \nu = 0.1, t_f = 3.14, t_s = 0.01, N = 2, N_s = 128, N_r = 256. \tag{7.14}$$

where t_s is the switching time from gPC to tKL and the number of collocation points in each parametric space is 16, hence the total number comes to 256 as we have two random variables.

The eigenvalues cross each other for this example as shown in Figure 7.10 and correspondingly M_{12}, that is $(1, 2)$-entry of matrix M defined in Equation (3.19), jumps sharply whenever the eigenvalues cross, and this causes the numerical instability for BO.

Figure 7.11 shows the L_2 error of the mean and variance for BO and DO and the numerical instability for BO arising when there is eigenvalue crossing. In order to avoid the singularity in the BO, it is proposed in [2] to freeze the stochastic coefficients temporarily and evolve only the basis when facing the eigenvalue crossing. However, the DO evolution equations does not suffer from the eigenvalue crossing.

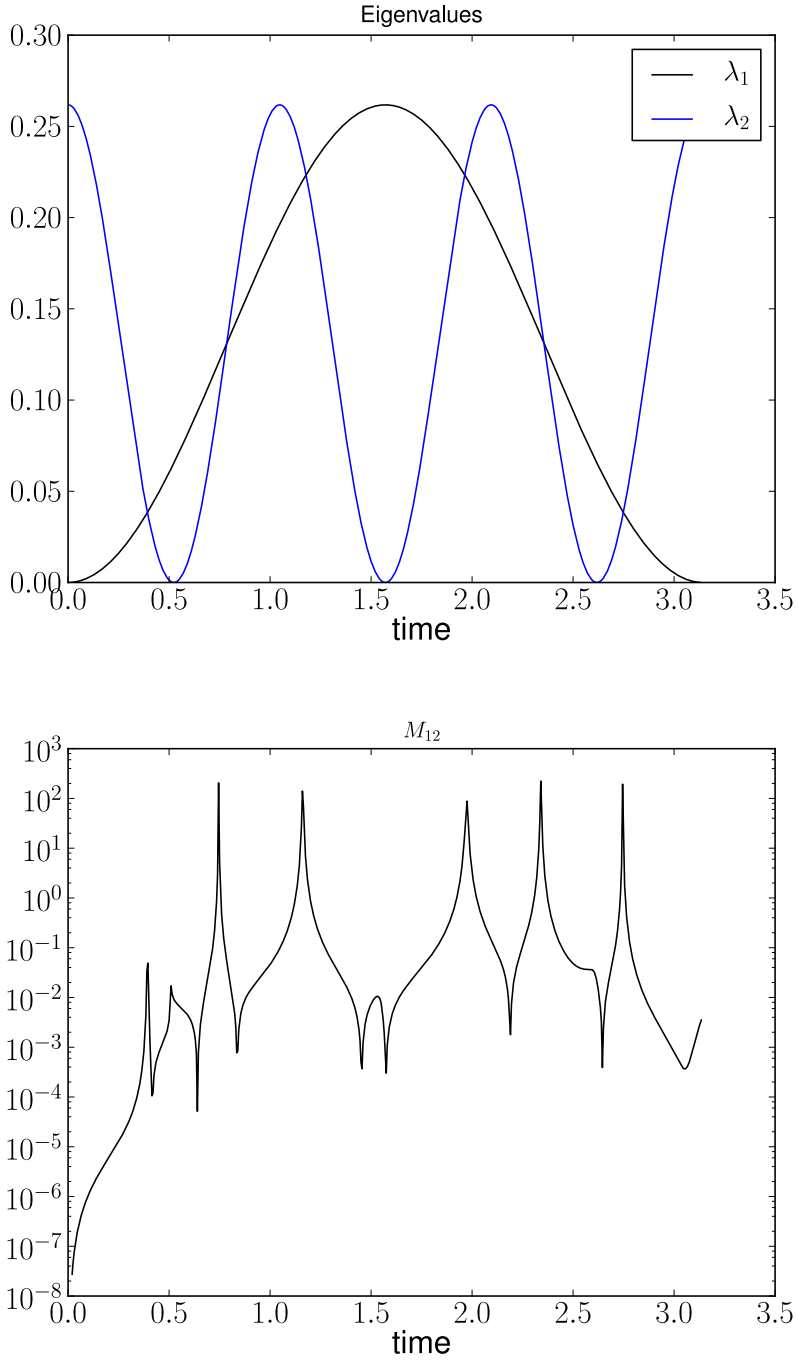

Figure 7.10: Left: eigenvalues, right: M_{12}. The eigenvalues cross out at the six locations at which M_{12} peaks as shown in the bottom Figure.

As introduced in Section 5.4.1, we can employ hybrid BO-DO by switching from the BO to DO utilizing the relation between the BO and DO in order to avoid the singularity due to eigenvalue crossing, that would be presented in the next section.

7.4 Adaptive algorithm

We consider the Burgers equation to demonstrate the adaptive algorithm presented in section 5.4:

$$u_t + uu_x = \nu u_{xx} + f(x,t;\omega). \tag{7.15}$$

We present two different Burgers example to describe two adaptive strategies: i) the hybrid BO-DO in subsection 7.4.1 and ii) adaptively adding and removing modes in subsection 7.4.2.

7.4.1 The hybrid BO-DO

For the illustration we assume that we know the solution that is random:

$$u_\infty(x,t;\omega) = \bar{u}(x,t) + \Phi_1(\xi_1(\omega))a_1(t)\cos(x-t) + \Phi_2(\xi_2(\omega))a_2(t)\cos(2x-3t) \tag{7.16}$$

where $\bar{u}(x,t) = \sin(x-t)$ and $\xi_1(\omega)$ and $\xi_2(\omega)$ are independent uniform random variables on $[0,1]$ and $\Phi_1(\xi_1)$ and $\Phi_2(\xi_2)$ are Legendre polynomials of the first order

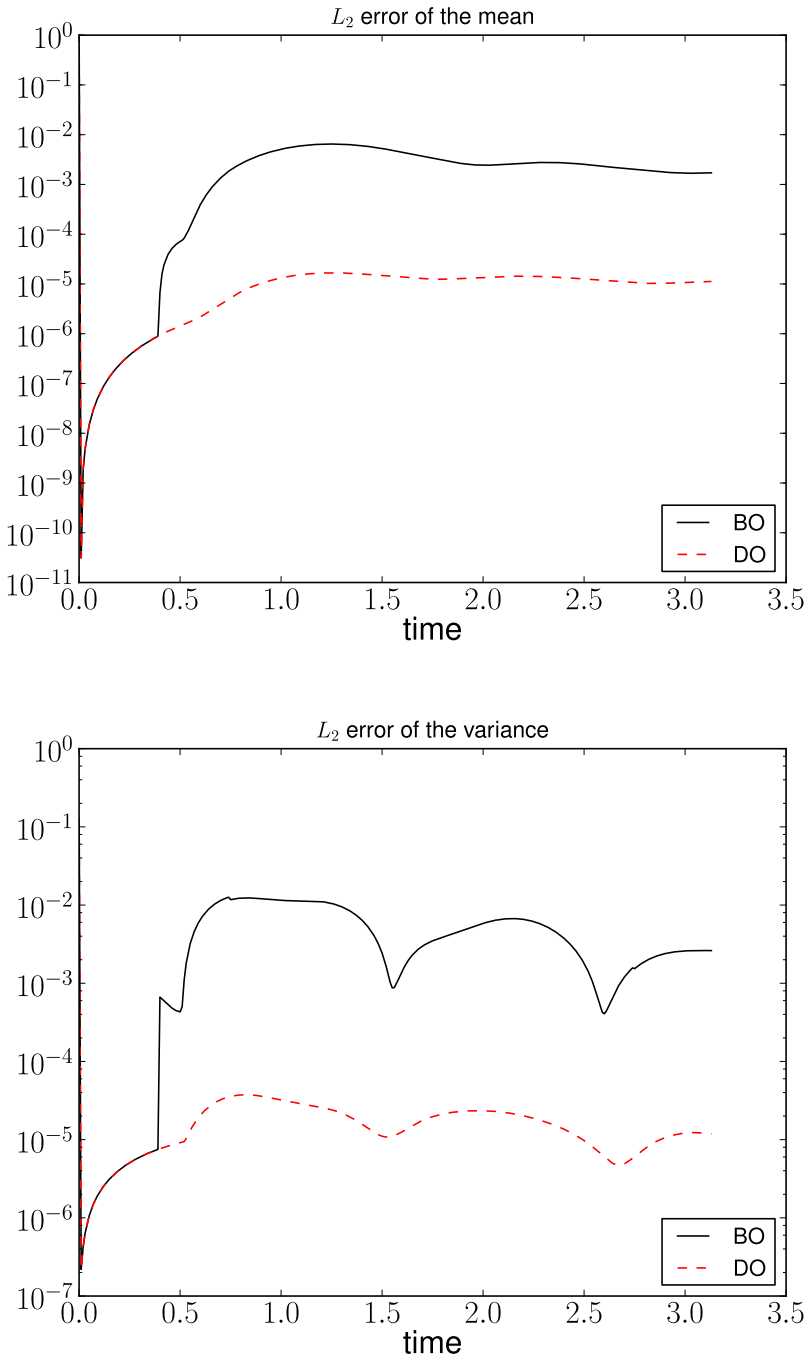

Figure 7.11: Left: mean, right: variance. Both the error of the mean and variance in BO jumps when the eigenvalues cross while the error in DO does not.

	DO	BO
mean	$\sin(x-t)$	$\sin(x-t)$
spatial basis	$u_1(x,t) = \frac{1}{\sqrt{\pi}}\cos(x-t)$ $u_2(x,t) = \frac{1}{\sqrt{\pi}}\cos(2x-3t)$	$u_1(x,t) = a_1(t)\cos(x-t)$ $u_2(x,t) = a_2(t)\cos(2x-3t)$
stochastic basis	$Y_1(t;\omega) = \sqrt{\pi}a_1(t)\Phi_1(\xi_1)$ $Y_1(t;\omega) = \sqrt{\pi}a_2(t)\Phi_2(\xi_2)$	$Y_1(t;\omega) = \Phi_1(\xi_1)$ $Y_2(t;\omega) = \Phi_2(\xi_2)$

Table 7.2: The exact BO and DO components.

such that $E[\Phi_i\Phi_j] = \delta_{ij}, i, j = 1, 2$, i.e.

$$\begin{aligned}\Phi_1(\xi_1) &= \sqrt{3}(2\xi_1 - 1)\\ \Phi_2(\xi_2) &= \sqrt{3}(2\xi_2 - 1).\end{aligned}$$

The forcing term is given accordingly.

Then we can compute the exact components for the BO and DO as shown in Table 7.2. Note that the stochastic basis for the BO is time-independent while both the spatial and stochastic basis for the DO are time-dependent.

The eigenvalues of the solution are given as follows:

$$\begin{aligned}\lambda_1(t) &= \pi a_1^2(t)\\ \lambda_2(t) &= \pi a_2^2(t).\end{aligned}$$

We choose $a_1(t)$ and $a_2(t)$ such that they have eigenvalue crossing as well as zero eigenvalues, which makes a good benchmark problem to test the adaptive algorithm. We choose two sets of functions as shown in Table 7.3.

	$a_1(t)$	$a_2(t)$
Case I	$1.5 + \sin(t)$	$1.5 + \cos(3t)$
Case II	$\sin(t)$	$\cos(3t)$

Table 7.3: Two cases of $(a_1(t), a_2(t))$.

Figure 7.12 shows the eigenvalues for cases I and II. The case I has three eigenvalue crossing between two modes while the case II has six eigenvalue crossing with three zero eigenvalues. For both cases we use three methods; i) BO, ii) DO, iii) hybrid BO-DO. Note that hybrid BO-DO starts with the BO and whenever the criteria in Algorithm 2 are satisfied it switch between them.

7.4.1.1 Case I

First we consider case I where we have $a_1(t) = 1.5 + \sin(t), a_2(t) = 1.5 + \cos(3t)$. We have eigenvalue crossing at three different times and do not have zero eigenvalue. Hence we expect that the DO works better than the BO because the latter suffers from the eigenvalue crossing while the former does not suffer from high condition number of the covariance matrix. Indeed, as shown in Figure 7.13 that shows the L_2 error for the mean and variance, the BO does suffer from the eigenvalue crossing while the DO works well. Note that the BO has jumps due to the numerical instability when there are eigenvalue crossing while other methods such as DO and hybrid BO-DO work fine. Hybrid BO-DO switch from the BO to the DO at about $t = 0.39$ when it faces first eigenvalue crossing and remains in the DO since there is no zero eigenvalue throughout the time interval. there is only one switching from the BO to the DO at about $t = 0.39$ for hybrid BO-DO.

We compare the spatial basis u_1 and u_2 derived from the DO evolution equations with the exact one in Table 7.2 at three different times. Figure 7.14 shows that the

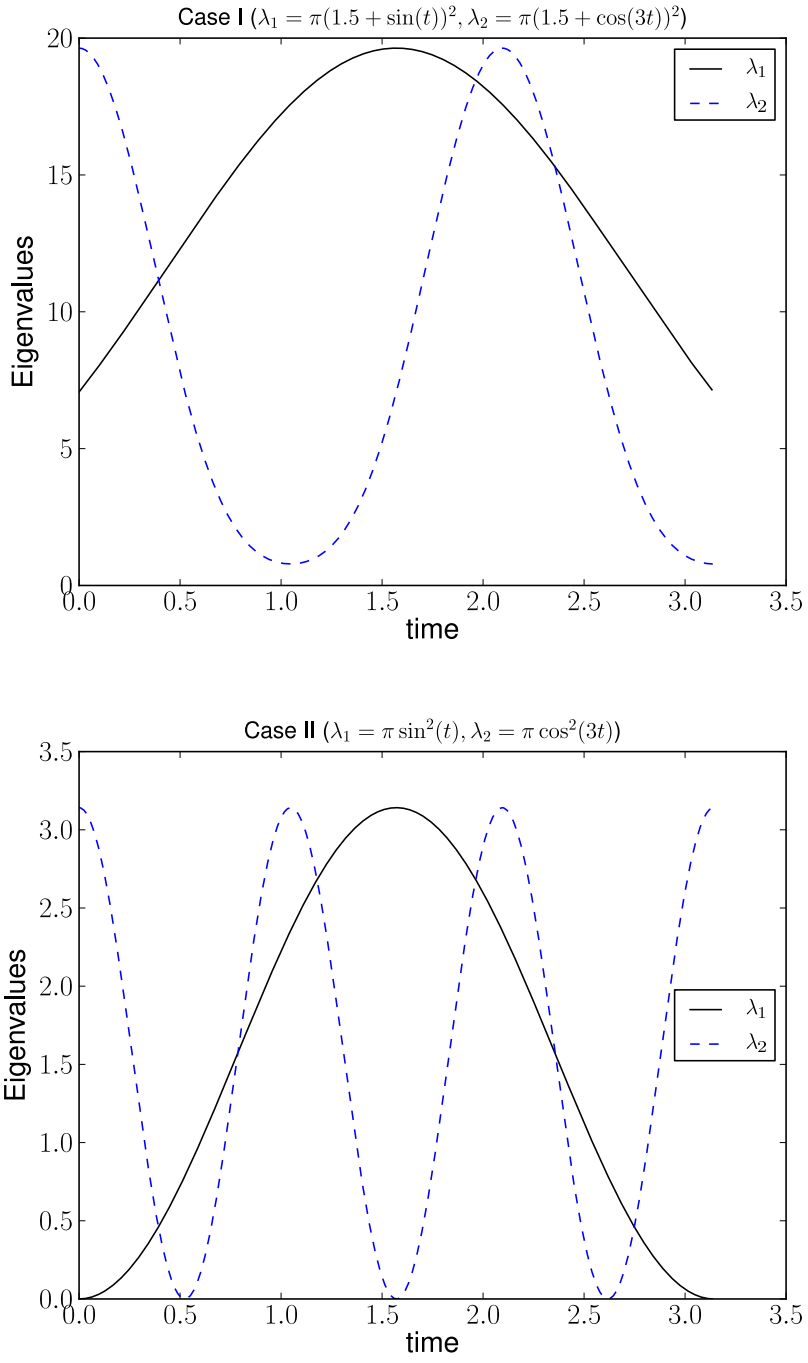

Figure 7.12: Eigenvalues in time for cases I (top) and case II (bottom).

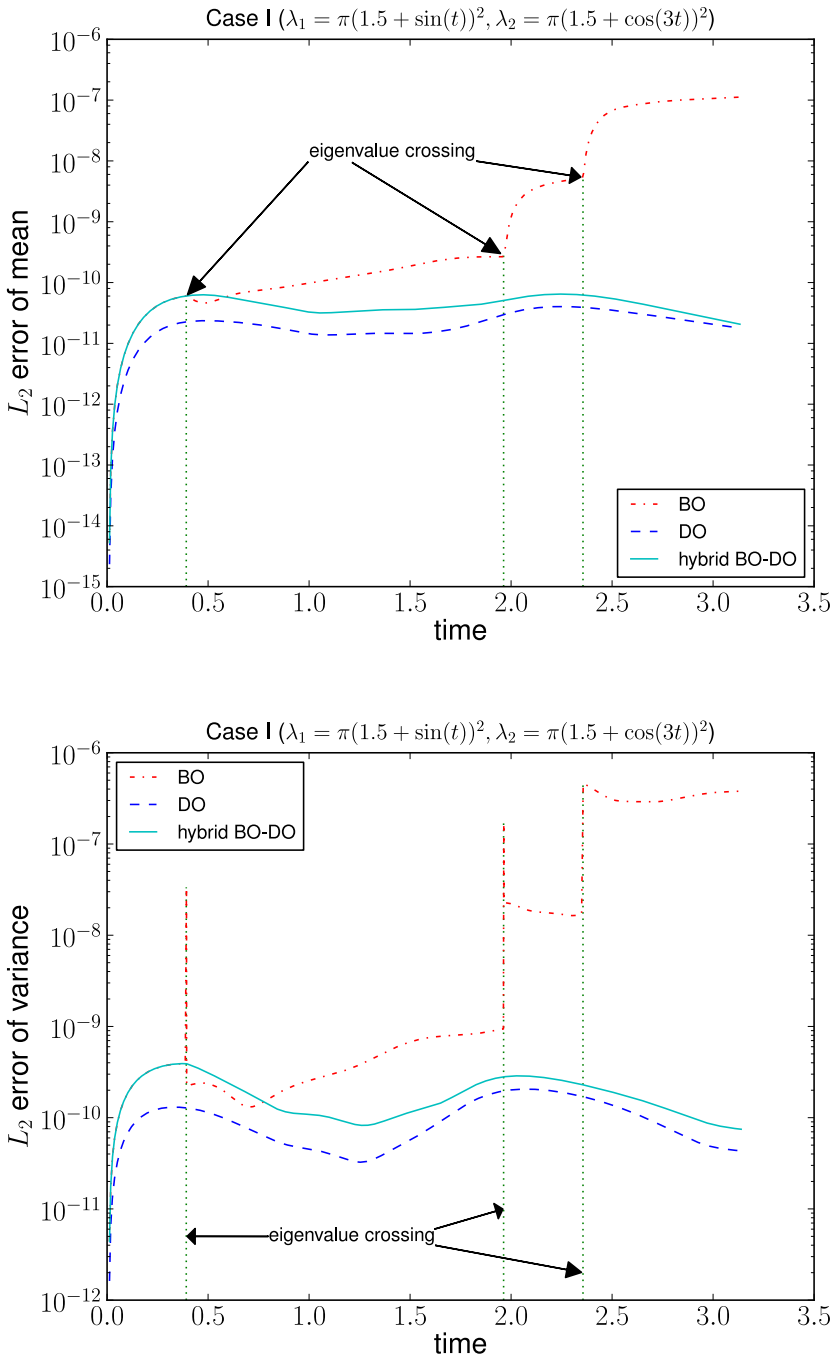

Figure 7.13: [Case I] L_2 errors for the mean (top) and variance (bottom). The BO has jumps due to the numerical instability when there are eigenvalue crossing while other methods work fine. Since there is no zero eigenvalue throughout the time interval, there is only one switching from the BO to the DO at about $t = 0.39$.

spatial basis from the DO evolution equations agrees very well with the exact DO spatial basis as expected.

7.4.1.2 Case II

We consider case II where we have $a_1(t) = \sin(t), a_2(t) = \cos(3t)$. We not only have eigenvalue crossing at six different times but also have zero eigenvalue at three different times. The L_2 error for the mean and variance is shown in Figure 7.15 where there is no BO because it diverges due to the numerical instability when facing eigenvalue crossing. Note also that the DO also suffers due to the numerical instability when the eigenvalue is getting close to the zero around $t = 0.52$. However, hybrid BO-DO works well. It starts with the BO and switch to the DO when facing eigenvalue crossing around $t = 0.4$ and switch back to the BO when facing zero eigenvalue around $t = 0.5$ and switch back to the DO when facing eigenvalue crossing around $t = 0.75$. However, when the next eigenvalue crossing happens around $t = 1.2$, it does not switch because it is already in the DO and hence does not suffer from the eigenvalue crossing. The choice of threshold plays an important role in maintaining the accuracy. The higher threshold $\epsilon_c = 10^{-5}$ gives better accuracy than the smaller threshold $\epsilon_c = 10^{-6}$ as it detects the small eigenvalue earlier and switches to BO.

We compare the spatial basis u_1 and u_2 derived from the hybrid BO-DO methods with the exact one in Table 7.2 at three different times $t = 0.7, 1.5, 3$. Note that the mode at $t = 0.7$ is the BO while the modes at $t = 1.5, 3$ are the DO. Figure 7.16 shows that the spatial basis derived from hybrid BO-DO agrees very well with the exact DO or BO spatial basis as expected.

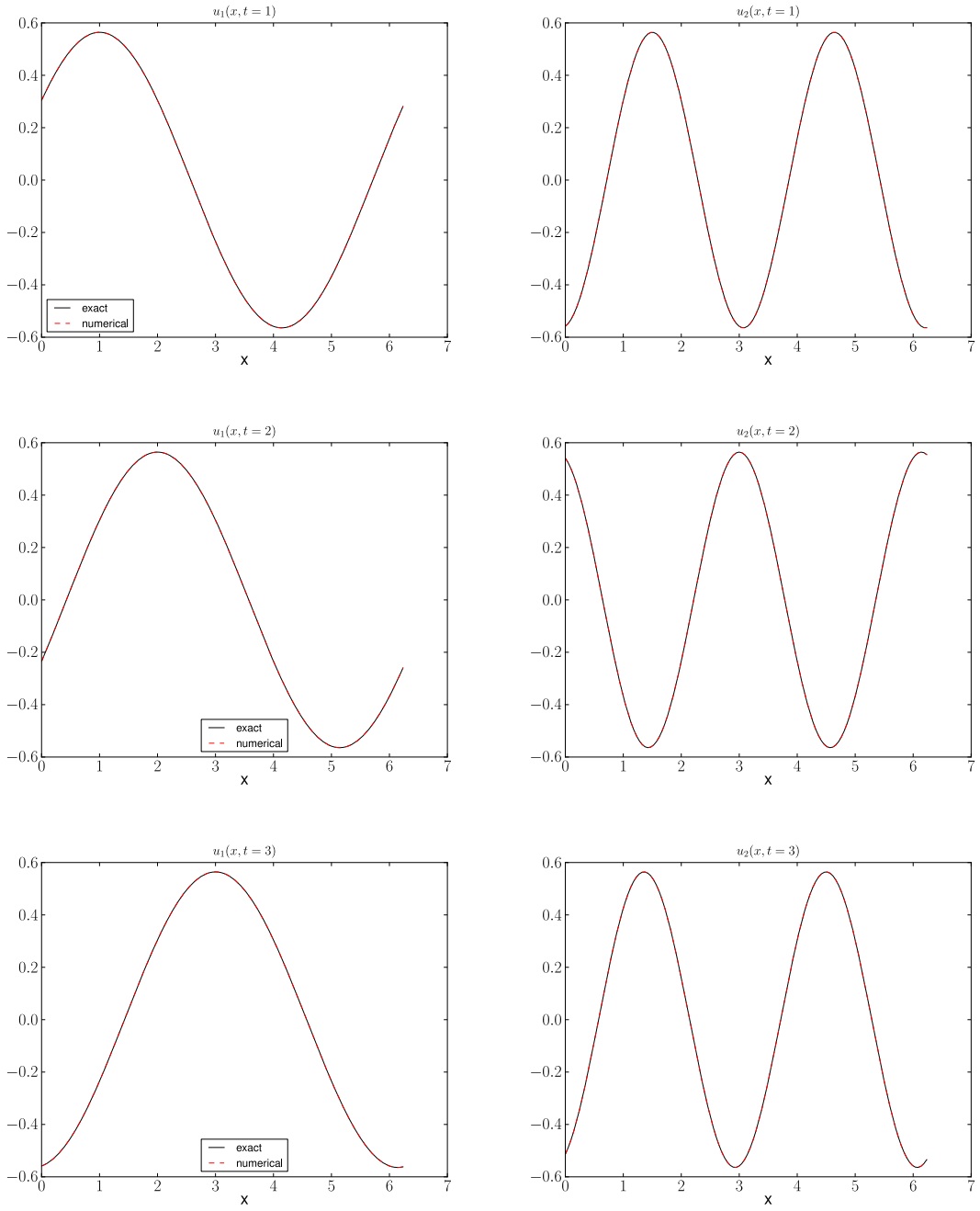

Figure 7.14: [Case I] DO spatial basis u_1 (left) and u_2 (right) at three different time $t = 1$ (top), 2 (middle) and 3 (bottom). They agree very well with the exact DO basis in Table 7.2.

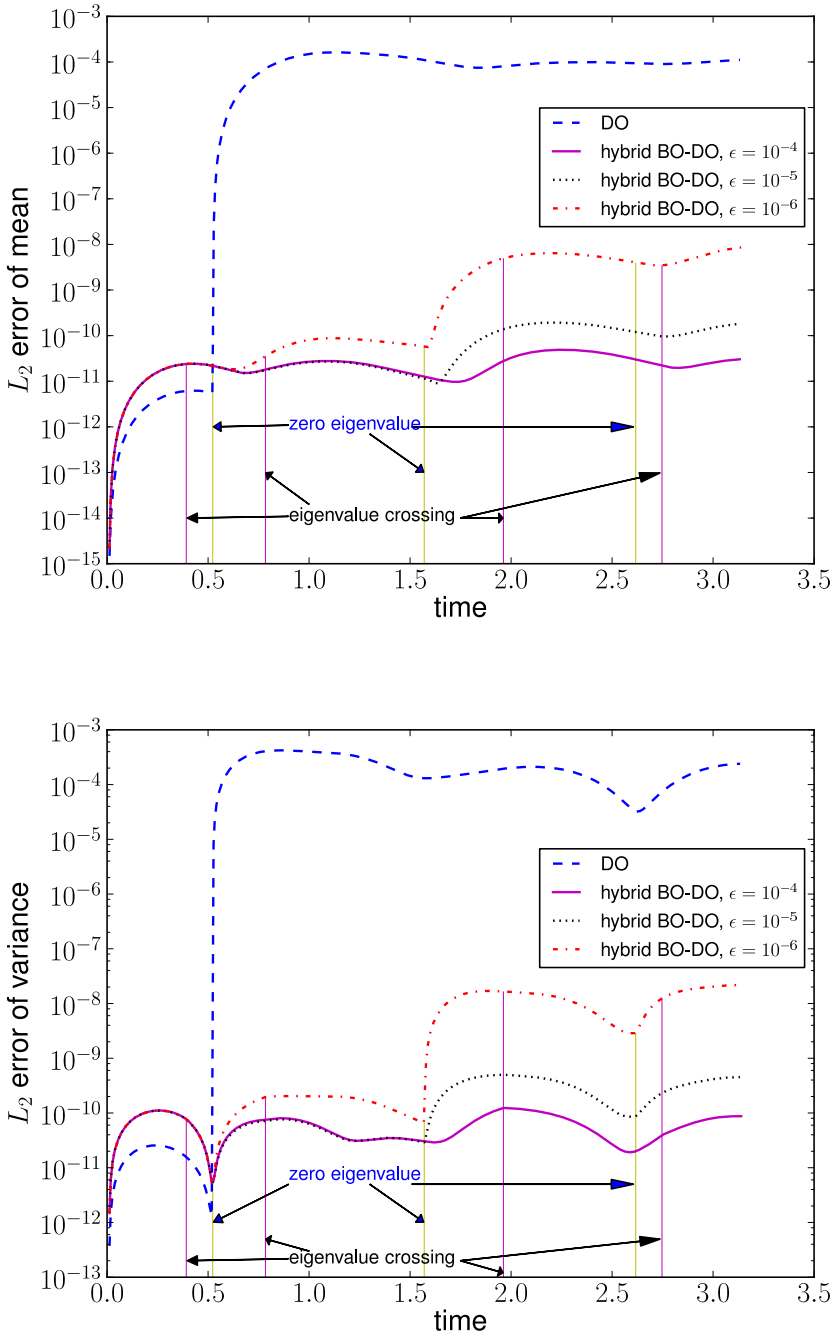

Figure 7.15: [Case II] L_2 errors for the mean (top) and variance (bottom). The BO diverges due to the numerical instability when facing eigenvalue crossing and the DO also suffers due to the numerical instability when the eigenvalue is getting close to the zero around $t = 0.52$. However, the adaptive methods works well. The higher threshold $\epsilon_c = 10^{-5}$ gives better accuracy than the smaller threshold $\epsilon_c = 10^{-6}$ as it detects the small eigenvalue earlier and switches to BO.

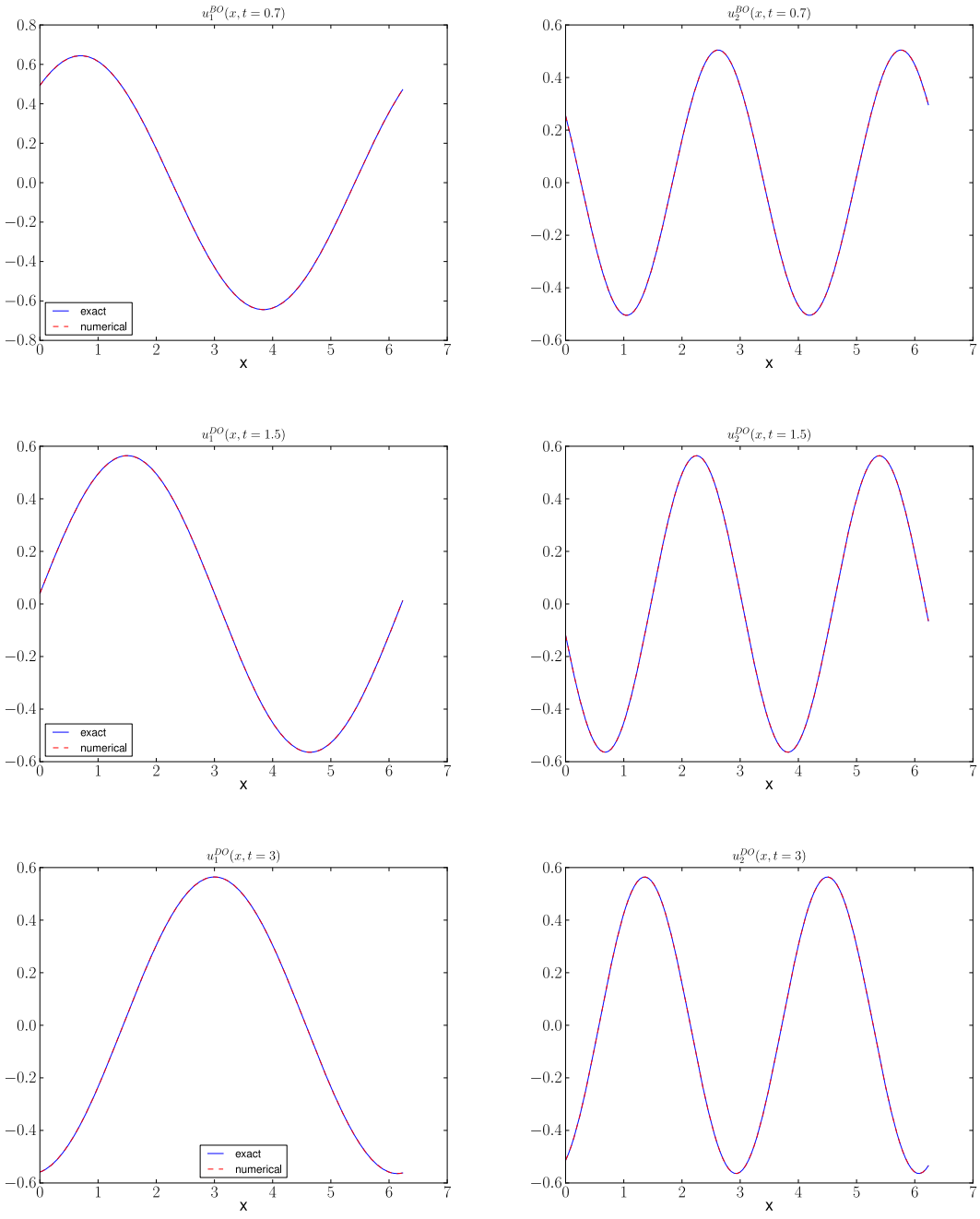

Figure 7.16: [Case II] DO or BO spatial basis u_1 (left) and u_2 (right) at three different time $t = 0.7$ (top), 1.5 (middle) and 3 (bottom) when using hybrid BO-DO. Note that hybrid BO-DO is in BO mode at $t = 0.7$ and is in DO mode at $t = 1.5, 3$. They agree very well with the exact DO or BO basis in Table 7.2.

7.4.2 Adaptively adding and removing modes

We consider again the stochastic Burgers problem in Section 7.2:

$$g_1(x) \equiv f(x,t;\omega) = \frac{1+\xi}{2}\sin(2\pi t) \tag{7.19}$$

where $\xi(\omega)$ is a uniformly distributed random variable on $[-1,1]$. The initial condition is given as follows:

$$u(x,0) = 0.5(\exp(\cos(x)-1.5)-1.5)\sin(x+2\pi\cdot 0.37). \tag{7.20}$$

Unlike in Section 7.2 where we had a fixed number of modes and showed the convergence with respect to the number of modes for the BO and DO, we now allow the system to adaptively add or remove modes according to Algorithm introduced in Subsection 5.4.2. The choice of the threshold for $(\epsilon_a^1, \epsilon_a^2)$ depends on the system. We have tested different sets of $(\epsilon_a^1, \epsilon_a^2)$ and would present only two cases. It is observed for this problem that when ϵ_a^1 is the same order of magnitude as ϵ_a^2, the adaptivity method works best. We choose the following threshold:

$$\epsilon_a^1 = \epsilon_a^2 = 10^{-9}.$$
$$\epsilon_a^1 = \epsilon_a^2 = 10^{-10}.$$

We tested the adaptive BO with the above threshold and BO with fixed number of modes for the comparison. The parameters are as follows:

$$dt = 10^{-3}, t_f = 25, N_s = 128, N_r = 64.$$

The third-order Runge-Kutta method is used as a time-integrator. Figure 7.17 shows

$(\epsilon_a^1, \epsilon_a^2)$	time (N)
$(10^{-9}, 10^{-9})$	4.38(7)
$(10^{-10}, 10^{-10})$	2.78(7), 4.58(8)

Table 7.4: The time at which a new mode is added.

the relative L_2 error for the mean and variance. The DO appears to be the same as the BO and hence is omitted in the figure.

The table 7.4 shows when a new mode is added for each threshold. It starts with $N = 6$. Only one mode is added at $t = 4.38$ for $\epsilon_a = 10^{-9}$ and two modes are added at $t = 2.78, 4.58$ for $\epsilon_a = 10^{-10}$. The lower the threshold is the more modes are added as expected. The accuracy also improves as more modes are added.

Figure 7.18 shows the eigenvalue for $\epsilon_a^1 = \epsilon_a^2 = 10^{-10}$. It clearly shows that the new modes are added when the smallest eigenvalue is larger than ϵ_a^1 at $t = 2.78$ and 4.58.

We now consider slightly different initial condition for the same Burgers equation

$$g_2(x) \equiv u(x, 0) = 0.5(\exp(\cos(x) - 1.5) - 1.5) \sin(2x + 2\pi \cdot 0.37). \tag{7.21}$$

This has more frequency in the physical space and makes the problem more interesting.

We have tested five different sets of $(\epsilon_a^1, \epsilon_a^2)$. The threshold is shown in Table 7.5. We tested the adaptive BO with the five different threshold and BO with fixed number of modes ($N = 10$) for the comparison. The parameters are as follows:

$$dt = 10^{-4}, t_f = 10, N_s = 256, N_r = 64.$$

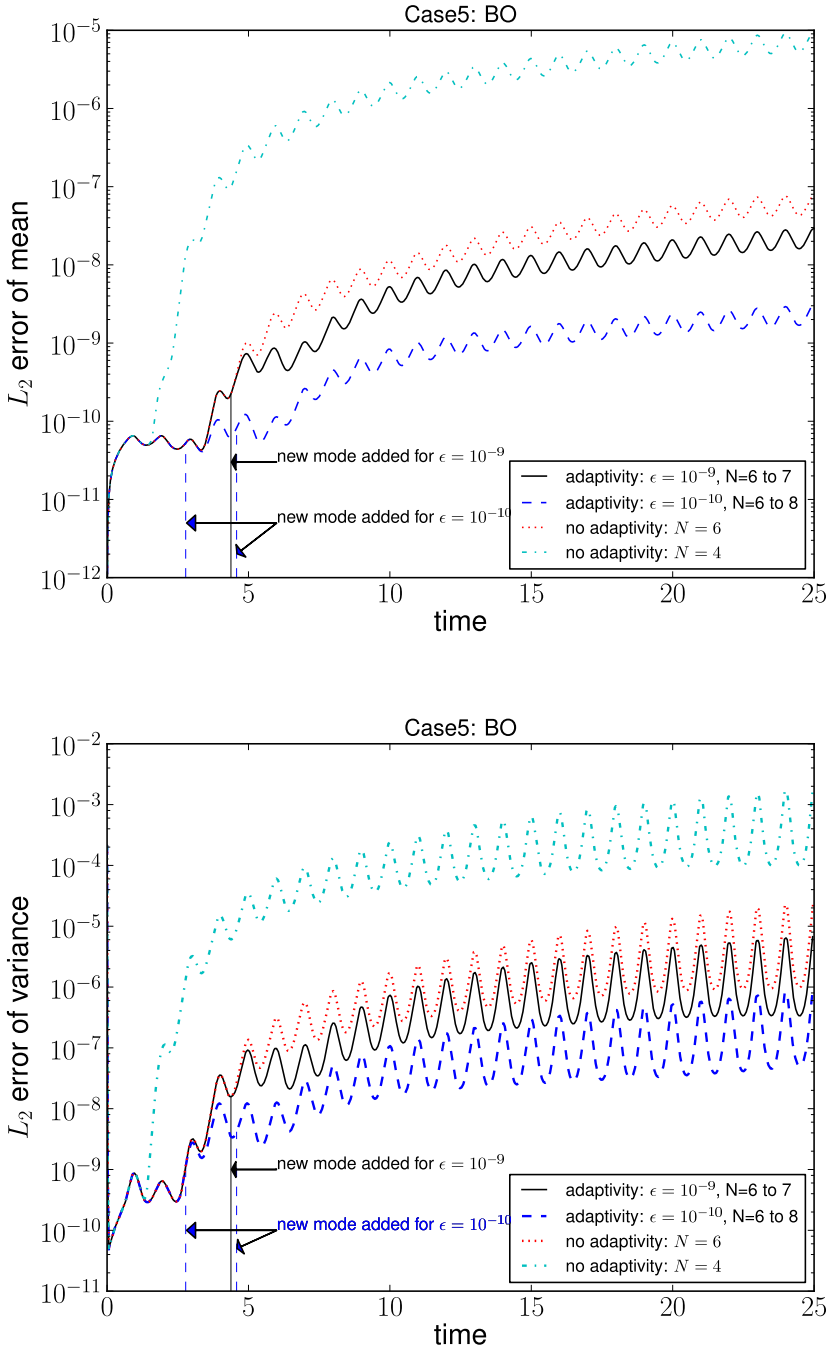

Figure 7.17: L_2 errors for the mean (top) and variance (bottom). The BO with two different fixed number of modes $N = 4, 6$ shows that higher mode gives better accuracy. The adaptive BOs (black solid line and blue dashed line) is much better than the BO with $N = 6$. The two adaptive BOs shows that the choice of the threshold is also important to get better accuracy.

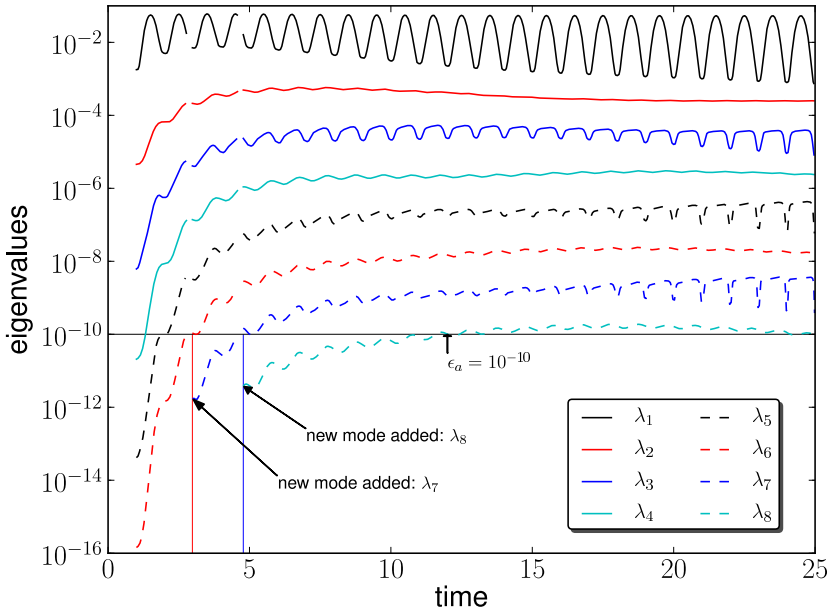

Figure 7.18: The eigenvalues for the adaptive BO for $\epsilon_a = 10^{-10}$. Two modes are added at $t = 2.78, 4.58$ so the modes are increased from 6 at the initial time to 8 at the final time. It starts with $N = 6$ and when the smallest eigenvalue λ_6 and the slope are larger than the threshold, a new mode (u_7, Y_7) is added at $t = 2.78$. The eigenvalue for newly added mode is about 10^{-12}. Another new mode is added at later time $t = 4.58$. λ_8 passes above the threshold at later time but a new mode is not added because the slope is not larger than the threshold. Indeed, even if new mode is added at this point, the numerical test shows that it does not improve the accuracy. This is why the slope is taken into account.

Cases	ϵ_a^1	ϵ_a^2
1.	10^{-7}	10^{-7}
2.	10^{-8}	10^{-8}
3.	10^{-9}	10^{-9}
4.	10^{-10}	10^{-10}
5.	10^{-11}	10^{-11}

Table 7.5: The threshold for the initial condition $g_2(x)$.

The third-order Runge-Kutta method is used as a time-integrator. Figure 7.19 shows the relative L_2 error for the mean and variance. It clearly shows that the accuracy improves when we add the modes when the smallest eigenvalue is larger than a prescribed threshold. The DO appears to be the same as the BO and hence is omitted in the figure.

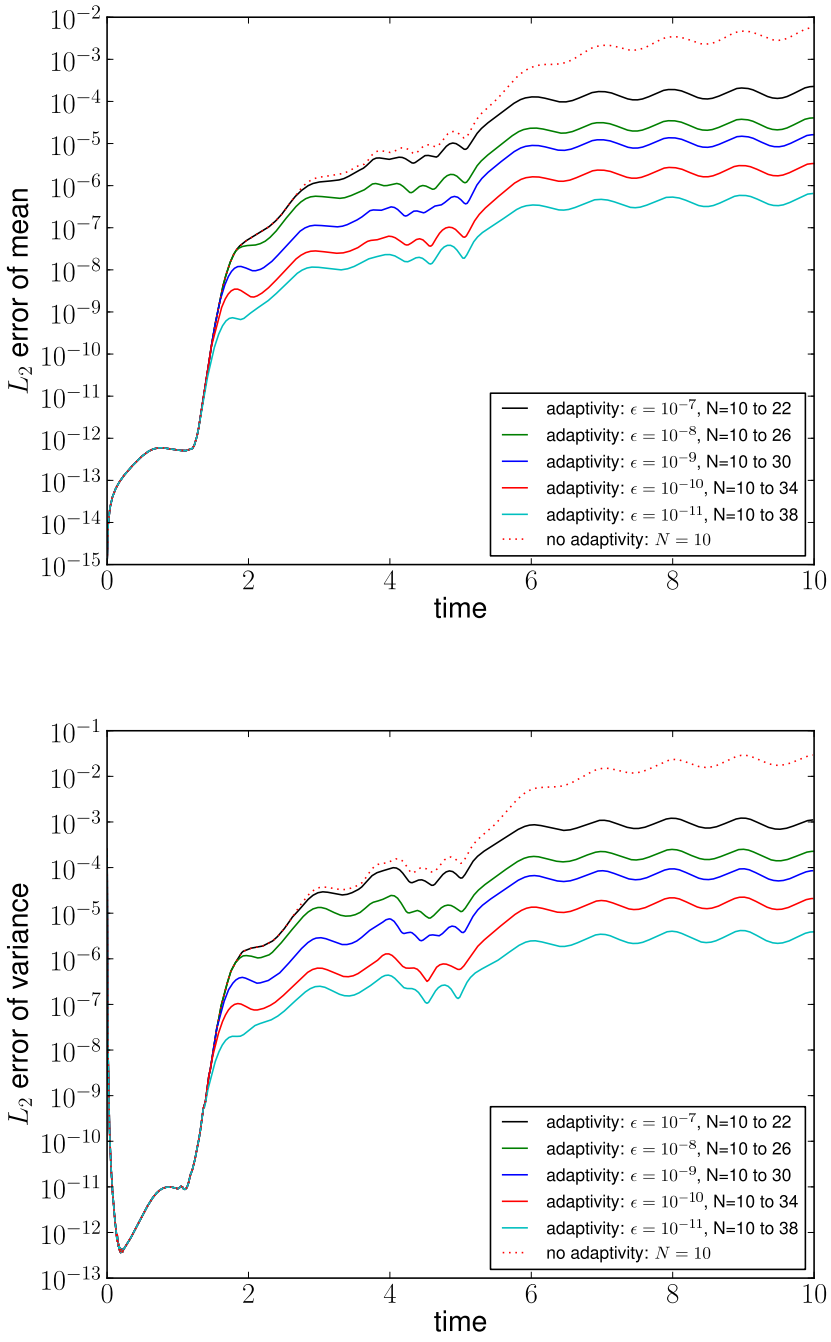

Figure 7.19: L_2 errors for the mean (top) and variance (bottom). The adaptive BOs are better than the BO with the fixed number of modes (N=10). The smaller the threshold is the better the accuracy is.

Chapter 8

Summary and Future Work

In this thesis we provided a unified-framework of time-dependent KL type methods for SPDEs that explore the low-dimensional structures on-the-fly in the L_2 sense. We introduced the DO evolution equations based on the dynamical constraints on the spatial basis, called DO condition, followed by the BO evolution equations based on the static constraints on the spatial and stochastic basis, called BO condition. We proved that both the spatial and stochastic basis for the BO and DO are related via an orthogonal matrix governed by orthogonal matrix differential equation. At any given time the spatial and stochastic basis of BO track exactly those of KL expansion and under the rotation or orthogonal linear transformation the DO enjoys the same property as the BO, i.e. low-dimensional structure. Each of the methods have disadvantages, e.g. when facing an eigenvalue crossing in BO or having a large condition number of the covariance matrix in DO. We utilized the orthogonal linear transformation between the two methods to overcome the aforementioned disadvantage achieving a unified-framework of time-dependent KL type methods for SPDEs. Another benefit employing the tKL representation may be the computa-

tional efficiency since extracting the most important modes of the KL expansion derived from other methods such as gPC or PCM at every time may require a large-scale computation. We applied the tKL methods to linear (advection) and nonlinear (Burgers, two-dimensional Navier-Stokes, etc) problems. We presented convergence properties of DO and BO in comparison with the PC method, where DO and BO methods converge exponentially fast with respect to the number of modes (for the problems considered) giving the same levels of computational accuracy comparable with the PC method but (in many cases) with substantially smaller computational cost compared to stochastic collocation, especially when the involved parametric space is high-dimensional. We showed the adaptive algorithms to add and remove modes based on the smallest eigenvalue to better capture the transient behavior. We developed a parallel solver for the tKL methods based on spectral h/p solver Nektar.

Lastly, we discuss a few ideas for future projects building upon the work presented in this thesis. The tKL modes can be splitted into the large and small scales in both spatial and random space; both the spatial and stochastic basis corresponding to large eigenvalue belong to the large scale in the spatial and random space, respectively while the modes corresponding to small eigenvalue belong to the small scale. We can employ adaptive discretization in both physical and parametric domains to further improve the efficiency of numerical implementation. The tKL modes track the most N energetic basis with N being the number of modes that results in a reduced-order modeling. The deterministic counterpart POD have been applied successfully in the numerical simulation for laminar flows. However, it is well known that it does not work well for turbulent flows because the discarded modes due to low energy have a significant impact on the dynamics. We need a closure model to take into account this non-negligible effect. We can employ an idea from the deterministic closure modeling such as variational multiscale models [79] to develop

a closure model in the stochastic framework.

Appendix A

Manual for parallel tKL Nektar solver

Parallel tKL Nektar solver is a BO and DO solver based on Nektar. It extends parallel Nektar solver for the deterministic partial differential equations to tKL solver for the stochastic partial differential equations. The probabilistic collocation method (PCM) is used for the discretization in parametric space while the spectral *hp* [74] method is used for the discretization in physical space. The BO and DO evolution equations for the mean, spatial and stochastic basis can be solved. It is assumed that the user knows the deterministic Nektar. If not, please see for more detail Nektar manuals - "nektar_UserGuide.pdf" and "nektar_ReferenceGuide.pdf".

A.1 User manual

The following is an example of the input file format for Nektar. It is a text file and filename extension is *.rea*. There are six main sections to this file:

- Parameters
- Mesh Data
- Curved Slide data
- Boundary Conditions
- Initial Conditions
- Drive Force Data

The main sections for parallel tKL Nektar are the same as those for parallel deterministic Nektar except that there are additional parameters in Parameters section. Hence Parameters section are explained only in this Appendix.

A.1.1 Model Problem

We consider the two-dimensional advection-diffusion equation with random advection velocity [80],

$$\frac{\partial \phi}{\partial t}(x,t;\omega) + u(x;\omega)\cdot\nabla\phi = \nu\nabla^2\phi \quad (x,t;\omega) \in D\times[0,T]\times\Omega, \tag{A.1}$$

where D is a bounded domain in R^2, Ω is the sample space in the probability space, and ν is the viscosity. For this problem, we will assume deterministic boundary and

initial conditions and that the advection velocity corresponds to a circular motion plus a constant random perturbation, i.e.,

$$u(x;\omega) = (y + a(\omega), -x - b(\omega)), \tag{A.2}$$

where $a(\omega)$ and $b(\omega)$ are random variables. The initial condition is given as

$$\phi(x, 0; \omega) = e^{-\frac{(x-x_0)^2+(y-y_0)^2}{2\lambda^2}}, \tag{A.3}$$

and the corresponding exact stochastic solution is

$$\phi_e(x, t; \omega) = \frac{\lambda^2}{\lambda^2 + 2\nu t} e^{-\frac{\hat{x}^2+\hat{y}^2}{2(\lambda^2+2\nu t)}}, \tag{A.4}$$

where

$$\hat{x} = x + b(\omega) - (x_0 + b(\omega))\cos(t) - (y_0 + a(\omega))\sin(t),$$
$$\hat{y} = y + a(\omega) + (x_0 + b(\omega))\sin(t) - (y_0 + a(\omega))\cos(t).$$

Here we set $\nu = 10^{-5}, \lambda = 1/8$ and $T = 1$. Since the initial condition is deterministic, we use the hybrid gPC-tKL introduced in Section 5.3. We consider two-dimensional parametric space assuming $a(\omega) = \sigma_1\xi_1$ and $b(\omega) = \sigma_2\xi_2$ where ξ_1 and ξ_2 are two independent random variables following uniform distribution on $[-1, 1]$.

A.1.2 Parameters

From advdiff.rea we read:

```
***** PARAMETERS *****
  NEKTAR SPLITTER
  2 DIMENSIONAL RUN
  21 PARAMETERS FOLLOW
        12             MODES
        0.00001        KINVIS
        1              TIMEMAX
        0.01           PCMTIMEMAX
        0.00001        DT
        TIMEMAX/DT     NSTEPS
        PCMTIMEMAX/DT  NPCMSTEPS
        0.             SLVTYPE
        1.             INTYPE
        1.             DOINTYPE
        1.             EQTYPE
        1000           IOSTEP
        1000           HISSTEP
        1000           STSTEP
        8              NCOLS_1D
        64             NCOLS
        2              NODOMODES
        0.2            SIGMA1
        0.1            SIGMA2
        1.0e-10        TOL
        0              ISKL
```

We will now list parameters necessary for the stochastic tKL methods and describe its purpose:

- **NPCMSTEPS** Sets the number of time steps for PCM to run for, i.e. sets the switching time t_s.
- **NCOLS_1D** The number of collocation points in 1-dimensional parametric space.
- **NCOLS** The number of collocation points in parametric space.
- **NODOMODES** Defines the number of tKL modes.
- **SIGMA1** Defines σ_1 in the above model problem.
- **SIGMA2** Defines σ_2 in the above model problem.
- **TOL** Defines the tolerance that is necessary to compute KL decomposition of the solution at $t = t_s$ in hybrid gPC-tKL.
- **ISKL** Defines if the KL decomposition is required. If ISKL is set to 1, then the KL decomposition is required at $t = t_s$. If ISKL is set to 0, then the modes $\bar{u}(x, t_s), \mathbf{U}(x, t_s), \mathbf{Y}(t_s; \omega)$ are loaded from files instead of computing the eigenfunctions and eigenvalues.

A.2 Developer manual

The highest level routines are all in drive.C as it is in the deterministic Nektar solver. Note that there are $(N + 1)$ deterministic PDEs for the mean and the spatial basis and N stochastic ODEs for the stochastic basis assuming that N is the number of

modes. The spectral hp method is employed for the deterministic PDEs while the stochastic collocation method is employed for the stochastic ODEs.

There are two files that perform tasks related to the tKL methods that would be described in the Appendix:

- **tkl_operation.C**: contains functions which compute the BO and DO components such as matrices M, S, G and vectors $\mathbf{h}, \mathbf{p}$.
- **eigfs_parpack.C**: contains functions which compute the KL decomposition.

A.2.1 tkl_operation.C

We remind the DO and BO evolution equations in Table A.1.

	DO	BO
mean	$\frac{\partial \bar{\mathbf{u}}^{DO}}{\partial t} = E[\mathcal{L}(u)]$	$\frac{\partial \bar{\mathbf{u}}^{BO}}{\partial t} = E[\mathcal{L}(u)]$
spatial basis	$\frac{\partial \mathbf{U}^{DO}}{\partial t} = (\mathbf{p} - \mathbf{U}^{DO} G) C^{-1}$	$\frac{\partial \mathbf{U}^{BO}}{\partial t} = \mathbf{U}^{BO} M + \mathbf{p}$
stochastic basis	$\frac{d\mathbf{Y}^{DO}}{dt} = \mathbf{h}$	$\frac{d\mathbf{Y}^{BO}}{dt} = (-\mathbf{Y}^{BO} S^T + \mathbf{h}) \Lambda^{-1}$

Table A.1: The BO and DO evolution equations. $\mathbf{U}^{DO}$ and $\mathbf{Y}^{DO}$ are the DO components of the basis and stochastic coefficients and $\mathbf{U}^{BO}$ and $\mathbf{Y}^{BO}$ are the BO components.

The vector and matrix in the evolution equations are defined as:

$$
\begin{aligned}
\Lambda &= diag(\lambda_1, ..., \lambda_N) \\
C_{ij} &= E[Y_i Y_j] \\
G_{ij} &= \langle E[\mathcal{L}[u] Y_j], u_i \rangle \\
M_{ij} &= \begin{cases} \frac{G_{ij}+G_{ji}}{-\lambda_i+\lambda_j}, & \text{if } i \neq j \\ 0, & \text{if } i = j \end{cases} \\
S_{ij} &= \begin{cases} G_{ij} + \lambda_i M_{ij}, & \text{if } i \neq j \\ G_{ii}, & \text{if } i = j \end{cases} \\
h_j &= \langle \tilde{\mathcal{L}}[u], u_j \rangle \\
p_j &= E[\mathcal{L}[u] Y_j].
\end{aligned}
$$

This source file compute components shown in the above equations which are listed below.

- `void Compute_EYY(Domain *omega)`

  Compute the covariance matrix of the stochastic basis $E[\mathbf{Y}^T\mathbf{Y}]$.

- `void Compute_iEYY(Domain *omega)`

  Compute the inverse of covariance matrix of the stochastic basis.

- `void Compute_EYYY(Domain *omega)`

  Compute the third-order moments of the stochastic basis $E[Y_i Y_j Y_k], i, j, k = 1, ..., N$.

- `void compute_cov_basis(Domain *omega)`

  Compute the covariance matrix of the spatial basis $\langle \mathbf{U}^T \mathbf{U} \rangle$.

- `void compute_h(Domain *omega)`

  Compute $\mathbf{h} = \langle \tilde{\mathcal{L}}[u]\mathbf{U} \rangle$.

- `void compute_p_explicit(Domain *omega)`

  Compute $\mathbf{p} = E[\mathcal{L}[u]\mathbf{Y}]$.

- `void compute_G(Domain *omega)`

  Compute $G = \langle \mathbf{U}^T E[\mathcal{L}[u]\mathbf{Y}] \rangle$.

- `void compute_M(Domain *omega)`

  Compute matrix M.

- `void compute_S(Domain *omega)`

  Compute matrix S.

A.2.2 eigfs_parpack.C

We need the KL decomposition for hybrid gPC-tKL at the switching time $t = t_s$. The procedure is described in Section 5.3. We need to compute the eigenvalue problem in order to get the eigenfunctions and eigenvalues that is often computationally

expensive. Parallel ARPACK (ARnoldi PACKage) library is used to solve this large scale eigenvalue problems.

- ```
  int Arpack_Socket(int N, Coord *gX, double* weight, double **cov,
                    int M, double tol, double *egvalue, double* egfunc)
  ```

  - `N` is the number of collocation points in physical domain.
  - `gX` is the structure containing the coordinates of the collocation points. The size of the array is N.
  - `weight` is the weights corresponding to the collocation points. The size of the array is N.
  - `cov` is the covariance matrix for which the eigenfunctions and eigenvalues are computed. The user have to compute the covariance matrix before calling this function. The size of the matrix is $N \times N$.
  - `M` is the number of the largest eigenvalues that would be computed.
  - `tol` is the tolerance to compute the eigenvalue problems used in ARPACK library.
  - `egvalue` contains the M largest eigenvalue of the covariance matrix.
  - `egfunc` contains the M eigenfunctions corresponding to the eigenvalues. The size of array is $N \cdot M$.

  If the output is equal to M, then the eigenvalues and eigenfunctions are computed successfully.
  ```

Bibliography

[1] T. Sapsis, P. Lermusiaux, Dynamically orthogonal field equations for continuous stochastic dynamical systems, Physica D 238 (2009) 2347–2360.

[2] M. Cheng, T. Hou, Z. Zhang, A dynamically bi-orthogonal method for time-dependent stochastic pdes i: Derivation and algortihms, Journal of Computational Physics 242 (2013) 843–868.

[3] M. Choi, T. Sapsis, G. E. Karniadakis, On the equivalence of dynamically orthogonal and dynamically bi-orthogonal methods: Theory and numerical simulations, Journal of Computational Physics 270 (2014) 1–20.

[4] K. Sobczyk, Stochastic Wave Propagation, Elsevier Publishing Company, 1985.

[5] V. Konotop, L. Vazquez, Nonlinear Random Waves, World Scientific, 1994.

[6] J. Fouque, J. Garnier, G. Papanicolaou, K. Solna, Wave Propagation and Time Reversal in Randomly Layered Media, Springer, 2007.

[7] T. Soong, M. Grigoriu, Random Vibration of Mechanical and Structural Systems, PTR Prentice Hall, 1993.

[8] Y. Lin, G. Cai, Probabilistic Structural Dynamics, McGraw-Hill Inc., 1995.

[9] J. Roberts, P. Spanos, Random Vibration and Statistical Linearization, Dover Publications, 2003.

[10] M. Giles, Multilevel monte carlo path simulation, Operations Research 56 (3) (2008) 607–617.

[11] R. Ghanem, P. Spanos, Stochastic Finite Elements: A Spectral Approach, Springer-Verlag, 1991.

[12] H. G. Matthies, A. Keese, Galerkin methods for linear and nonlinear elliptic stochastic partial differential equations, Computer Methods in Applied Mechanics and Engineering 194 (12) (2005) 1295–1331.

[13] R. A. Todor, C. Schwab, Convergence rates for sparse chaos approximations of elliptic problems with stochastic coefficients, IMA Journal of Numerical Analysis 27 (2) (2007) 232–261.

[14] X. Wan, G. E. Karniadakis, Multi-element generalized polynomial chaos for arbitrary probability measures, SIAM Journal on Scientific Computing 28 (3) (2006) 901–928.

[15] D. Xiu, J. Hesthaven, High order collocation methods for differential equations with random inputs, SIAM J. Sci. Comput. 27(3) (2005) 1118–1139.

[16] D. Xiu, G. E. Karniadakis, The Wiener–Askey polynomial chaos for stochastic differential equations, SIAM Journal on Scientific Computing 24 (2002) 619–644.

[17] J. Foo, X. Wan, G. E. Karniadakis, The multi-element probabilistic collocation method: error analysis and simulation, J. Comput. Phys. 227 (2008) 9572–9595.

[18] I. Babuska, F. Nobile, R. Tempone, A stochastic collocation method for elliptic partial differential equations with random input data, SIAM J. Numer. Anal 45 (2007) 1005–1034.

[19] M. K. Deb, I. M. Babuška, J. T. Oden, Solution of stochastic partial differential equations using galerkin finite element techniques, Computer Methods in Applied Mechanics and Engineering 190 (48) (2001) 6359–6372.

[20] P. Frauenfelder, C. Schwab, R. A. Todor, Finite elements for elliptic problems with stochastic coefficients, Computer methods in applied mechanics and engineering 194 (2) (2005) 205–228.

[21] B. Ganapathysubramanian, N. Zabaras, Sparse grid collocation schemes for stochastic natural convection problems, Journal of Computational Physics 225 (1) (2007) 652–685.

[22] P. Holmes, J. Lumley, G. Berkooz, Turbulence, Coherent Structures, Dynamical Systems and Symmetry, Cambridge University Press, 1996.

[23] L. Sirovich, Turbulence and the dynamics of coherent structures, parts I, II and III, Quart. Appl. Math. XLV (1987) 561–590.

[24] J. Cusumano, M. Sharkady, B. Kimble, Experimental measurements of dimensionality and spatial coherence in the dynamics of a flexible-beam impact oscillator, Philos. Trans. R. Soc. London 347 (1994) 421–438.

[25] B. Feeny, R. Kappagantu, On the physical interpretation of proper orthogonal modes in vibrations, J. Sound Vibr. 211 (1998) 607–616.

[26] A. Rosenfeld, A. C. Kak, Digital picture processing, Vol. 1, Elsevier, 2014.

[27] N. Wiener, The homogeneous chaos, American Journal of Mathematics 60 (4) (1938) 897–936.

[28] T. Hou, W. Luo, B. Rozovskii, H.-M. Zhou, Wiener chaos expansions and numerical solutions of randomly forced equations of fluid mechanics, Journal of Computational Physics 216 (2) (2006) 687–706.

[29] R. Ghanem, J. Red-Horse, Propagation of probabilistic uncertainty in complex physical systems using a stochastic finite element approach, Physica D 133 (1-4) (1999) 137–144.

[30] A. Sarkar, R. Ghanem, Mid-frequency structural dynamics with parameter uncertainty, Computer Methods in Applied Mechanics and Engineering 191 (47-48) (2003) 93–100.

[31] A. J. Chorin, Gaussian fields and random flow, Journal of Fluid Mechanics 63 (01) (1974) 21–32.

[32] O. P. L. Matre, O. M. Knio, H. N. Najm, R. G. Ghanem, A stochastic projection method for fluid flow I. basic formulation, J. Comput. Phys. 173 (2001) 481–511.

[33] D. Xiu, G. E. Karniadakis, Modeling uncertainty in flow simulations via generalized polynomial chaos, J. Comput. Phys. 187 (2003) 137–167.

[34] O. Knio, O. L. Maitre, Uncertainty propagation in cfd using polynomial chaos decomposition, Fluid Dyn. Res 38 (2006) 616–640.

[35] S. Das, R. Ghanem, S. Finette, Polynomial chaos representation of spatio-temporal random fields from experimental measurements, J. Comput. Phys. 228 (2009) 8726–8751.

[36] S. Smolyak, Quadrature and interpolation formulas for tensor products of certain classes of functions, Soviet Math. Dokl. 4 (1963) 240–243.

[37] A. Keese, H. Matthies, Numerical methods and smolyak quadrature for nonlinear partial differential equations.

[38] E. Novak, K. Ritter, High dimensional integration of smooth functions over cubes, Numer. Math.

[39] E. Novak, K. Ritter, Simple cubature formulas with high polynomial exactness, Constr. Approx.

[40] E. N. V. Barthelmann, K. Ritter, High dimensional polynomial interpolation on sparse grids, Adv. Comput. Math.

[41] K. Petras, On the smolyak cubature error for analytic functions, Adv. Comput. Math.

[42] I. Babuska, F. Nobile, R. Tempone, A sparse grid stochastic collocation method for partial differential equations with random input data, SIAM J. Numer. Anal 46 (2008) 2309–2345.

[43] F. Nobile, R. Tempone, C. Webster, An anisotropic sparse grid stochastic collocation method for partial differential equations with random input data, SIAM J. Numer. Anal 46 (2008) 2411–2442.

[44] R. Fisher, Statistical Methods for Research Workers, Oliver and Boyd, 1925.

[45] W. Hoeffding, et al., A class of statistics with asymptotically normal distribution, The Annals of Mathematical Statistics 19 (3) (1948) 293–325.

[46] M. Griebel, Sparse grids and related approximation schemes for higher dimensional problems, SFB 611, 2005.

[47] M. Bieri, C. Schwab, Sparse high order fem for elliptic spdes, Computer Methods in Applied Mechanics and Engineering 198 (13) (2009) 1149–1170.

[48] J. Foo, G. E. Karniadakis, Multi-element probabilistic collocation in high dimensions, J. Comput. Phys. 229 (2009) 1536–1557.

[49] X. Yang, M. Choi, G. Lin, G. E. Karniadakis, Adaptive anova decomposition of stochastic incompressible and compressible flows, Journal of Computational Physics 231 (2012) 1587–1614.

[50] D. Venturi, X. WAN, G. Karniadakis, Stochastic bifurcation analysis of rayleigh-benard convection, J. Fluid Mech 650 (2010) 391–413.

[51] D. Venturi, X. WAN, G. Karniadakis, Stochastic low-dimensional modelling of a random laminar wake past a circular cylinder, J. Fluid Mech 606 (2008) 339–367.

[52] T. Sapsis, H. A. Dijkstra, Interaction of additive noise and nonlinear dynamics in the double-gyre wind-driven ocean circulation, Journal of Physical Oceanography 43 (2013) 366–381.

[53] T. Sapsis, M. Ueckermann, P. Lermusiaux, Global analysis of navier-stokes and boussinesq stochastic flows using dynamical orthogonality, Journal of Fluid Mechanics 734 (2013) 83–113.

[54] M. Ueckermann, P. Lermusiaux, T. Sapsis, Numerical schemes for dynamically orthogonal equations of stochastic fluid and ocean flows, Journal of Computational Physics 233 (2013) 272–294.

[55] T. Sapsis, A. Majda, Statistically accurate low order models for uncertainty quantification in turbulent dynamical systems, Proceedings of the National Academy of Sciences 110 (2013) 13705–13710.

[56] M. Choi, T. Sapsis, G. E. Karniadakis, A convergence study for SPDEs using combined polynomial chaos and dynamically-orthogonal condition, Journal of Computational Physics 245 (2013) 281–301.

[57] A. Majda, J. Harlim, Filtering Complex Turbulent Systems, Cambridge University Press, 2012.

[58] A. Bain, D. Crisan, Fundamentals of stochastic filtering, stochastic modeling and applied probability, Springer, New York, 2009.

[59] P. F. J. Lermusiaux, Uncertainty estimation and prediction for interdisciplinary ocean dynamics, J. Comp. Phys. 217 (2006) 176–199.

[60] A. Majda, D. Qi, T. Sapsis, Blended particle filters for large dimensional chaotic dynamical systems, Proceedings of the National Academy of Sciences in press.

[61] S. Lall, J. E. Marsden, S. Glavaski, A subspace approach to balanced truncation for model reduction of nonlinear control systems, Int. J. Robust Nonlinear Control 12 (2002) 519.

[62] Z. Ma, C. W. Rowley, G. Tadmor, Snapshot-based balanced truncation for linear time-periodic systems, IEEE Trans. Autom. Control 55 (2010) 469.

[63] J.-F. Gerbeau, D. Lombardi, Reduced-Order Modeling based on Approximated Lax Pairs, ArXiv e-printsarXiv:1211.4153.

[64] X. Wan, G. E. Karniadakis, An adaptive multi-element generalized polynomial chaos method for stochastic differential equations, J. Comput. Phys. 209 (2005) 617–642.

[65] T. P. Sapsis, Attractor local dimensionality, nonlinear energy transfers, and finite-time instabilities in unstable dynamical systems with applications to 2D fluid flows, Proceedings of the Royal Society A 469 (2153) (2013) 20120550.

[66] T. P. Sapsis, P. F. J. Lermusiaux, Dynamical criteria for the evolution of the stochastic dimensionality in flows with uncertainty, Physica D 241 (2012) 60.

[67] M. Cheng, T. Hou, Z. Zhang, A dynamically bi-orthogonal method for time-dependent stochastic pdes ii: Adaptivity and generalizations, Journal of Computational Physics 242 (2013) 753–776.

[68] O. L. Maitre, O. M. Knio, Spectral Methods for Uncertainty Quantification With Applications to Computational Fluid Dynamics, Springer, 2010.

[69] R. H. Cameron, W. T. Martin, The orthogonal development of non-linear functionals in series of fourier-hermite functionals, The Annals of Mathematics 48 (2) (1947) 385–392.

[70] M. Loeve, Probabilistic Theory II, Springer-Verlag, 1978.

[71] B. Øksendal, Stochastic differential equations, Springer, 2003.

[72] R. G. G. Olivier P. Le Matre, Habib N. Najm, O. M. Knio, Multi-resolution analysis of wiener-type uncertainty propagation schemes, J. Comput. Phys. 197 (2004) 502–531.

[73] M. Gerritsma, J.-B. van der Steen, P. Vos, G. E. Karniadakis, Time-dependent generalized polynomial chaos, J. Comput. Phys. 229 (2010) 8333–8363.

[74] G. E. Karniadakis, S. J. Sherwin, Spectral/hp Element Methods for Computational Fluid Dynamics, Oxford University Press, Second Edition, 2005.

[75] D. Gottlieb, S. A. Orszag, C. H. I. MA, Numerical analysis of spectral methods, Vol. 2, SIAM, 1977.

[76] J. S. Hesthaven, S. Gottlieb, D. Gottlieb, Spectral methods for time-dependent problems, no. 21, Cambridge University Press, 2007.

[77] M. Jardak, C.-H. Su, G. E. Karniadakis, Spectral polynomial chaos solutions of the stochastic advection equation, J. Sci. Comput. 17 (2002) 319–338.

[78] J. Jacod, P. Protter, Probability Essentials, Springer-Verlag, 2004.

[79] T. J. Hughes, A. A. Oberai, L. Mazzei, Large eddy simulation of turbulent channel flows by the variational multiscale method, Physics of Fluids (1994-present) 13 (6) (2001) 1784–1799.

[80] X. Wan, D. Xiu, G. E. Karniadakis, Stochastic solutions for the two-dimensional advection-diffusion equation, SIAM Journal on Scientific Computing 26 (2004) 578–590.